Chapter 4
Figures

98ϕ918ϕϕ48
Part 2

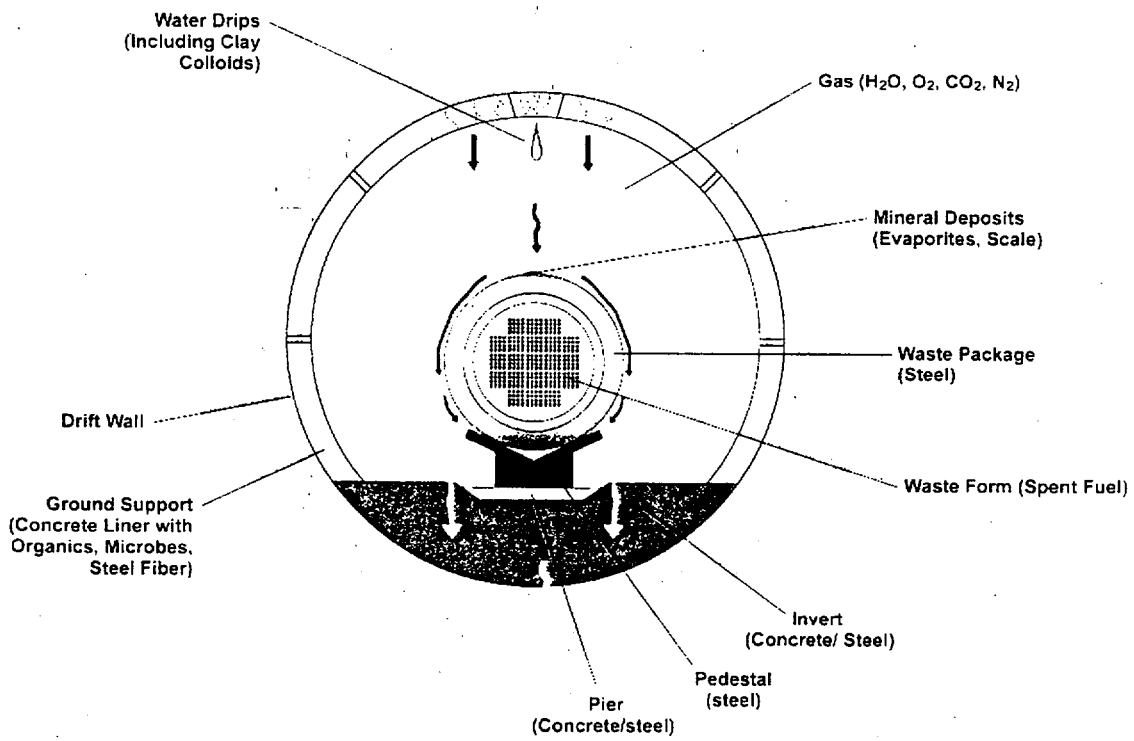

Figure 4-1. General near-field geochemical environment (NFGE) conceptual processes, phases, and design materials. This TSPA-VA component describes changing compositions of gas, water, colloids, and solids within the potential emplacement drifts.

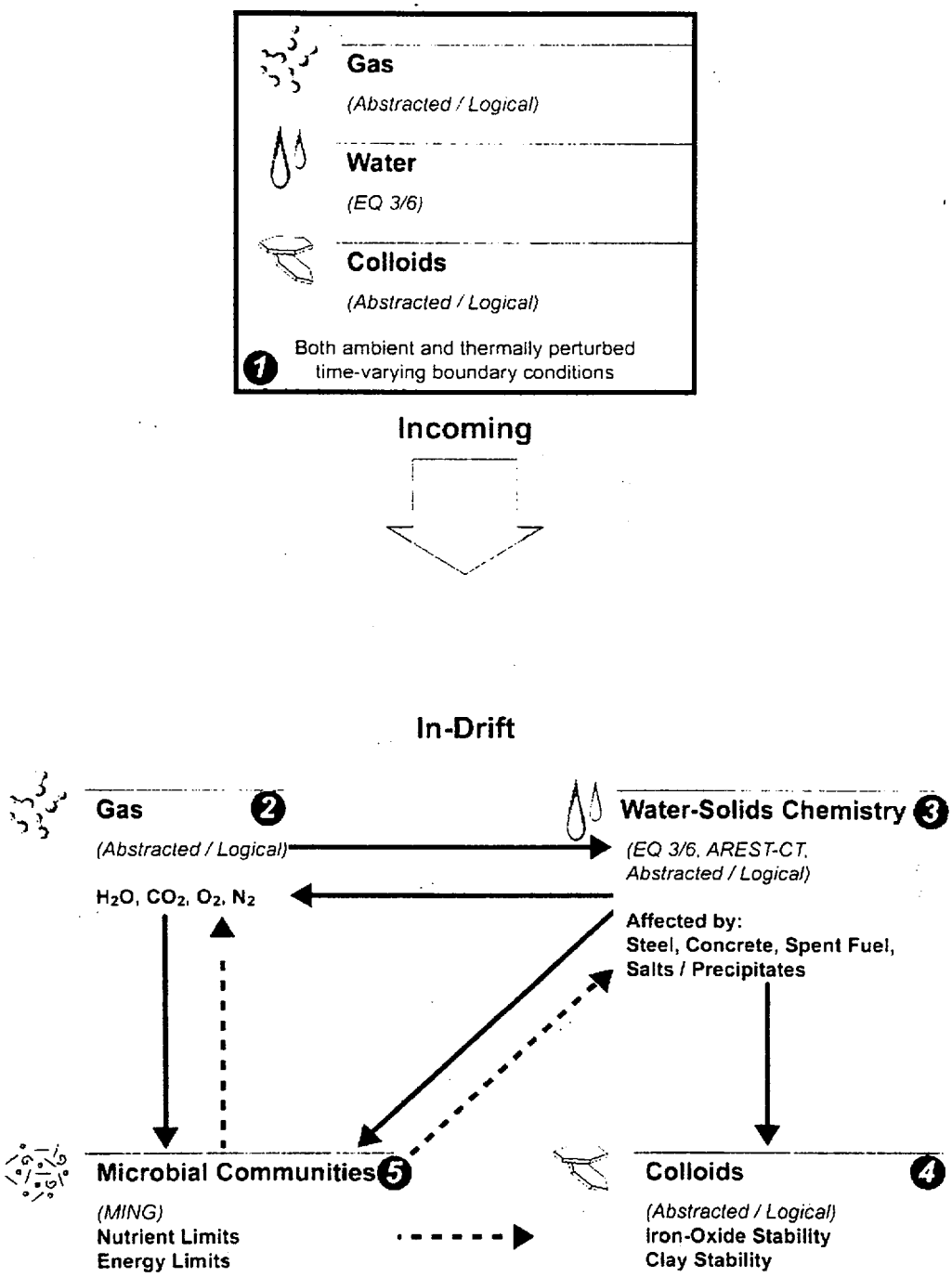

Figure 4-2. Relations between the five (5) NFGE models.

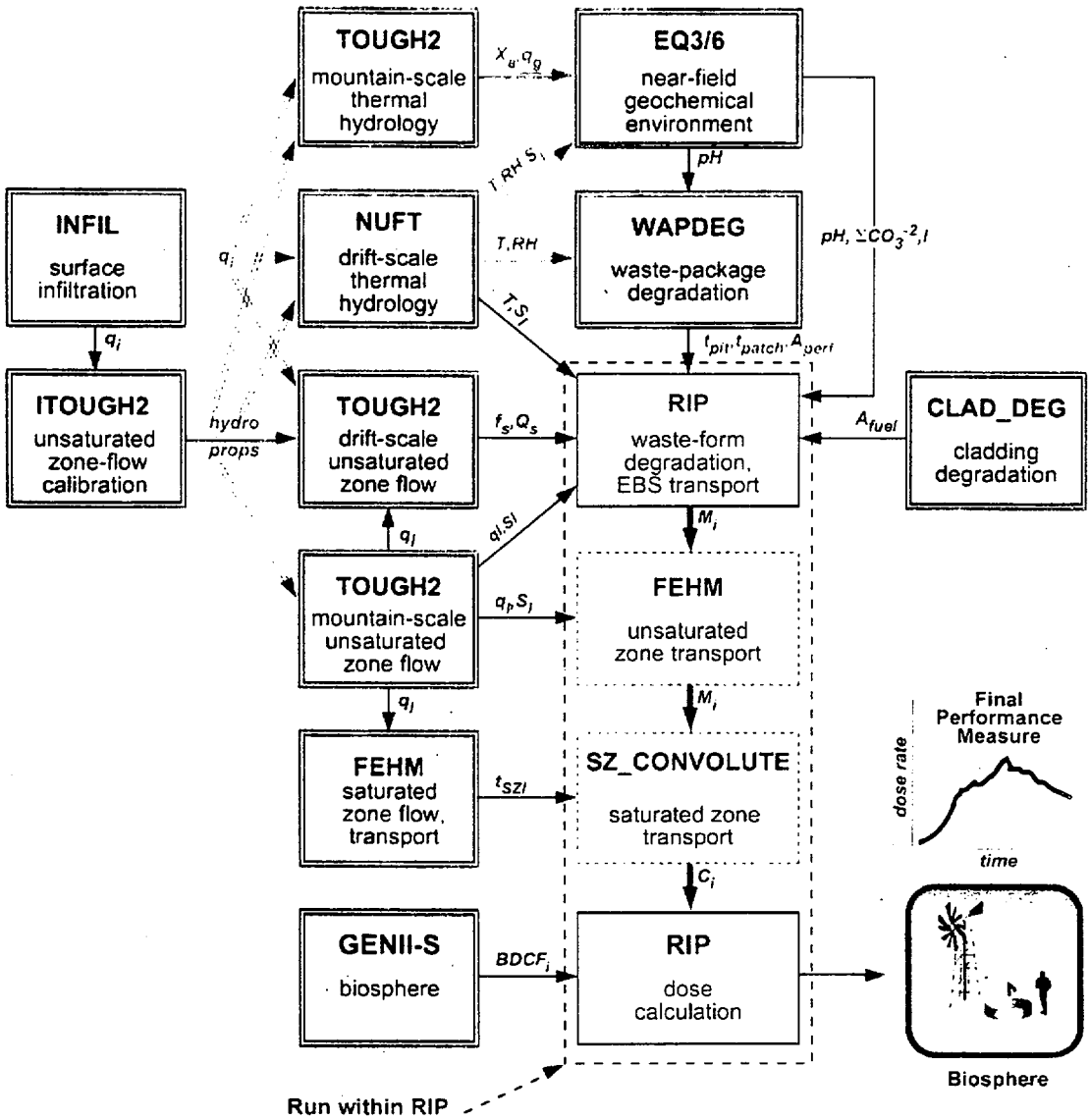

OUTPUT Parameters

T	Temperature	Q_S	Seep flow rate
RH	Relative humidity	pH	pH
S_l	Liquid saturation	ΣCO_3^{-2}	Carbonate concentration
X_a	Air mass fraction	I	Ionic strength
q_g	Gas flux	t_{pit}	Initial-pit-penetration time
q_l	Liquid flux	t_{patch}	Initial-patch-penetration time
q_i	Infiltration flux	A_{perf}	Perforated container area
M_i	Radionuclide mass flux	A_{fuel}	Exposed fuel area
C_i	Radionuclide concentration	t_{SZi}	Saturated zone transport time
f_S	Fraction of WPs with seeps	$BDCF_i$	Biosphere dose conversion factor
		EBS	Engineered Barrier System

Legend

- *External Process Model*
- *RIP Cells*
- *Rip Calls External Code*
- *Response Surface Between Process Models*
- *Response Surface from Process Model to RIP*
- *Between RIP Cells and External Code*

Figure 4-3. TSPA-VA code configuration: information flow among TSPA component computer codes.

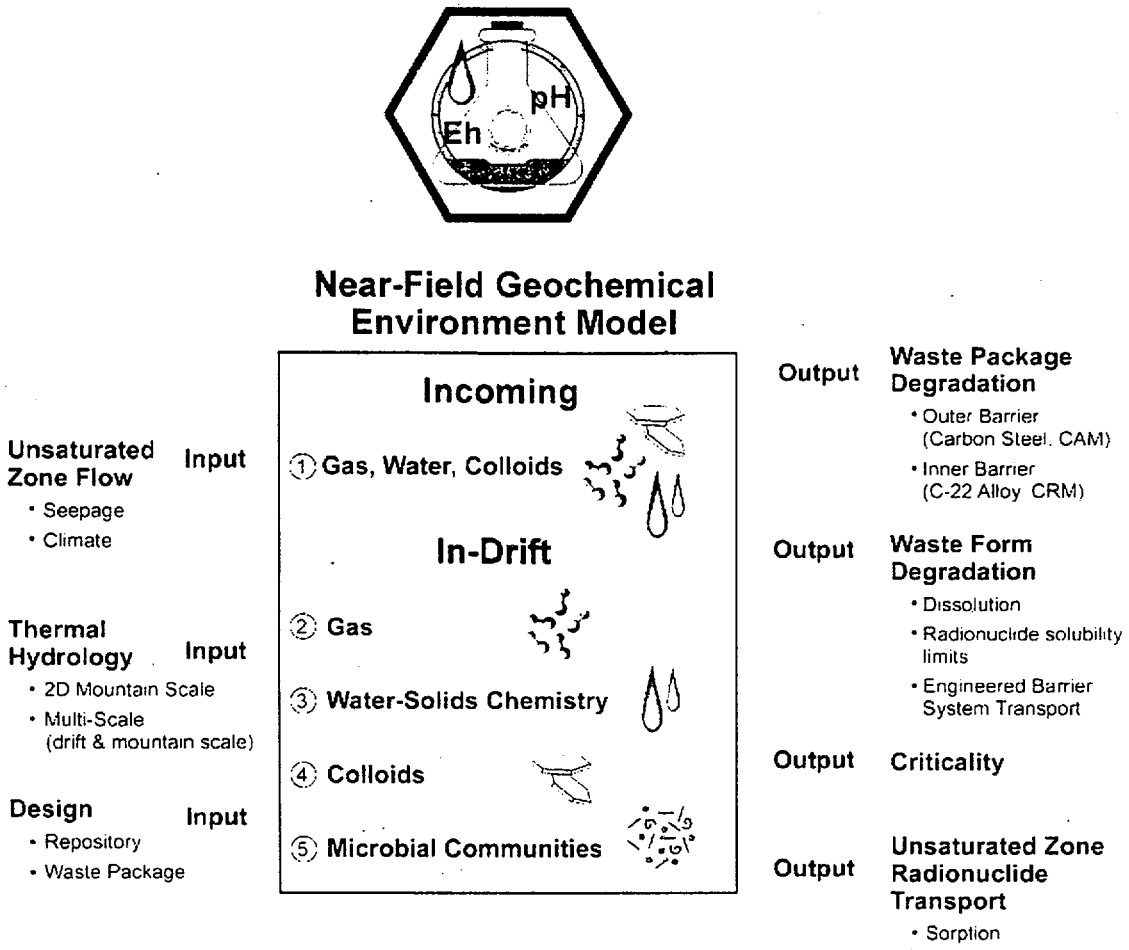

Figure 4-4. Interconnects between NFGE component and other TSPA-VA components.

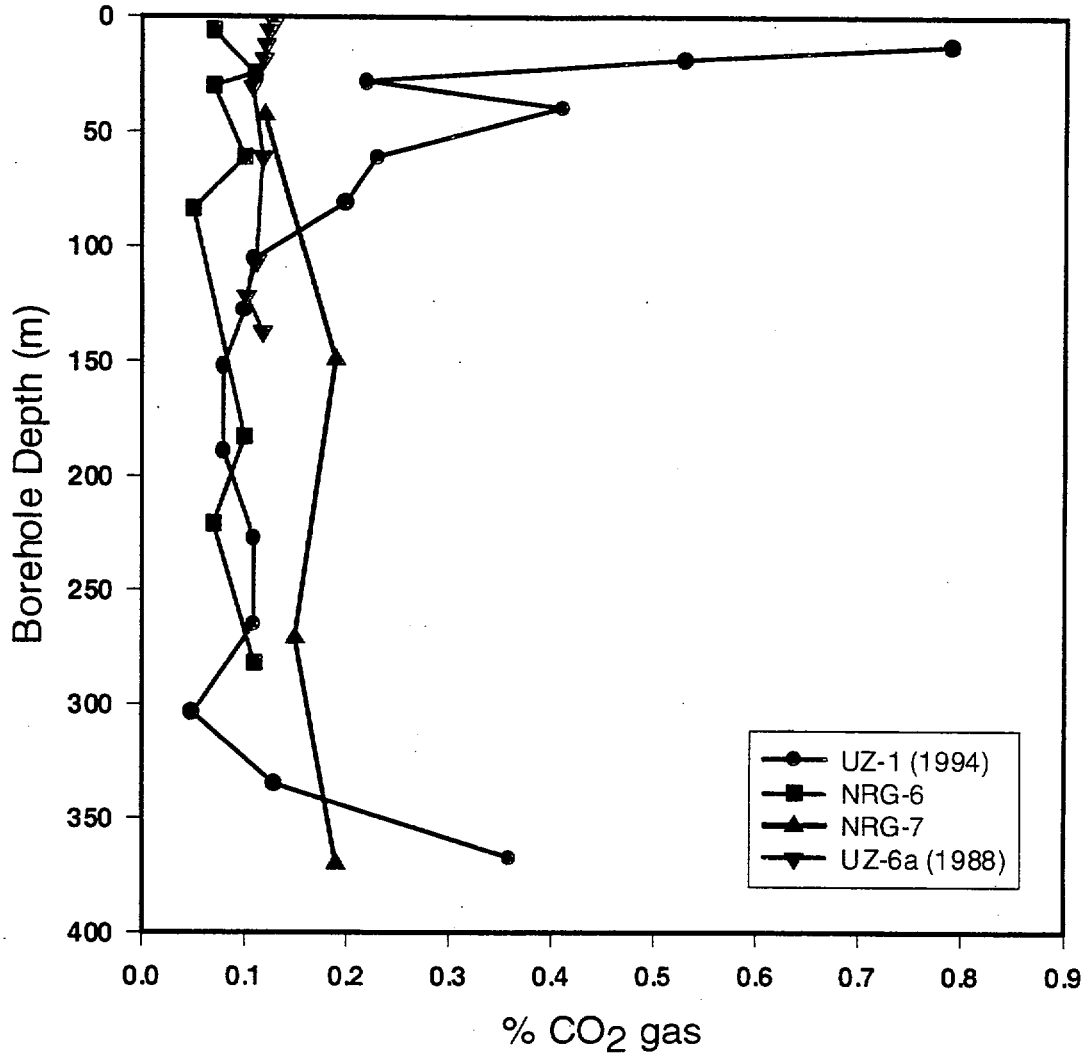

Figure 4-5. CO_2 gas abundance from various boreholes in the UZ of Yucca Mountain. Data taken from Yang et al. (1985, 1993, 1996) and Thorstensen et al. (1990).

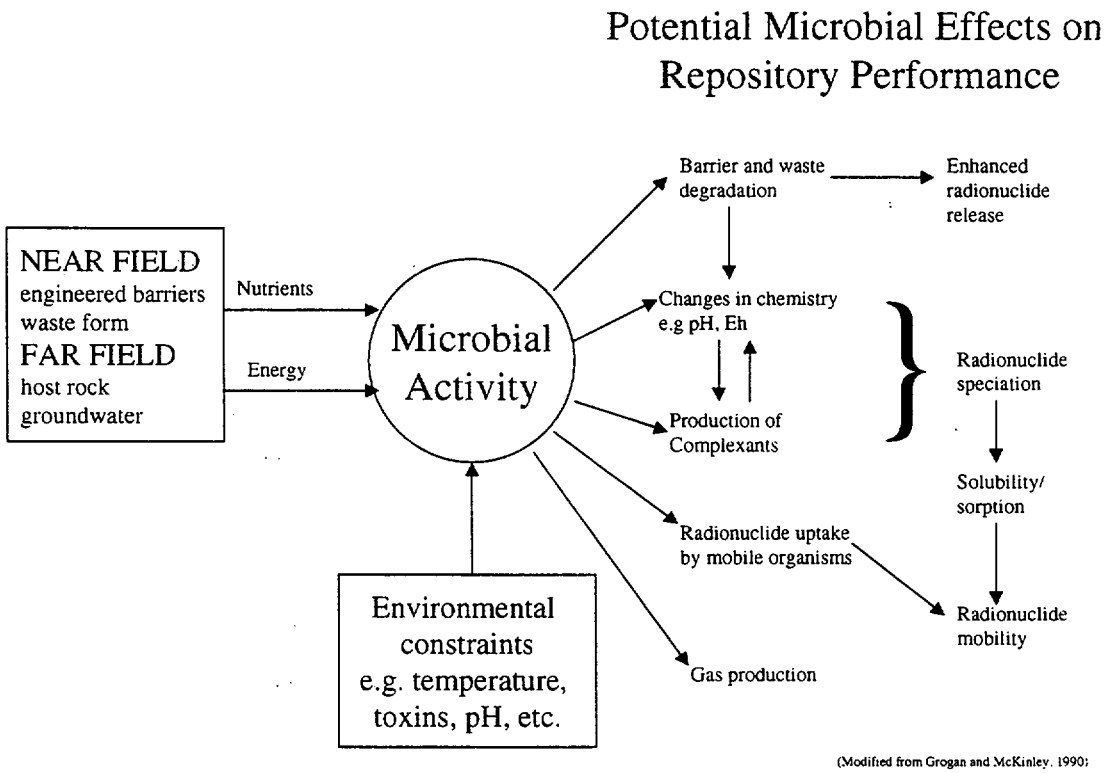

Figure 4-6. Simplified flow diagram of the potential effects of microbial activity on repository performance.

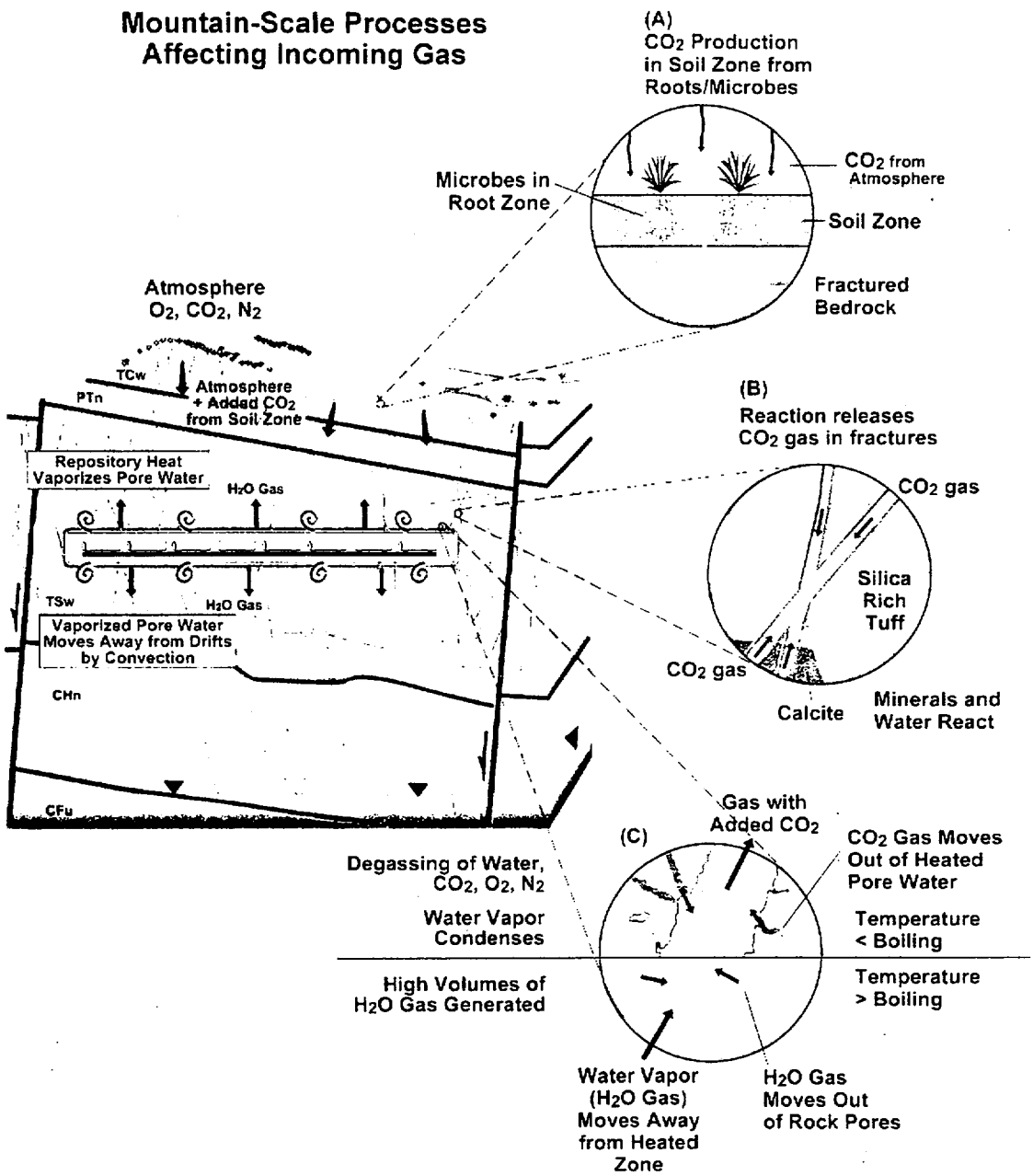

Figure 4-7. Mountain-scale conceptual picture of Incoming-Gas model processes.

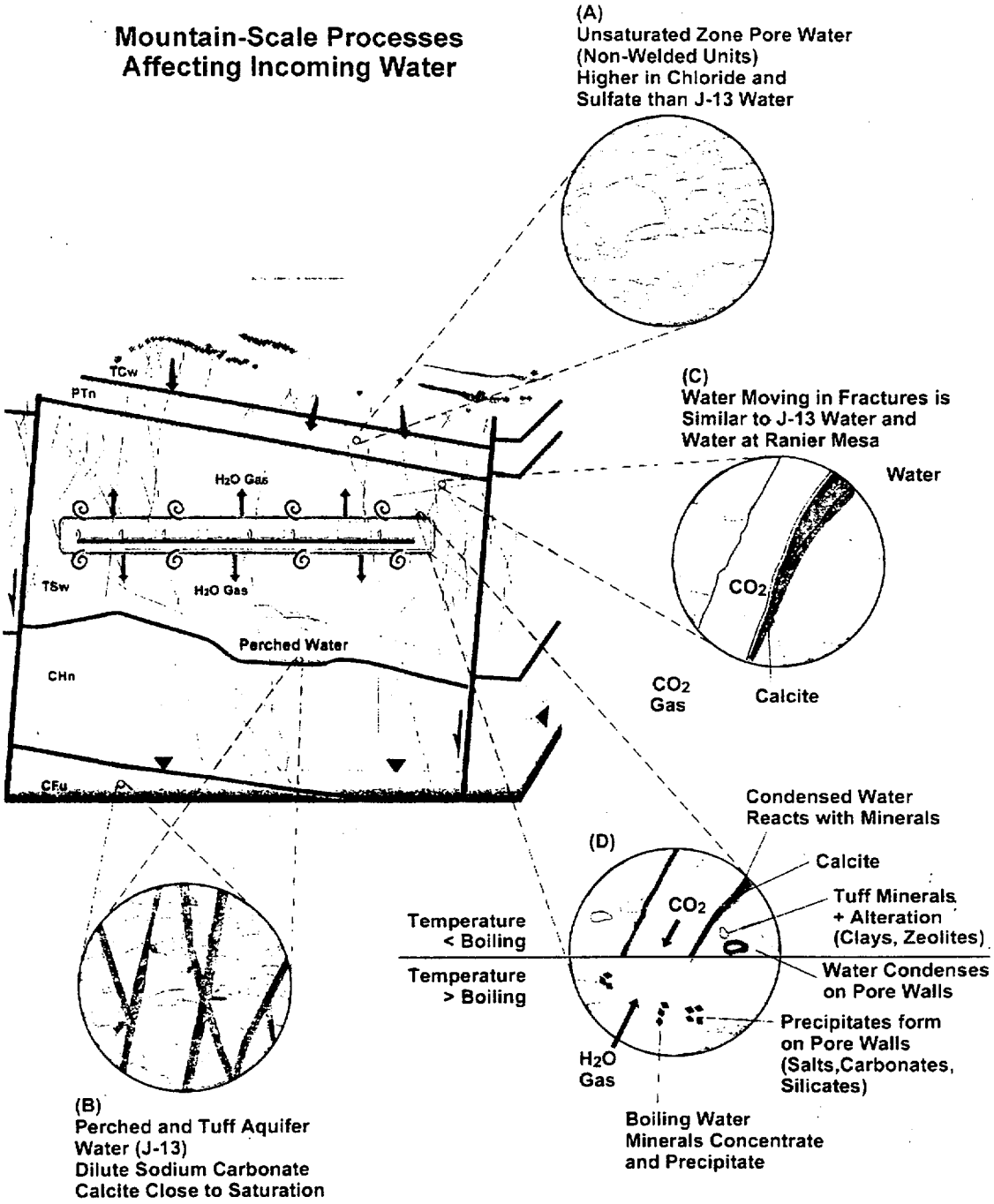

Figure 4-8. Mountain-scale conceptual picture of Incoming-Water model processes.

Time Frame 1 First Few 100s of Years

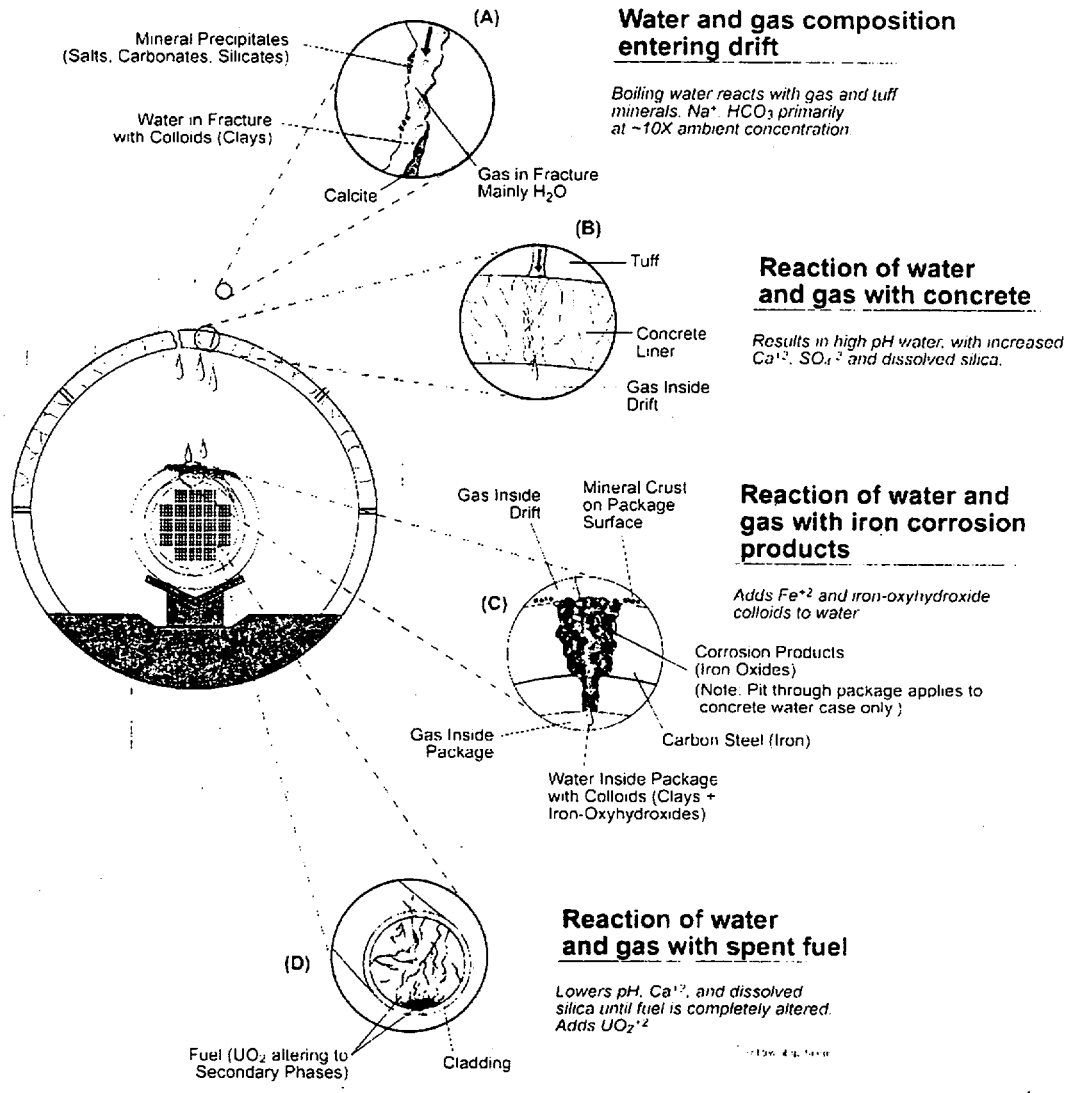

Figure 4-9. Drift-scale NFGE conceptual processes Time Frame 1 (first few 100 years).

Time Frame 2 ~500 Years to 10,000 Years

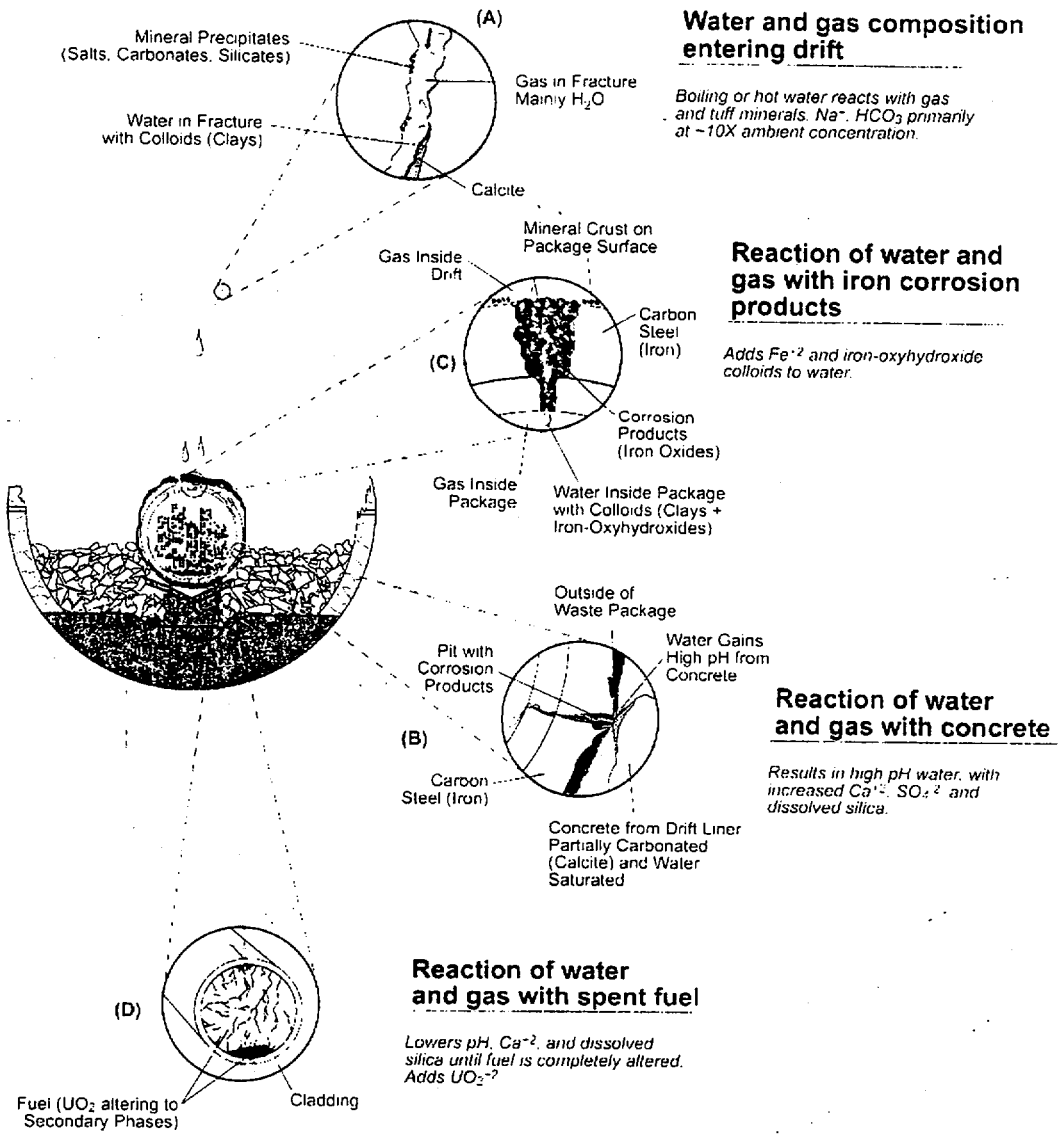

Figure 4-10. Drift-scale NFGE conceptual processes Time-Frame 2 (about 500 to 10,000 years).

Time Frame 3 ~10,000 Years to 100,000 Years

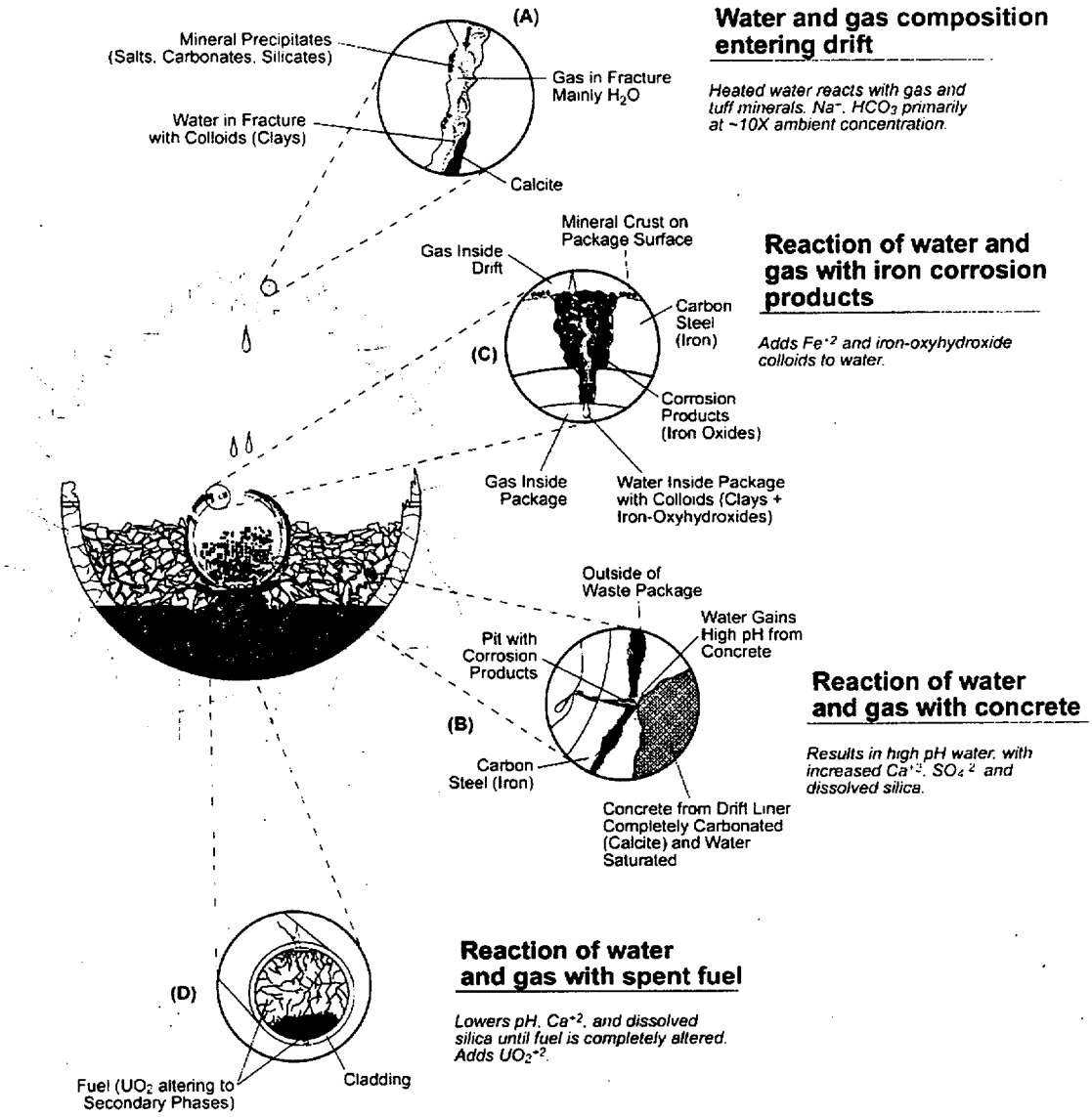

Figure 4-11. Drift-scale NFGE conceptual processes Time-Frame 3 (about 10,000 to 100,000 years).

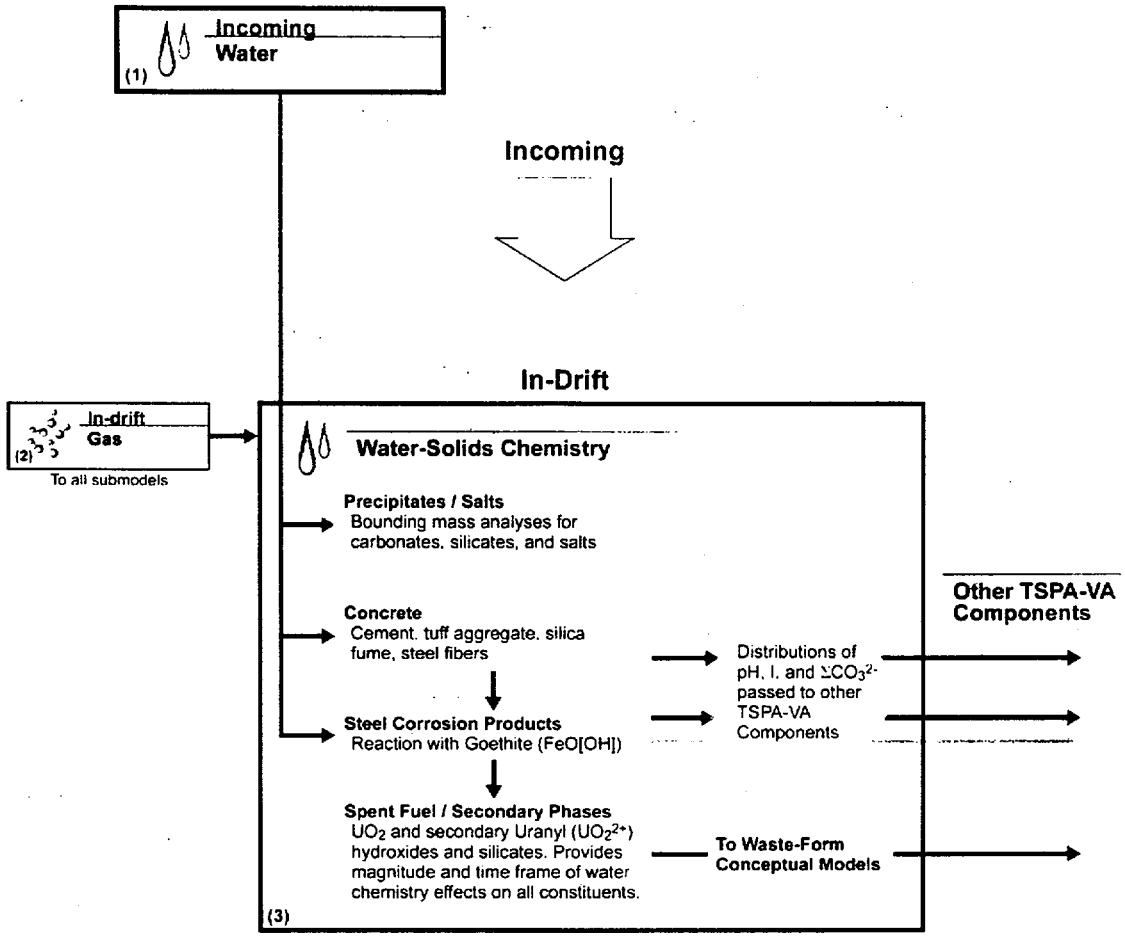

Figure 4-12. Connections among the water-solids chemistry submodels.

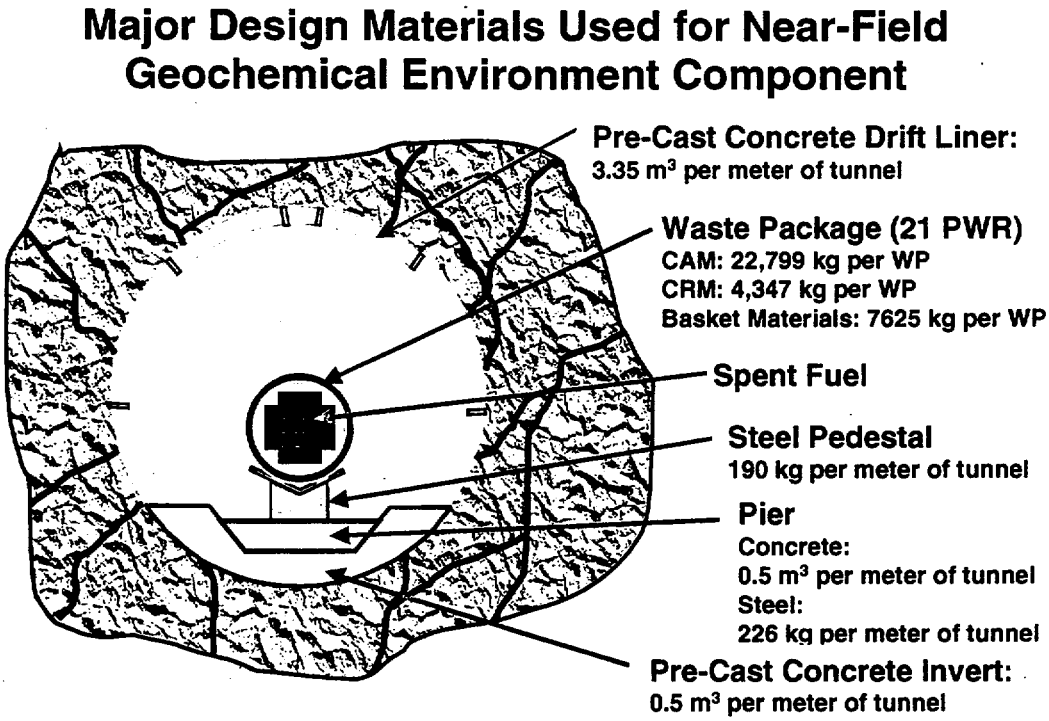

Figure 4-13. Major design materials used for NFGE component.

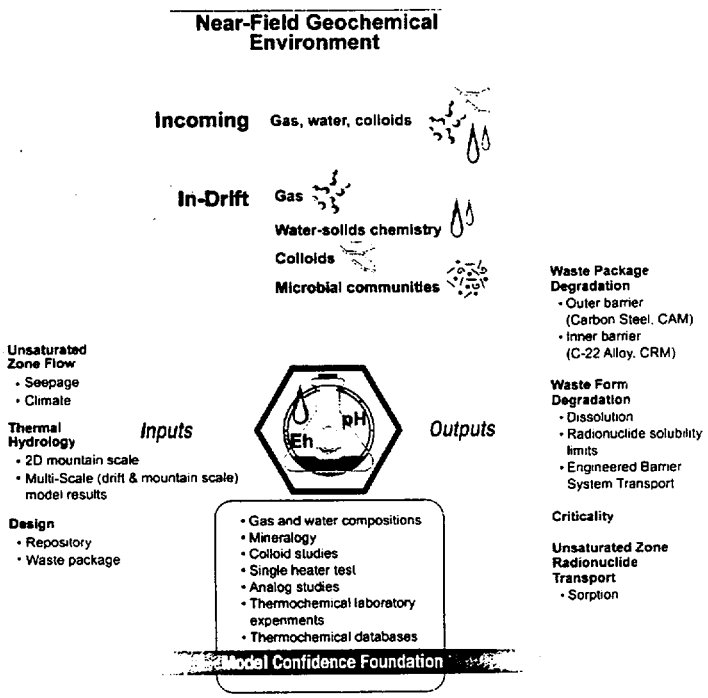

Figure 4-14. Inputs, outputs, and bases for the TSPA-VA NFGE component.

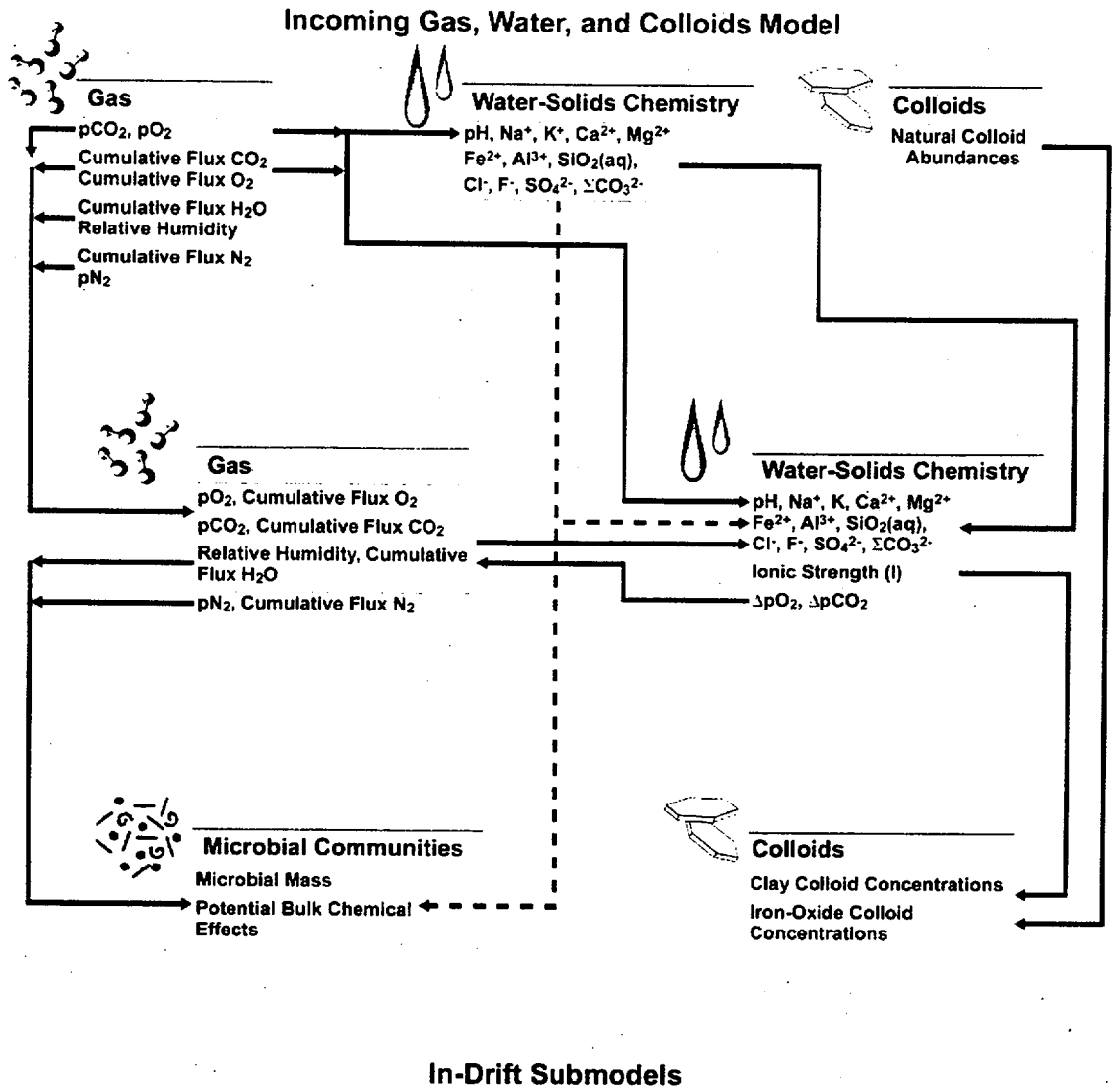

Figure 4-15. Box plot of all NFGE models and their specific parameter handoffs between each of them.

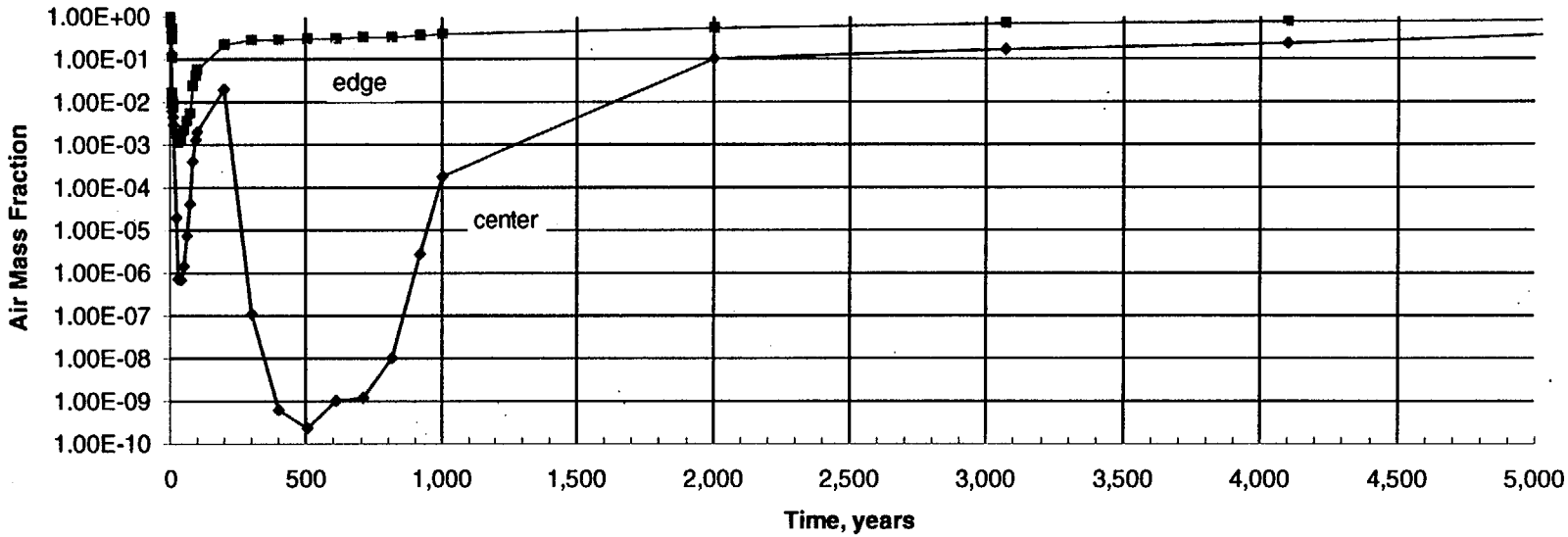

Figure 4-16. The 2-D mountain-scale results for air mass fraction to 5,000 years at both center and edge locations for the 233,400 cross section through the center of the potential repository. The infiltration and climate history are those for the base-case TSPA-VA analyses (I-dry to 5,000 years, I-LTA from 5,000 to 95,000, I-dry 95,000 to 100,000—see Chapter 3 for a detailed discussion).

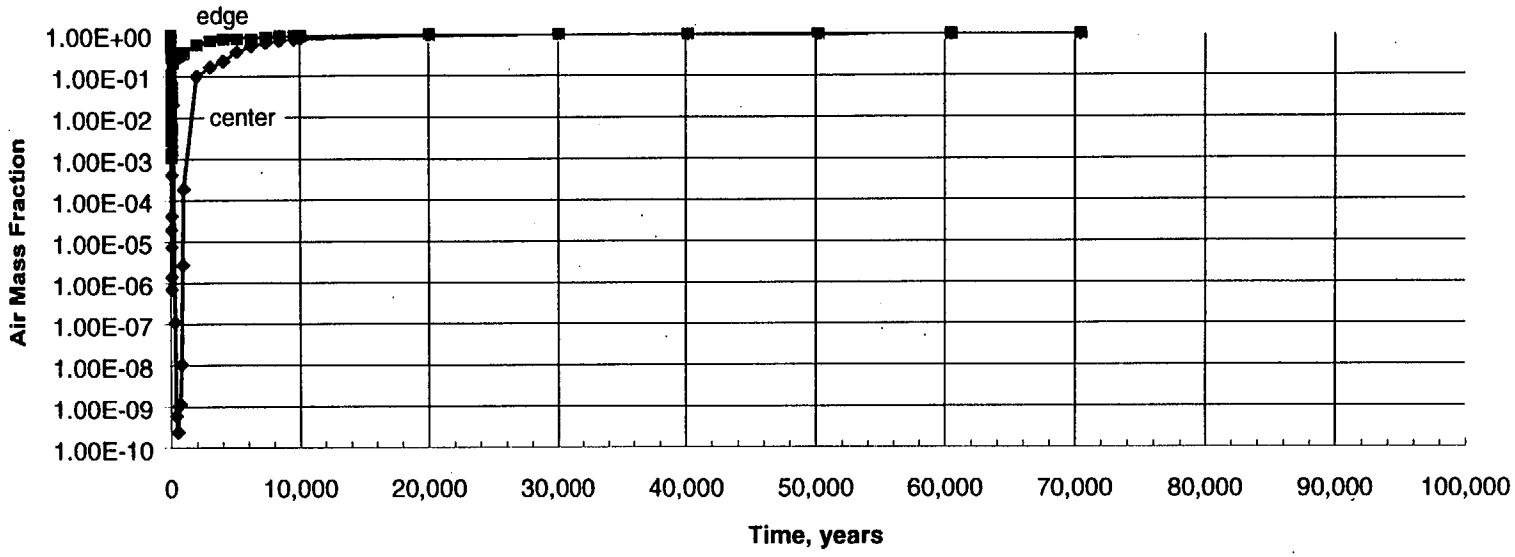

Figure 4-17. The 2-D mountain-scale results for air mass fraction to 100,000 years at both center and edge locations for the 233,400 cross section through the center of the potential repository. The infiltration and climate history are those for the base-case TSPA-VA analyses (I-dry to 5,000 years, I-LTA from 5,000 to 95,000, I-dry 95,000 to 100,000—see Chapter 3 for a detailed discussion).

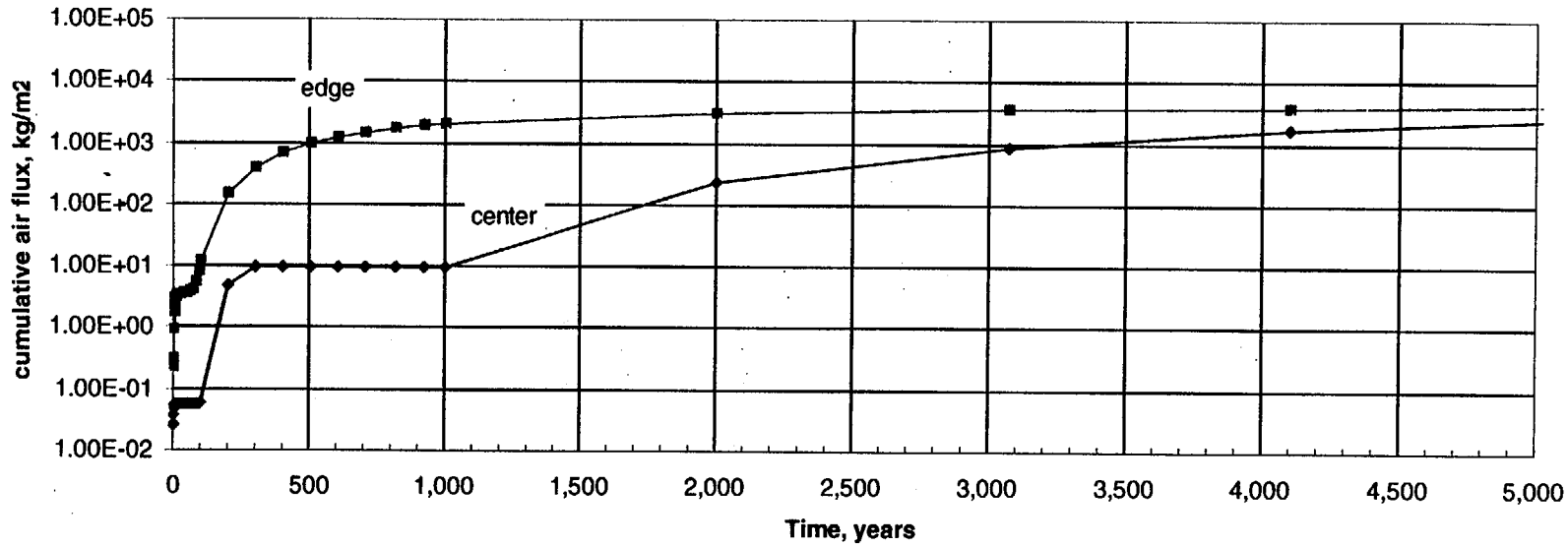

Figure 4-18. The 2-D mountain-scale results for cumulative air flux to 5,000 years at both center and edge locations for the 233,400 cross section through the center of the potential repository. The infiltration and climate history are those for the base-case TSPA-VA analyses (I-dry to 5,000 years, I-LTA from 5,000 to 95,000, I-dry 95,000 to 100,000—see Chapter 3 for a detailed discussion).

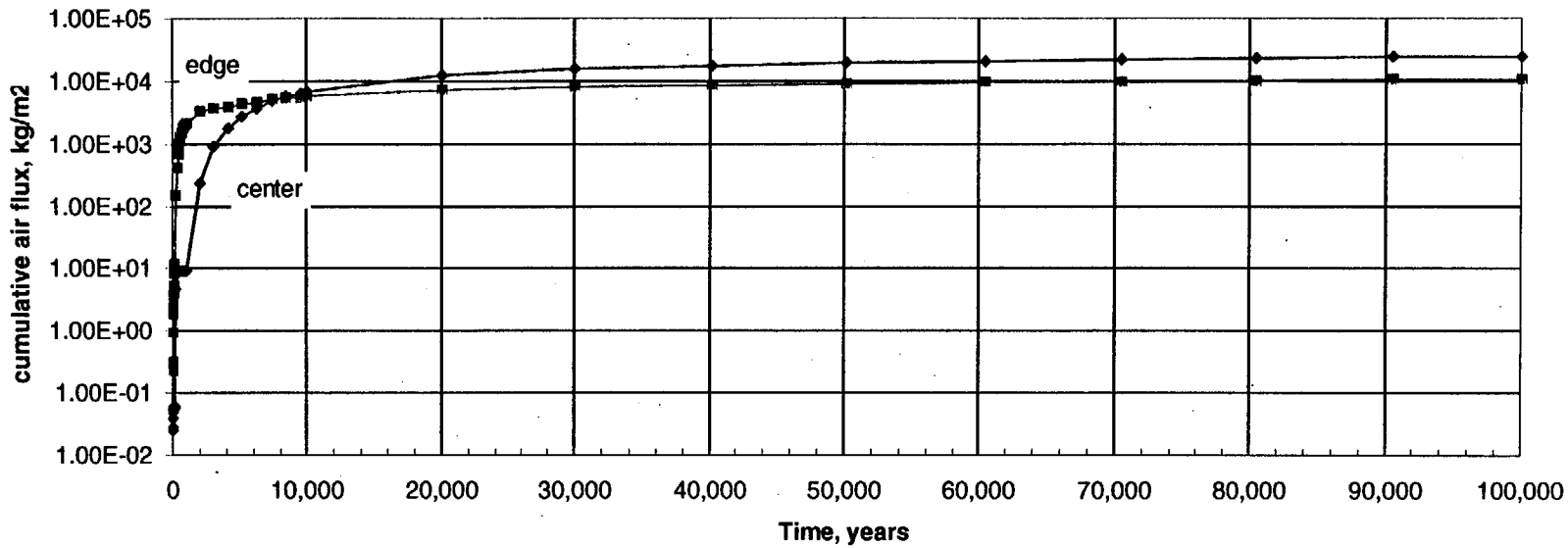

Figure 4-19. The 2-D mountain-scale results for cumulative air flux to 100,000 years at both center and edge locations for the 233,400 cross section through the center of the potential repository. The infiltration and climate history are those for the base-case TSPA-VA analyses (I-dry to 5,000 years, I-LTA from 5,000 to 95,000, I-dry 95,000 to 100,000—see Chapter 3 for a detailed discussion).

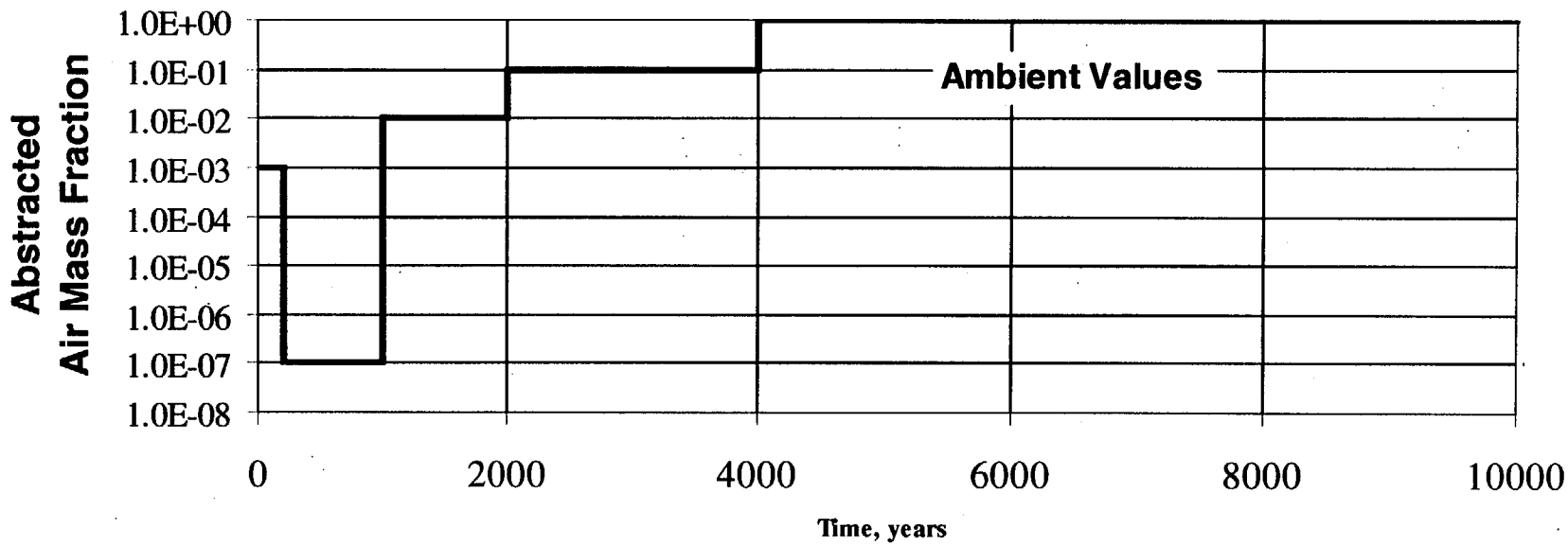

Figure 4-20. The abstracted values of air mass fraction to 10,000 years. Values return to ambient at 4,000 years and are based on the 2-D mountain-scale results for air mass fraction at the center location for the 233,400 cross section through the center of the potential repository. The infiltration and climate history are those for the base-case TSPA-VA analyses (I-dry to 5,000 years, I-LTA from 5,000 to 95,000, I-dry 95,000 to 100,000—see Chapter 3 for a detailed discussion).

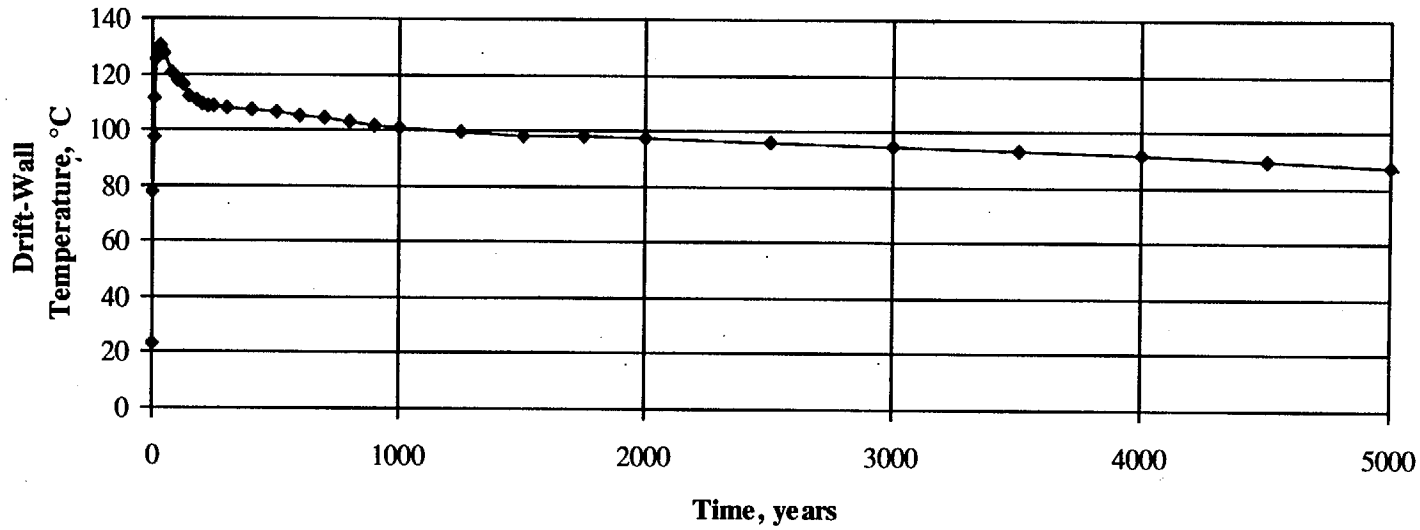

Figure 4-21. The temperatures at the drift wall to 5,000 years based on the drift-scale results of the multi-scale thermal-hydrologic models for the representative spent nuclear fuel waste package in the Region CC (repository center). These results represent the infiltration and climate history for the base-case TSPA-VA analyses (I-dry to 5,000 years, I-LTA from 5,000 to 100,000—see Chapters 2 and 3 for detailed discussion) by using the I-dry results to 5,000 years and then switching to those for the long-term average climate.

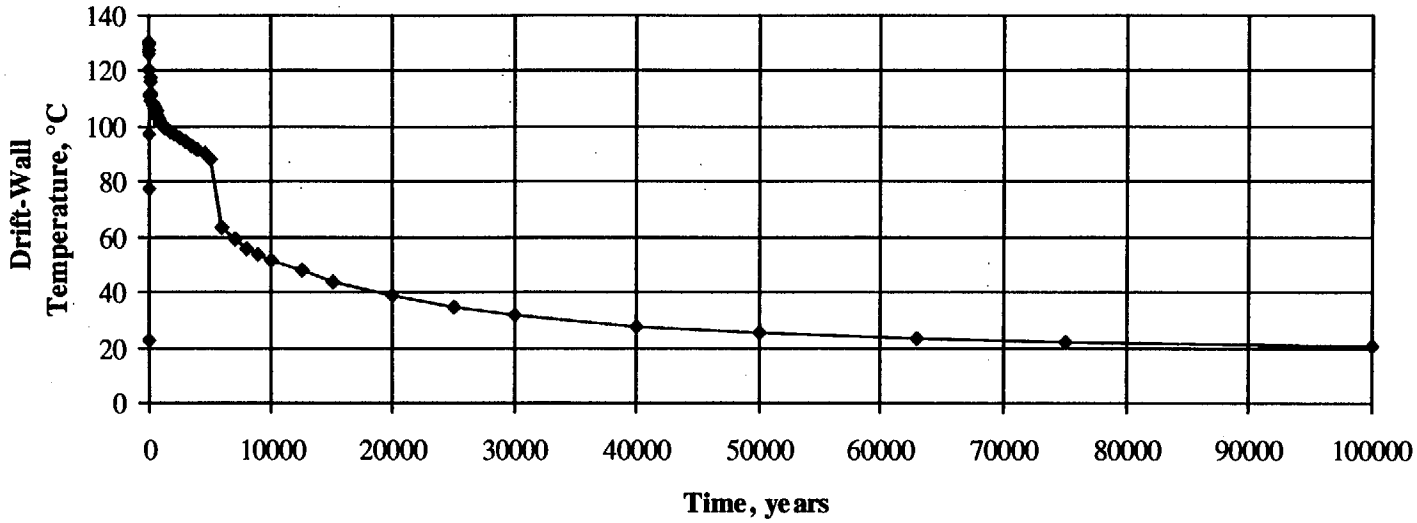

Figure 4-22. The temperatures at the drift wall to 100,000 years based on the drift-scale results of the multi-scale thermal-hydrologic models for the representative spent nuclear fuel waste package in the Region CC (repository center). These results represent the infiltration and climate history for the base-case TSPA-VA analyses (I-dry to 5,000 years, I-LTA from 5,000 to 100,000—see Chapters 2 and 3 for detailed discussion) by using the I-dry results to 5,000 years and then switching to those for the long-term average climate.

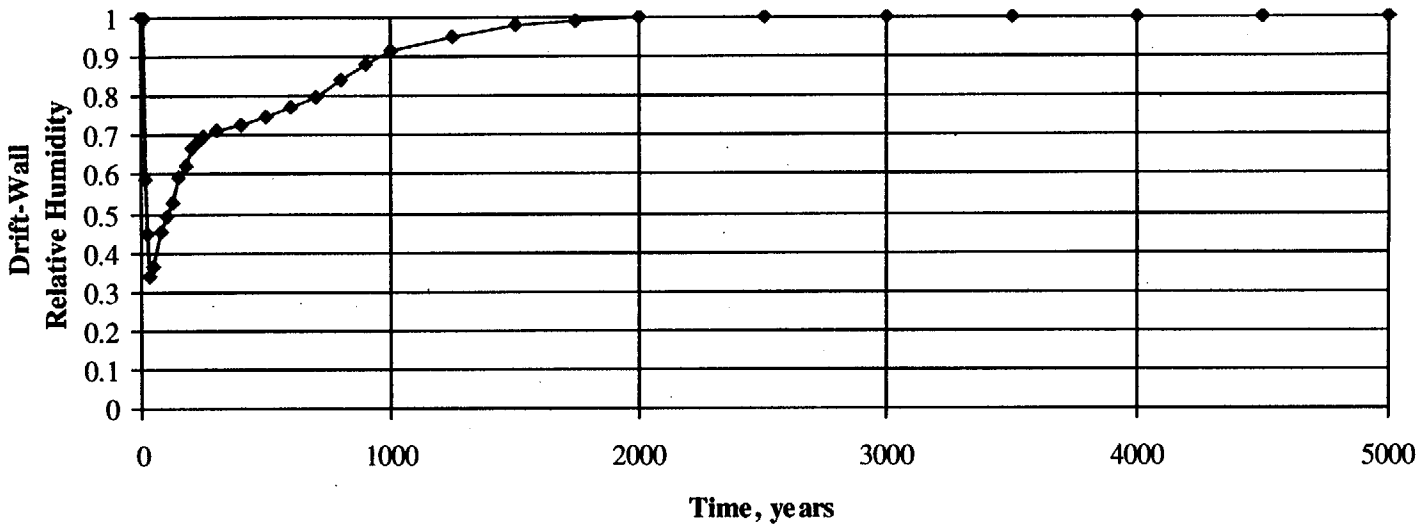

Figure 4-23. The relative humidity at the drift wall to 5,000 years based on the drift-scale results of the multi-scale thermal-hydrologic models for the representative spent nuclear fuel waste package in the Region CC (repository center). These results represent the infiltration and climate history for the base-case TSPA-VA analyses (I-dry to 5,000 years, I-LTA from 5,000 to 100,000—see Chapters 2 and 3 for detailed discussion) by using the I-dry results to 5,000 years and then switching to those for the long-term average climate.

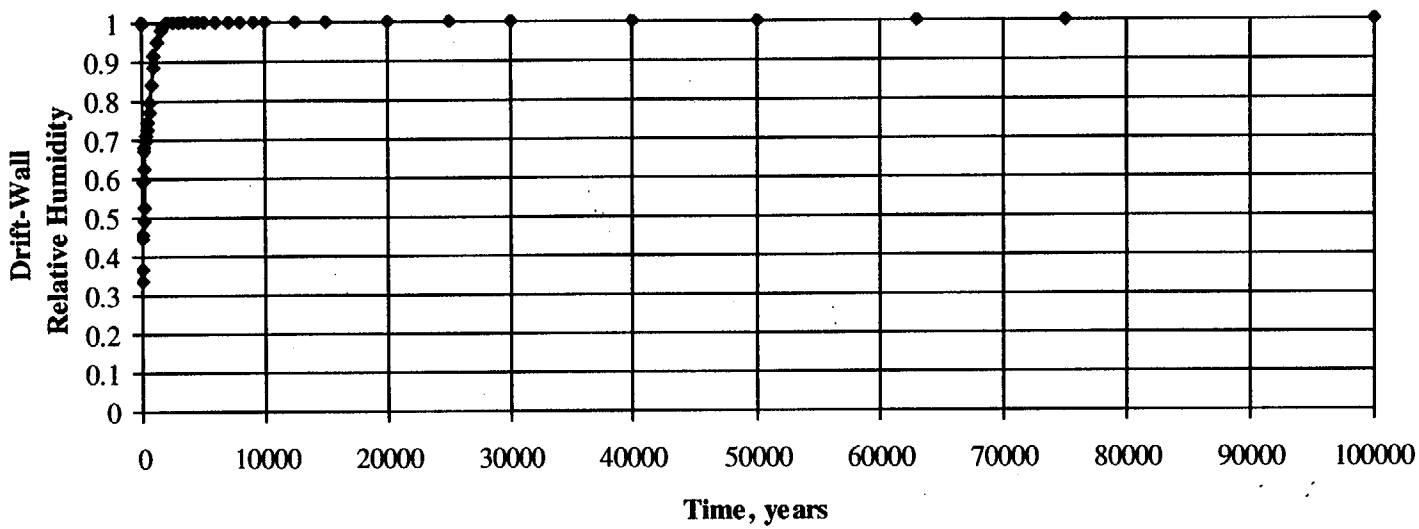

Figure 4-24. The relative humidity at the drift wall to 100,000 years based on the drift-scale results of the multi-scale thermal-hydrologic models for the representative spent nuclear fuel waste package in the Region CC (repository center). These results represent the infiltration and climate history for the base-case TSPA-VA analyses (I-dry to 5,000 years, I-LTA from 5,000 to 100,000—see Chapters 2 and 3 for detailed discussion) by using the I-dry results to 5,000 years and then switching to those for the long-term average climate.

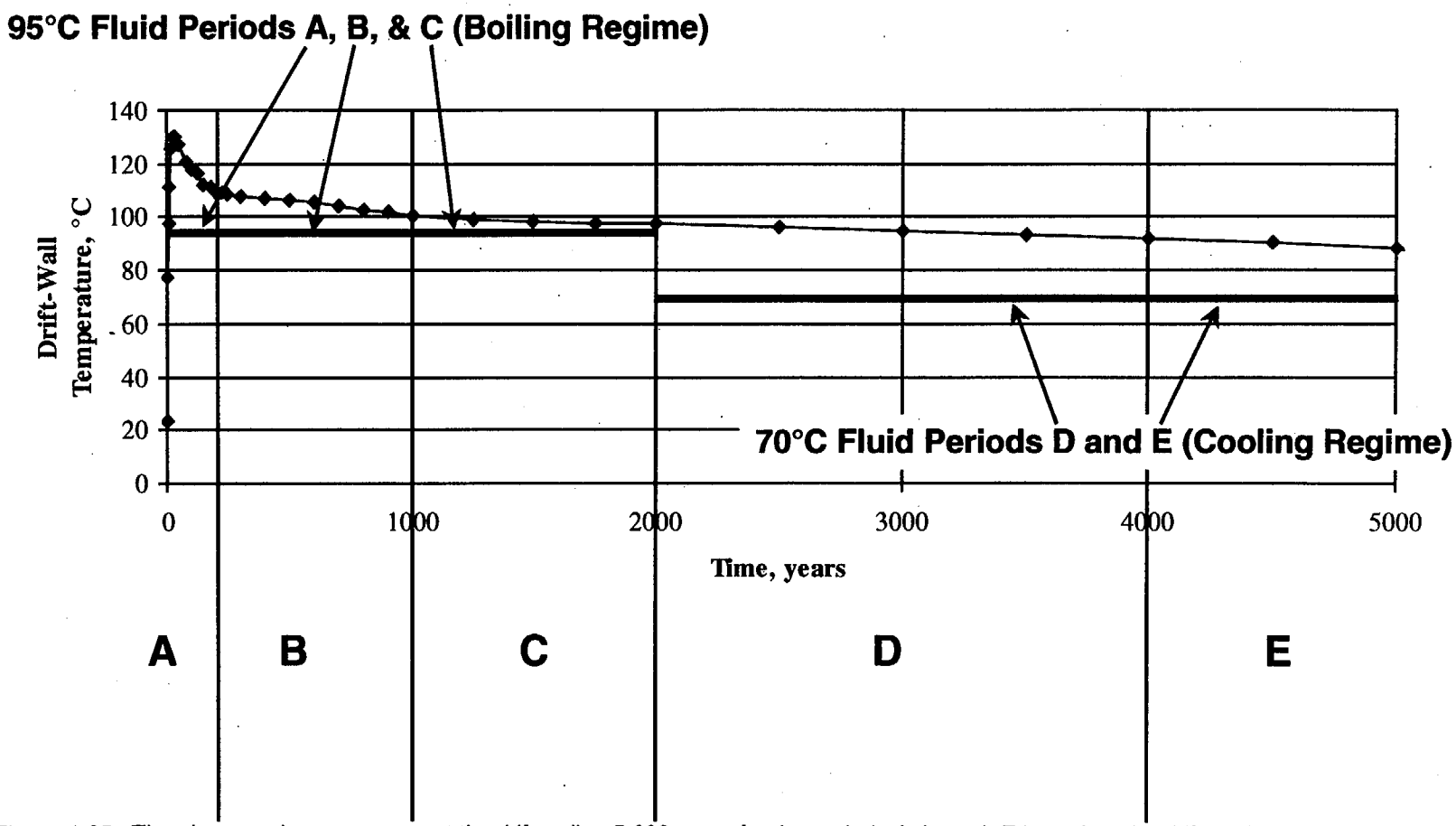

Figure 4-25. The abstracted temperatures at the drift wall to 5,000 years for the periods A through E based on the drift-scale results of the multi-scale thermal-hydrologic models for the representative spent nuclear fuel waste package in the Region CC (repository center). These results represent the infiltration and climate history for the base-case TSPA-VA analyses (I-dry to 5,000 years, I-LTA from 5,000 to 100,000—see Chapters 2 and 3 for detailed discussion) by using the I-dry results to 5,000 years and then switching to those for the long-term average climate.

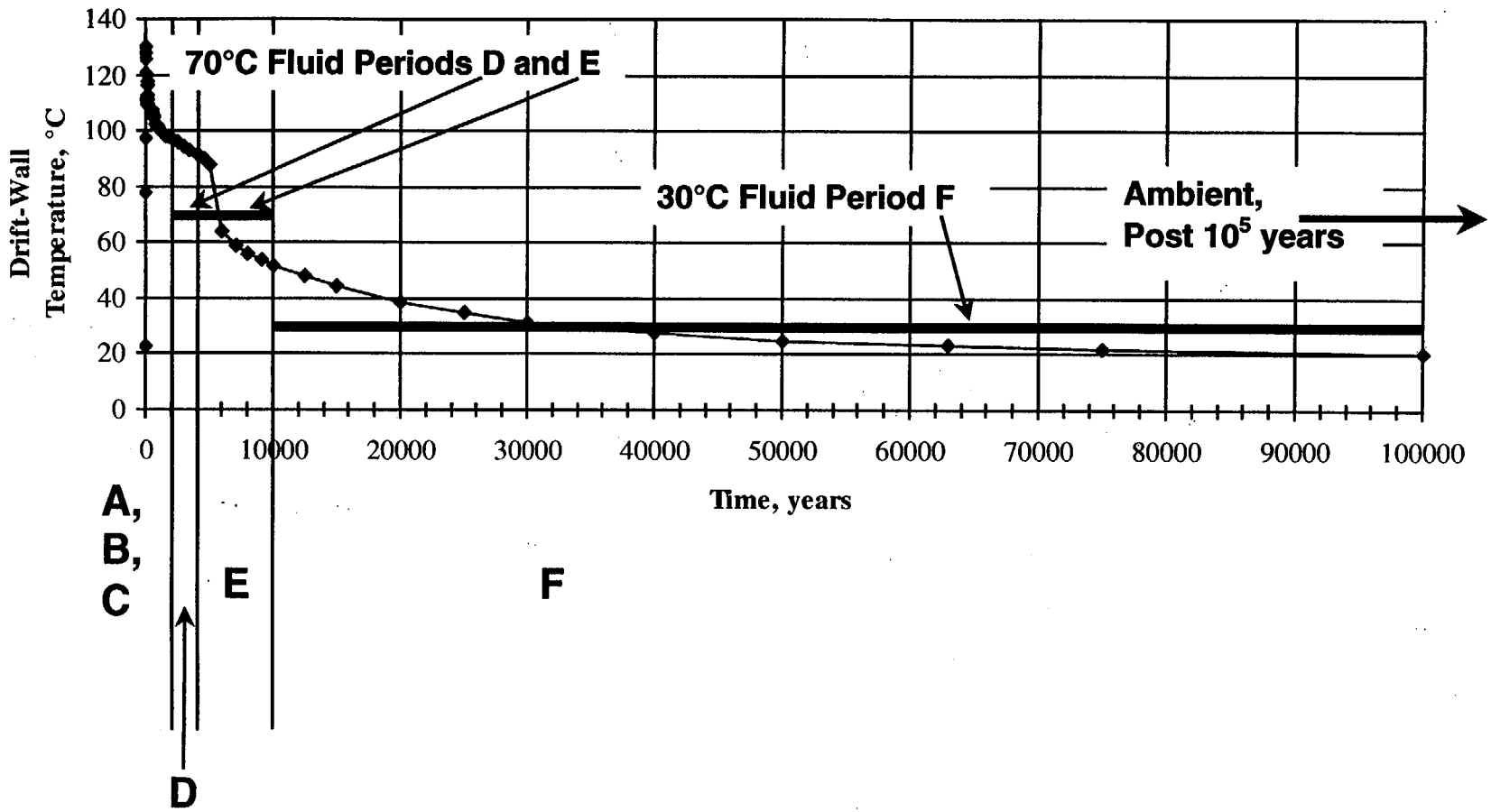

Figure 4-26. The abstracted temperatures at the drift wall to 100,000 years for the periods A through F based on the drift-scale results of the multi-scale thermal-hydrologic models for the representative spent nuclear fuel waste package in the Region CC (repository center). These results represent the infiltration and climate history for the base-case TSPA-VA analyses (I-dry to 5,000 years, I-LTA from 5,000 to 100,000—see Chapters 2 and 3 for detailed discussion) by using the I-dry results to 5,000 years and then switching to those for the long-term average climate.

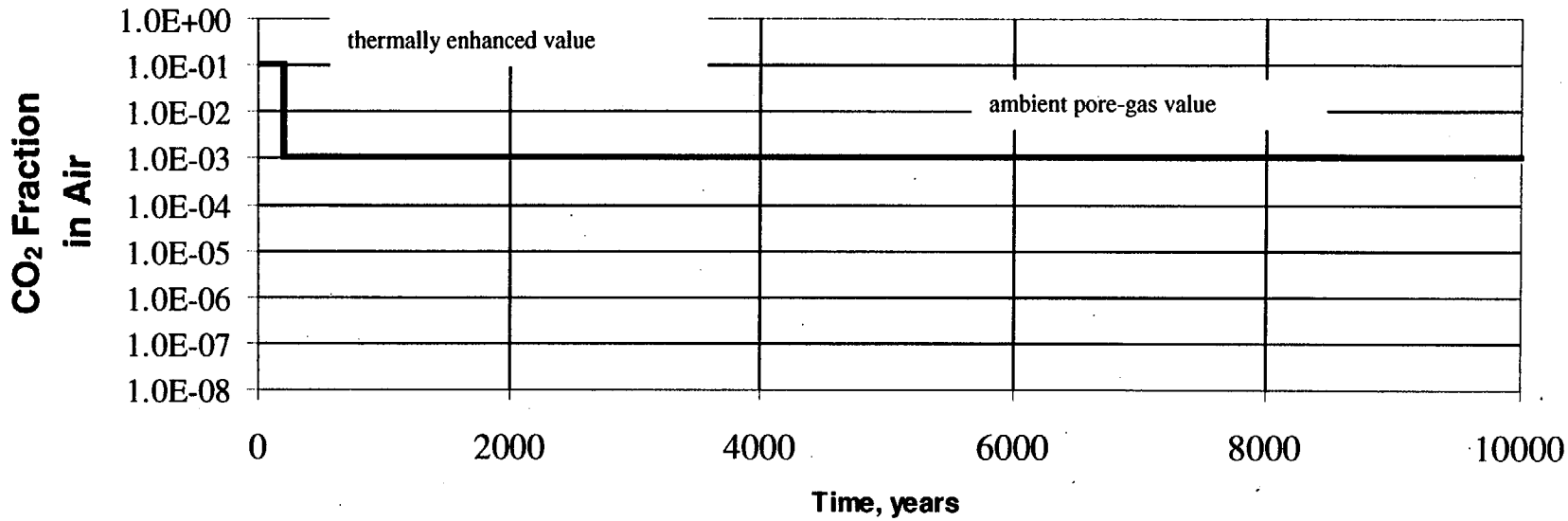

Figure 4-27. The abstracted values of the CO_2 fraction in air to 10,000 years. The composition is composed of two parts—a short transient period that has enhanced CO_2 and followed by a return to the ambient pore-gas values for the site. These values, when combined with the abstracted air-mass fraction values, provide the gas composition through time for CO_2. See text for discussion and for the values of nitrogen and oxygen in air that were taken from the atmospheric values.

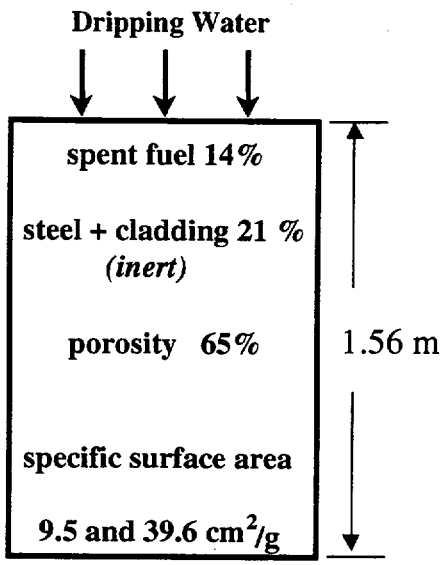

Figure 4-28. Schematic of simulation configurations.

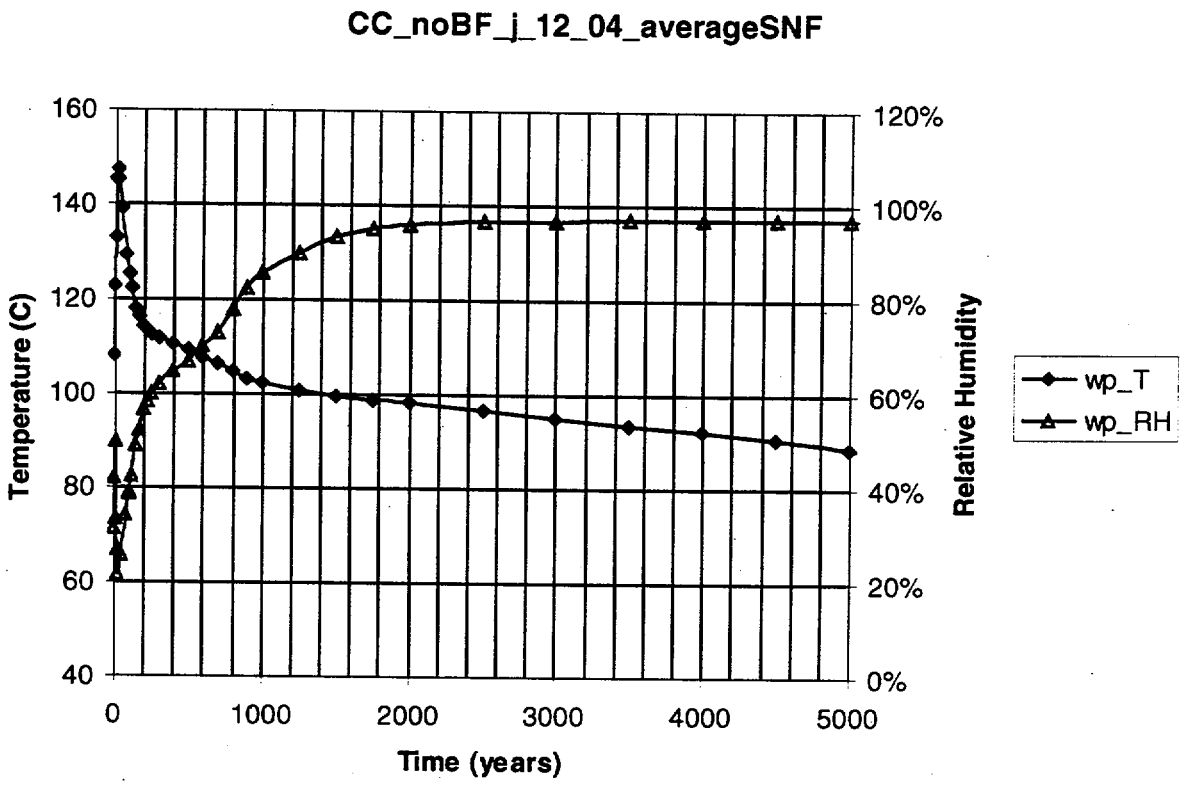

Figure 4-29. Thermal-hydrology results from Chapter 3 for the CC_noBF_j_12_04_averageSNF.

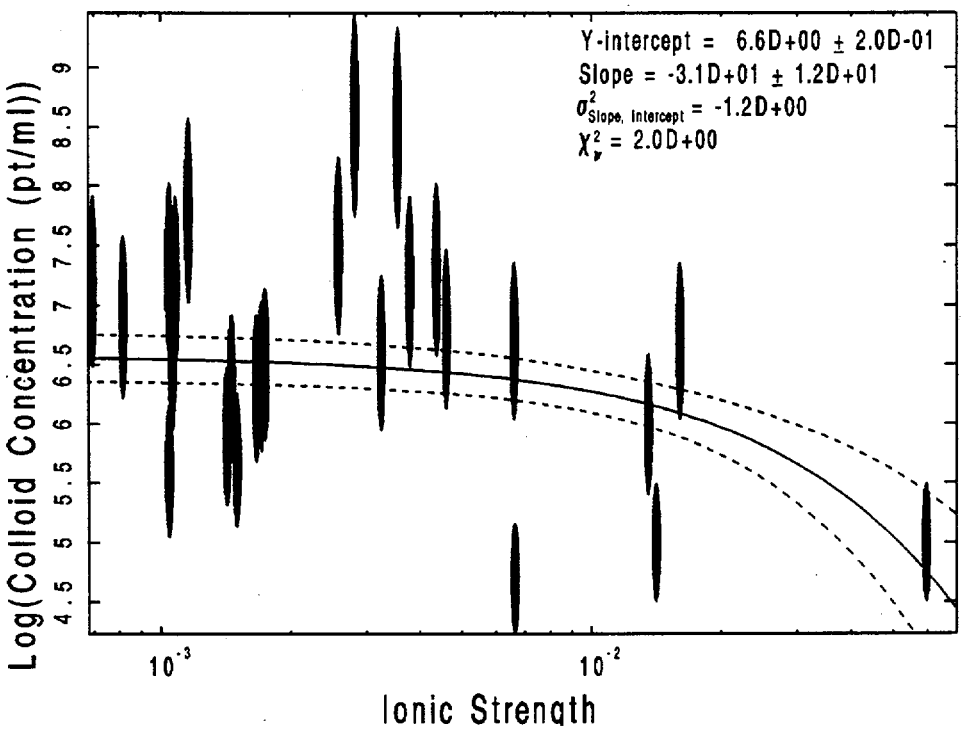

Figure 4-30. A linear fit to all of the available data.

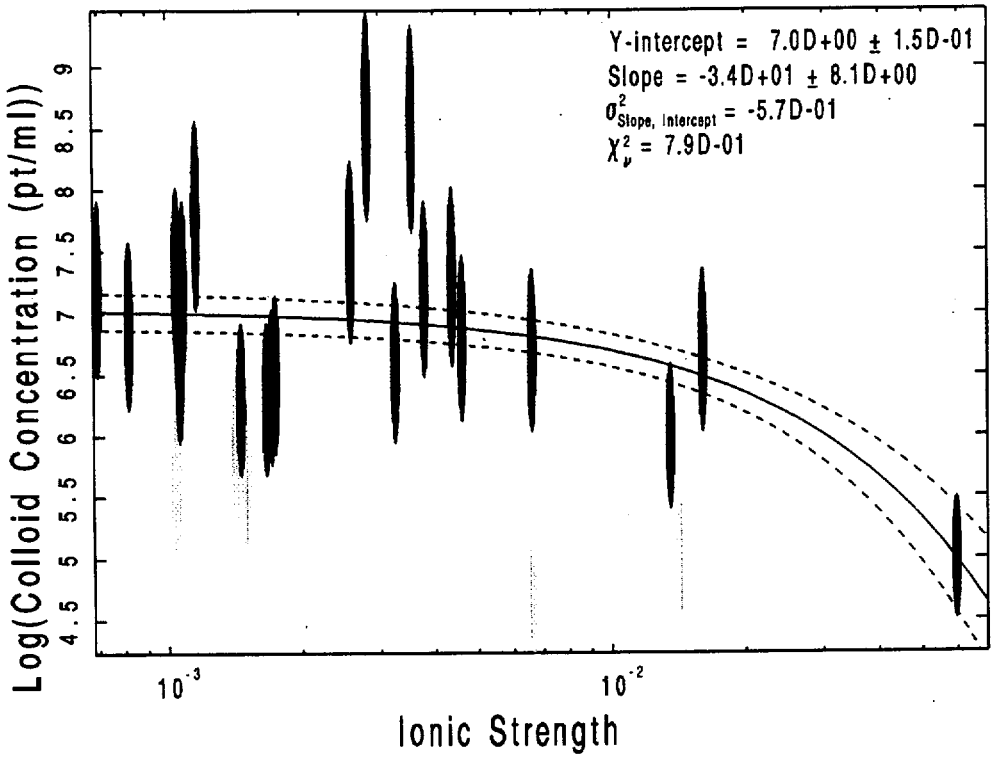

Figure 4-31. Presents a similar fit to the data except that 5 of the data that show lower than expected colloid concentrations have been omitted from the fit compared to that shown in Figure 4-30.

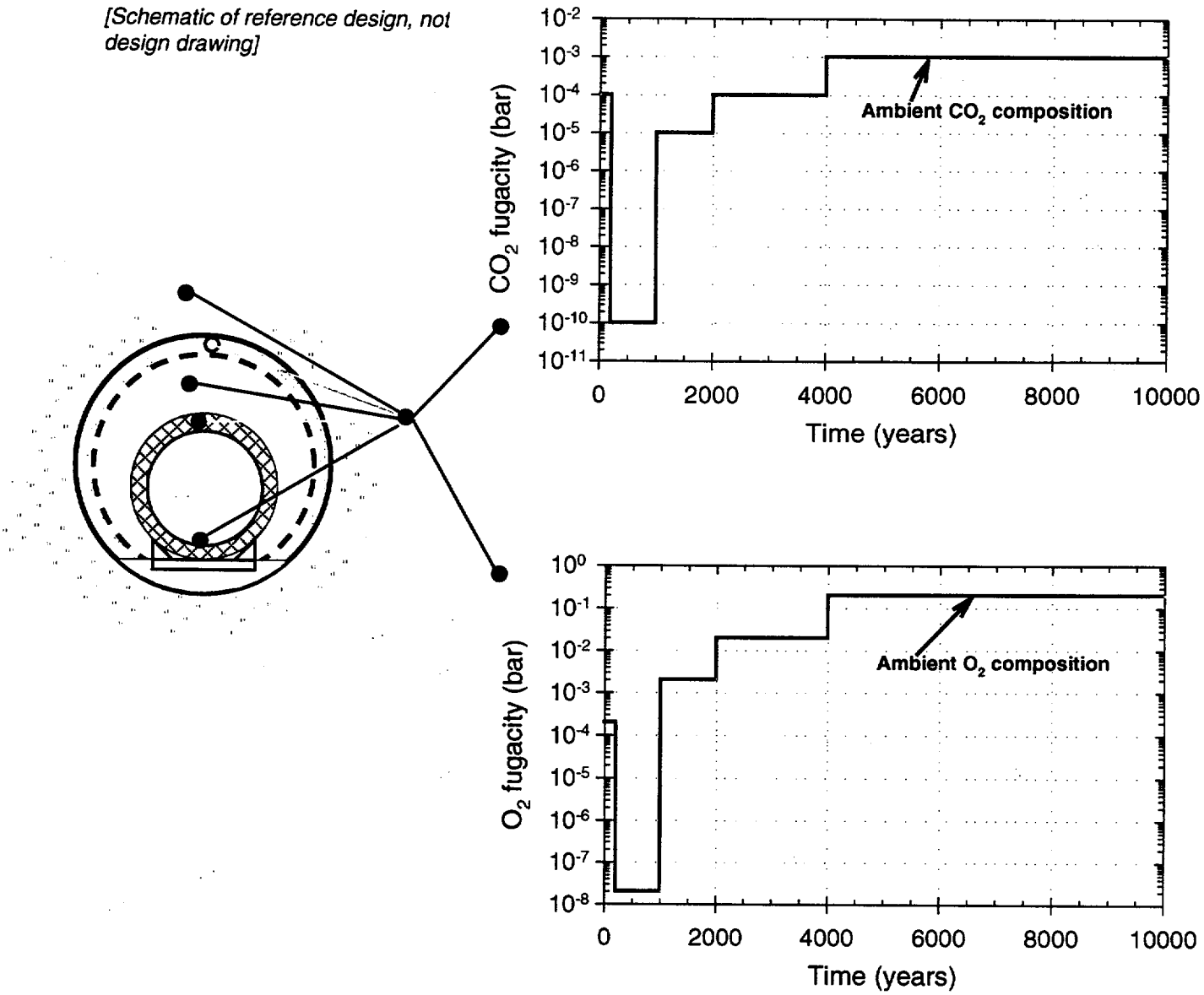

Figure 4-32. Near-field geochemical environment (NFGE) gas composition results for carbon dioxide and oxygen from time of waste emplacement to 10,000 years later. As indicated by reference to the schematic of a drift cross section and waste package, these gas compositions apply to the entire region within and near the drift, including inside of the waste package.

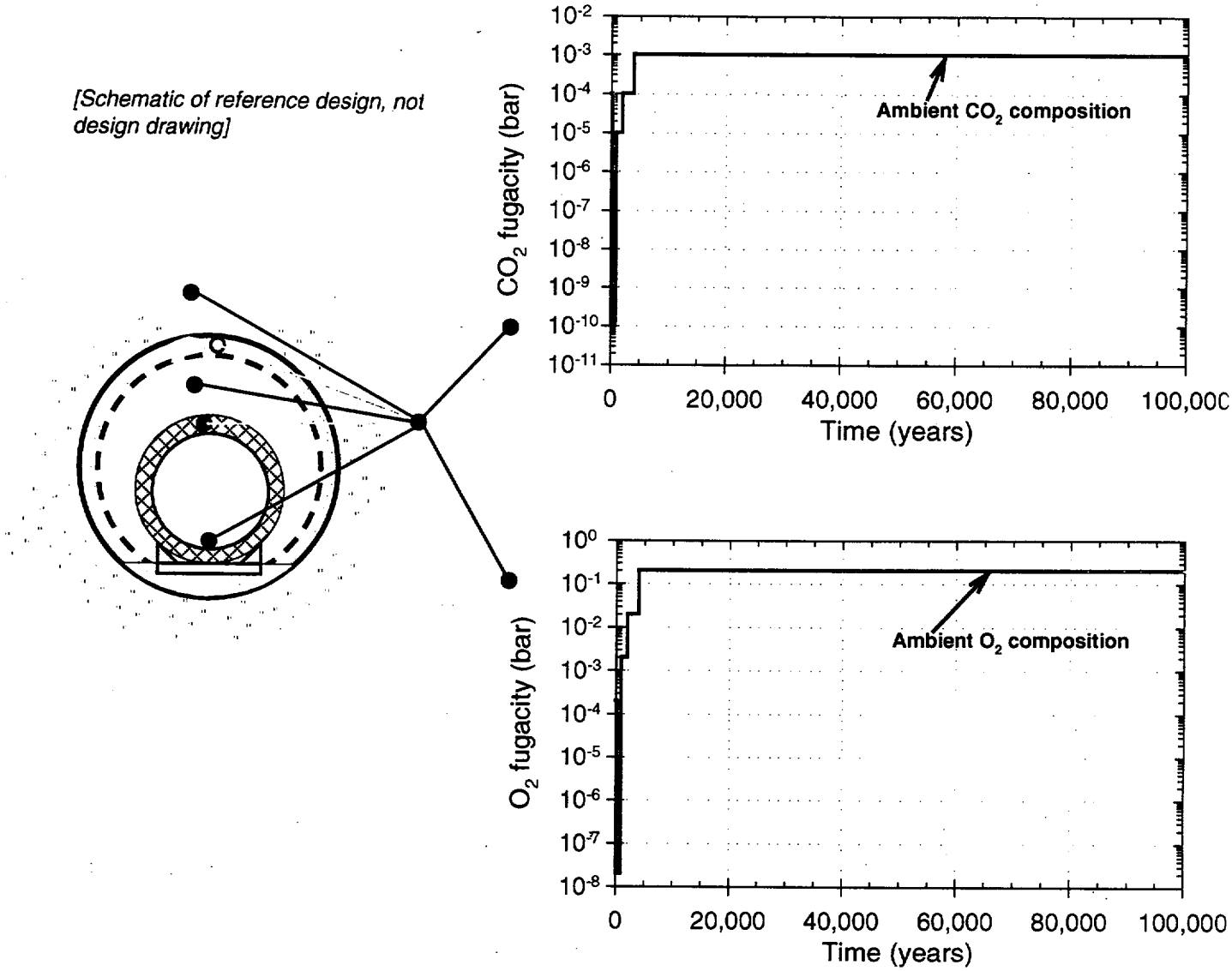

Figure 4-33. Near-field geochemical environment (NFGE) gas composition results for carbon dioxide and oxygen from time of waste emplacement to 100,000 years later. As indicated by the reference to the schematic of a drift cross section and waste package, these gas compositions apply to the entire region within and near the drift, including inside of the waste package.

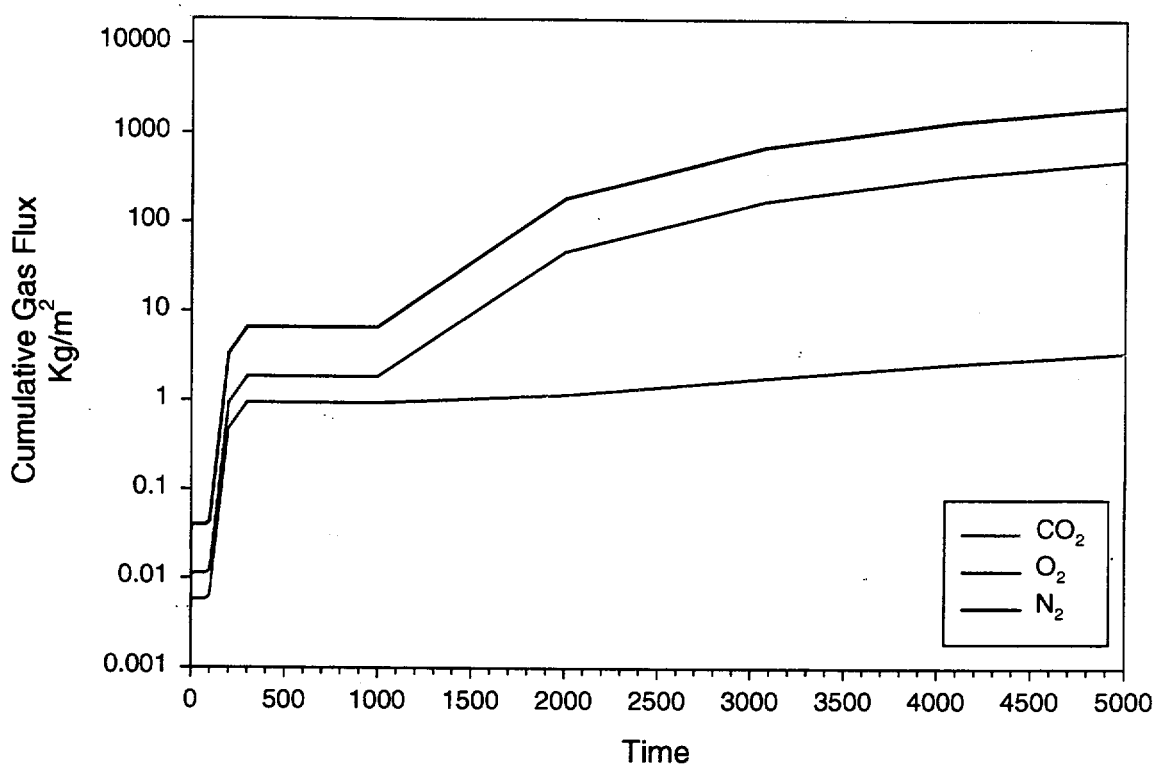

Figure 4-34. The cumulative fluxes of CO_2, O_2, and N_2 into the drift to 5,000 years based on the air composition and the 2-D mountain-scale results for cumulative air flux to 100,000 years at the center location for the 233,400 cross section through the center of the potential repository. The infiltration and climate history are those for the base-case TSPA-VA analyses (I-dry to 5,000 years, I-LTA from 5,000 to 95,000, I-dry 95,000 to 100,000—see Chapter 3 for a detailed discussion).

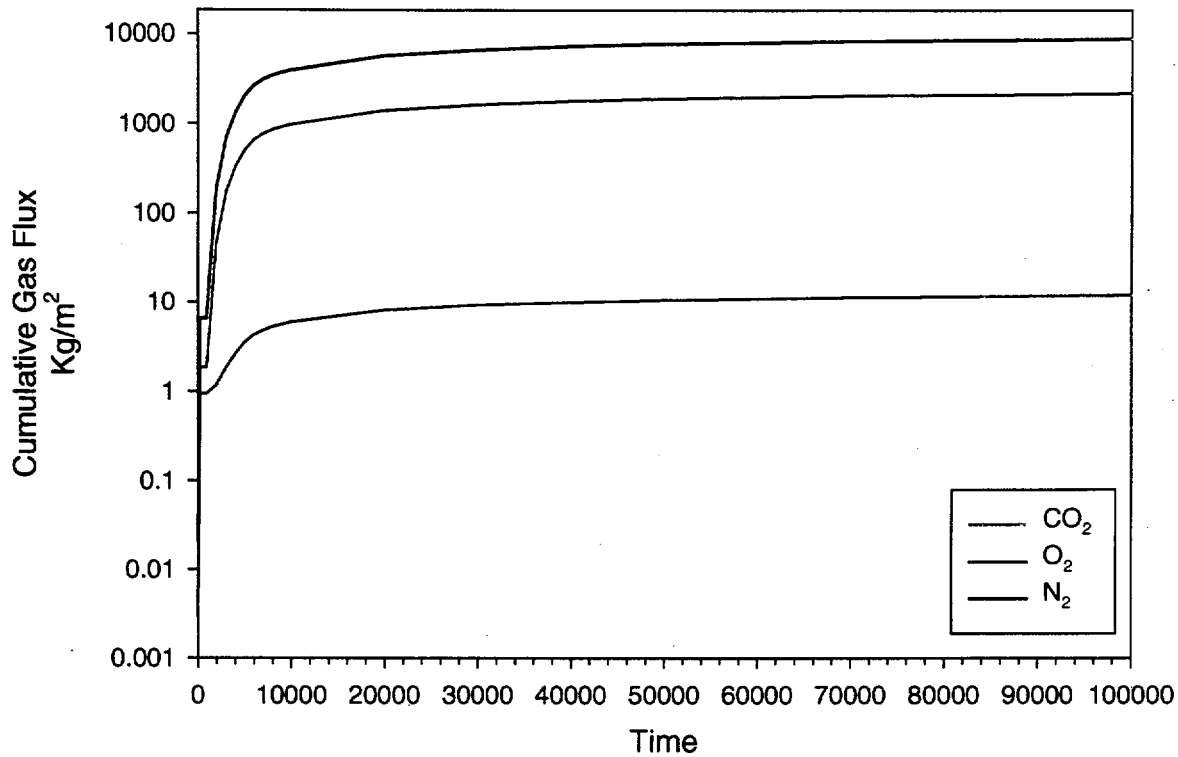

Figure 4-35. The cumulative fluxes of CO_2, O_2, and N_2 into the drift to 100,000 years based on the air composition and the 2-D mountain-scale results for cumulative air flux to 100,000 years at the center location for the 233,400 cross section through the center of the potential repository. The infiltration and climate history are those for the base-case TSPA-VA analyses (I-dry to 5,000 years, I-LTA from 5,000 to 95,000, I-dry 95,000 to 100,000—see Chapter 3 for a detailed discussion).

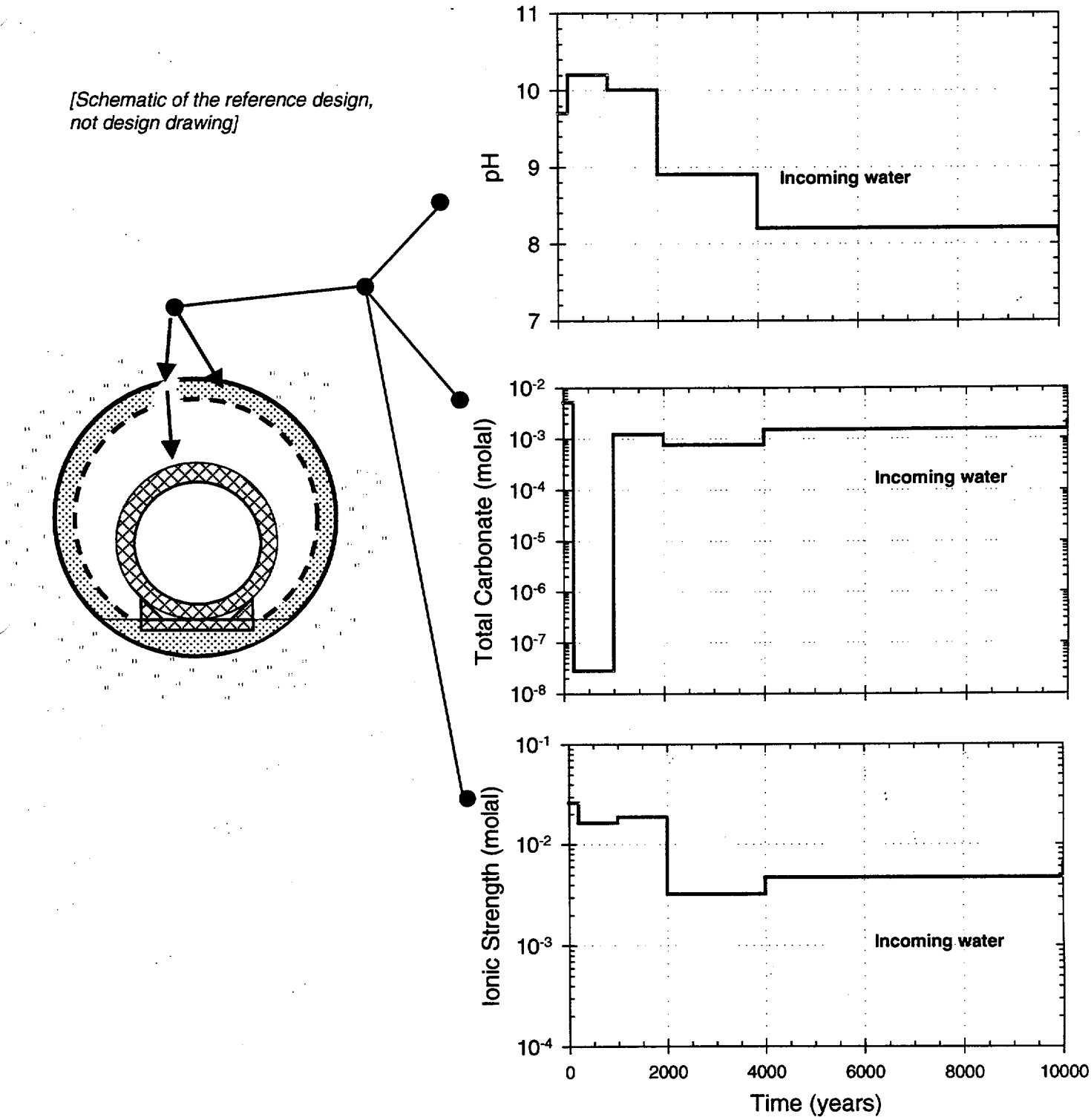

Figure 4-36. The resultant fluid compositions for incoming water to 10,000 years shown in terms of the pH, total dissolved carbonate (ΣCO_3^{2-}), and the ionic strength.

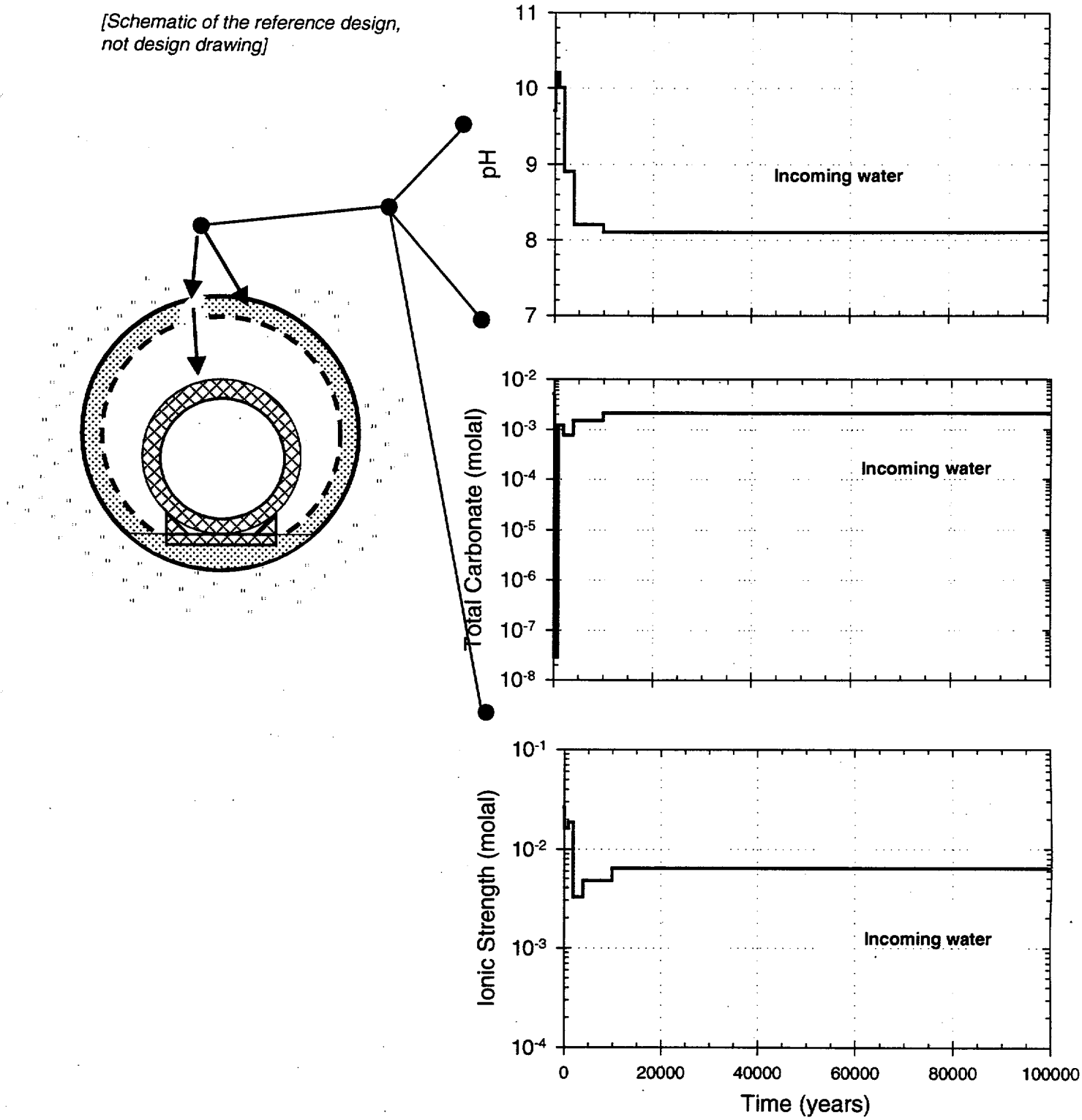

Figure 4-37. The resultant fluid compositions for incoming water to 100,000 years shown in terms of the pH, total dissolved carbonate (ΣCO_3^{2-}), and the ionic strength.

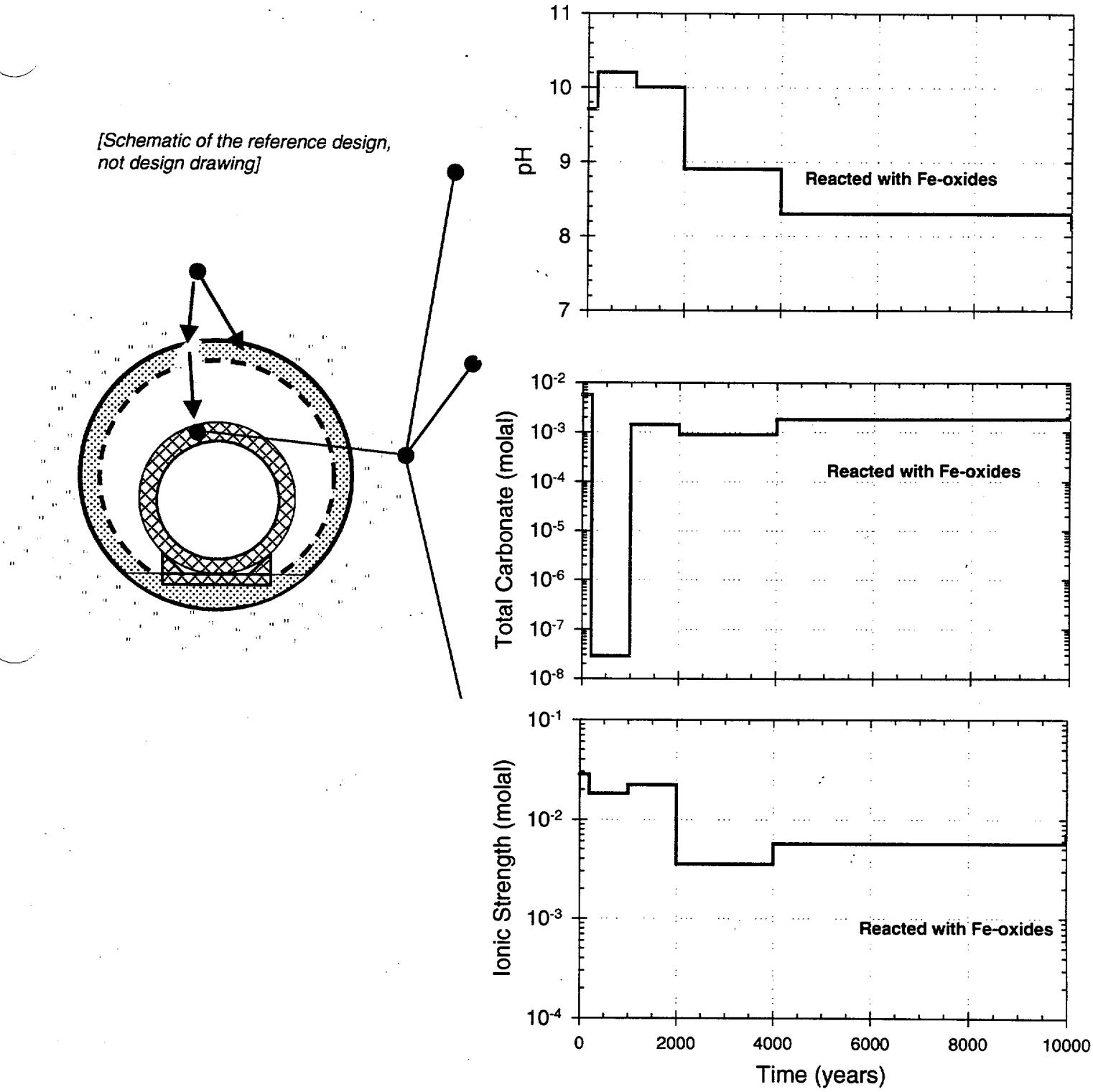

Figure 4-38. The resultant fluid compositions for water reacted with corrosion products to 10,000 years shown in terms of the pH, total dissolved carbonate (ΣCO_3^{2-}), and the ionic strength.

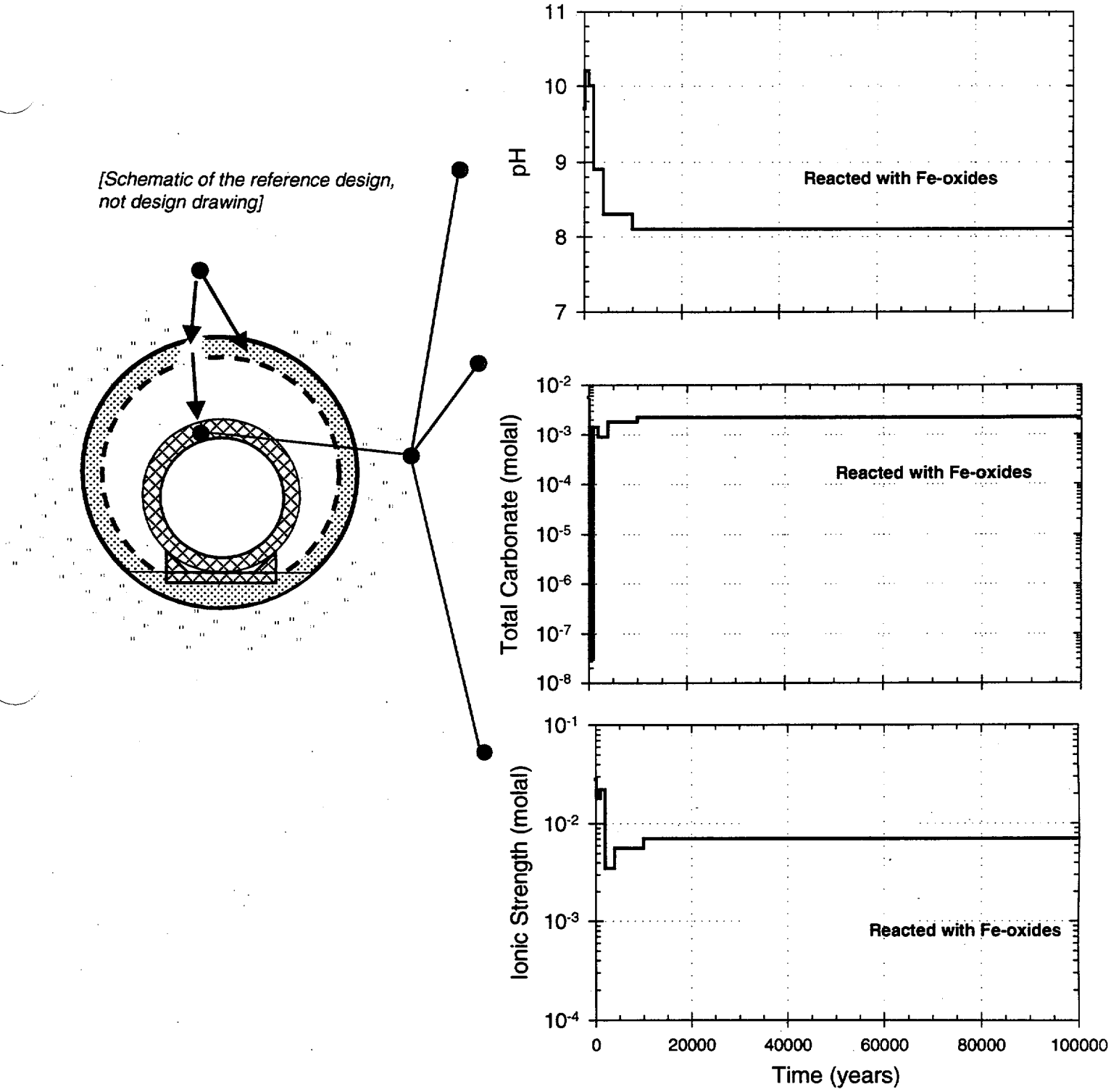

Figure 4-39. The resultant fluid compositions for water reacted with corrosion products to 100,000 years shown in terms of the pH, total dissolved carbonate (ΣCO_3^{2-}), and the ionic strength.

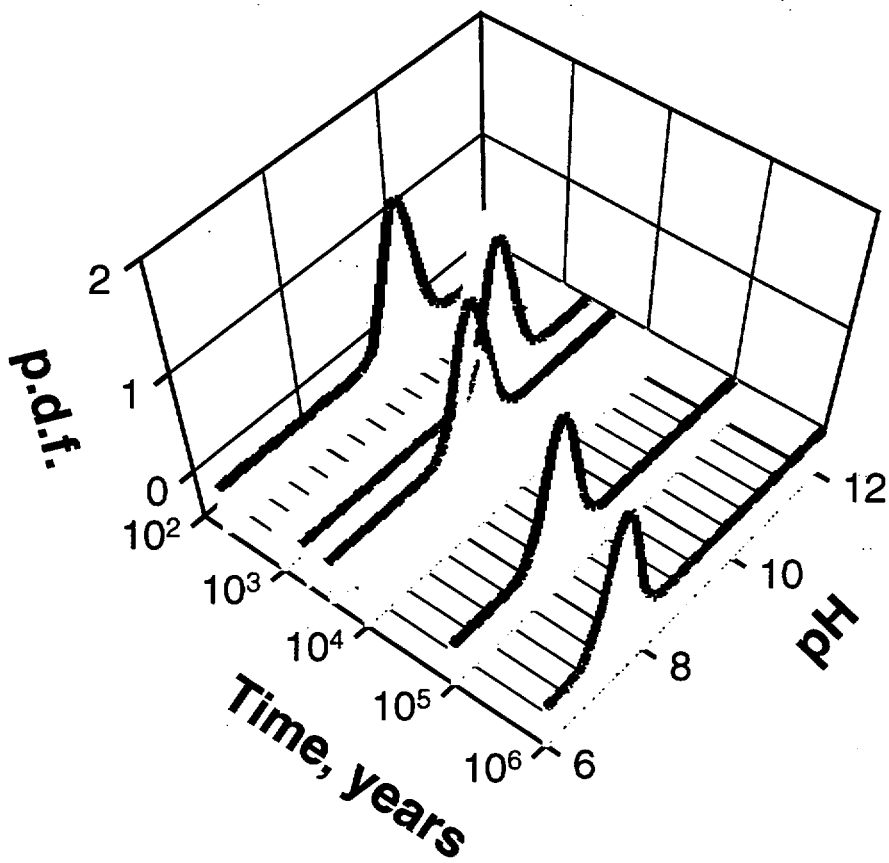

Figure 4-40. Example of input to the TSPA-VA from the near-field geochemical environment component showing distributions of pH for incoming water reacted with iron-oxides. Distributions are shown as probability density functions (p.d.f).

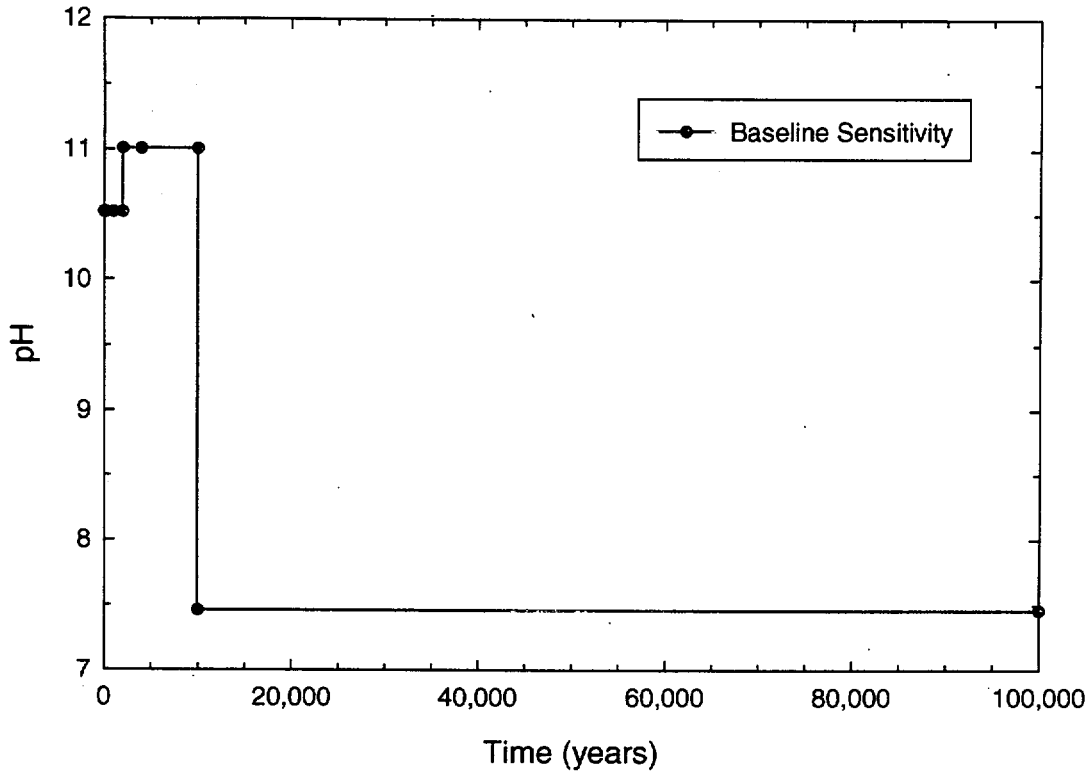

Figure 4-41. Baseline sensitivity simulations of concrete reacted fluid, pH vs. time.

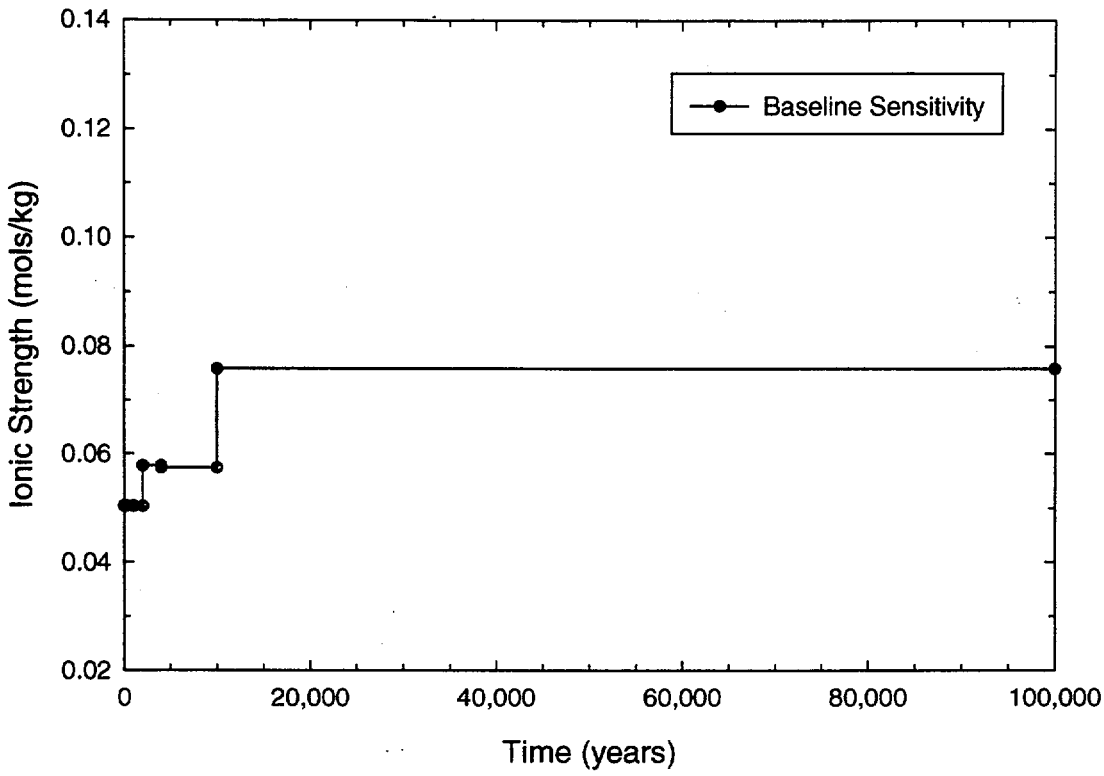

Figure 4-42. Baseline sensitivity simulations of concrete reacted fluid, ionic strength vs. time.

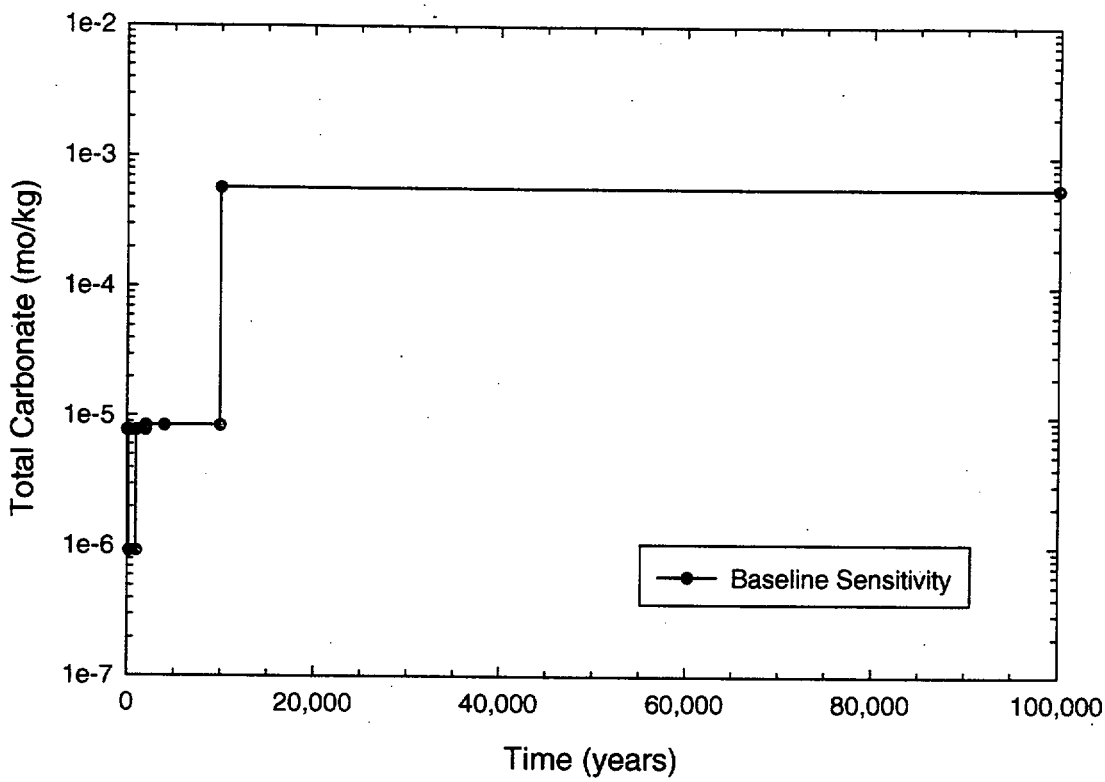

Figure 4-43. Baseline sensitivity simulations of concrete reacted fluid, total carbonate vs. time.

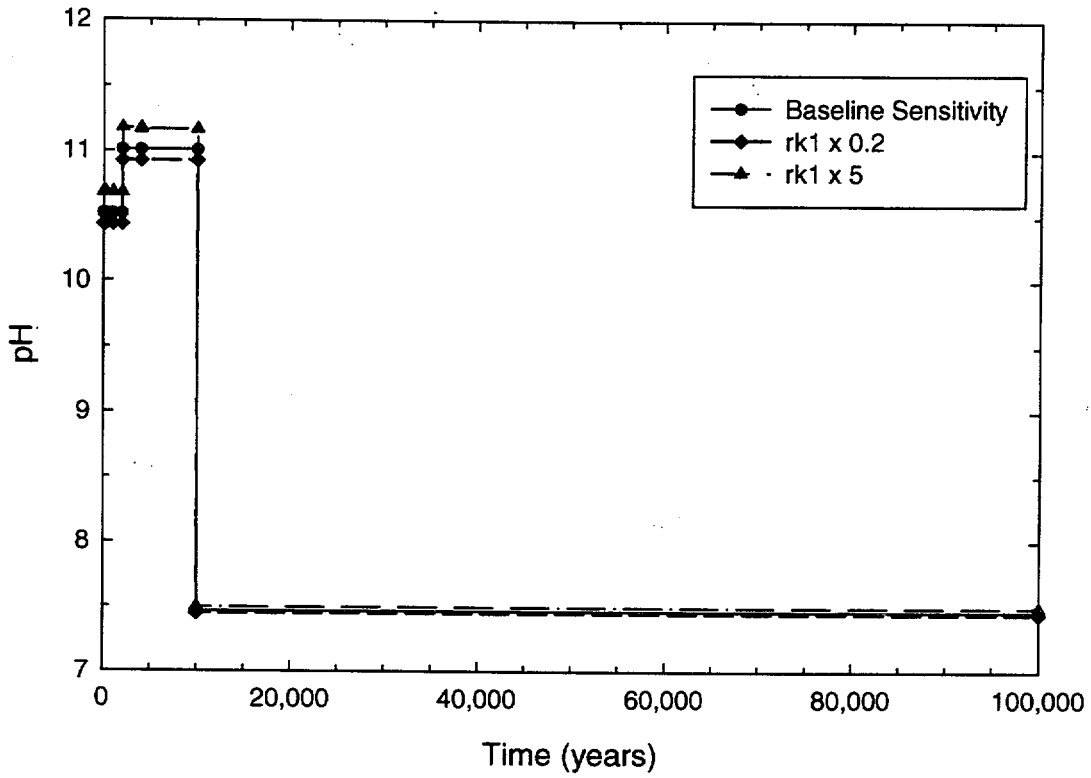

Figure 4-44. Sensitivity study showing the effect of relative reaction rates on concrete reacted fluid chemistry, pH vs. time.

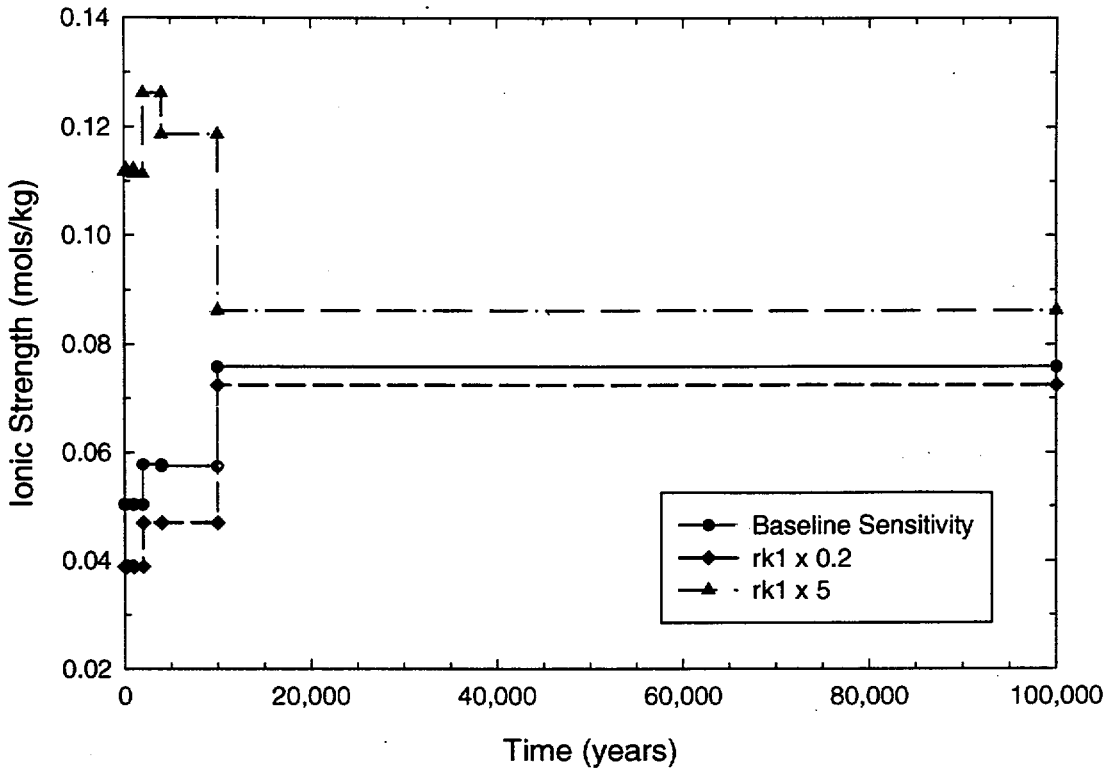

Figure 4-45. Sensitivity study showing the effect of relative reaction rates on concrete reacted fluid chemistry, ionic strength vs. time.

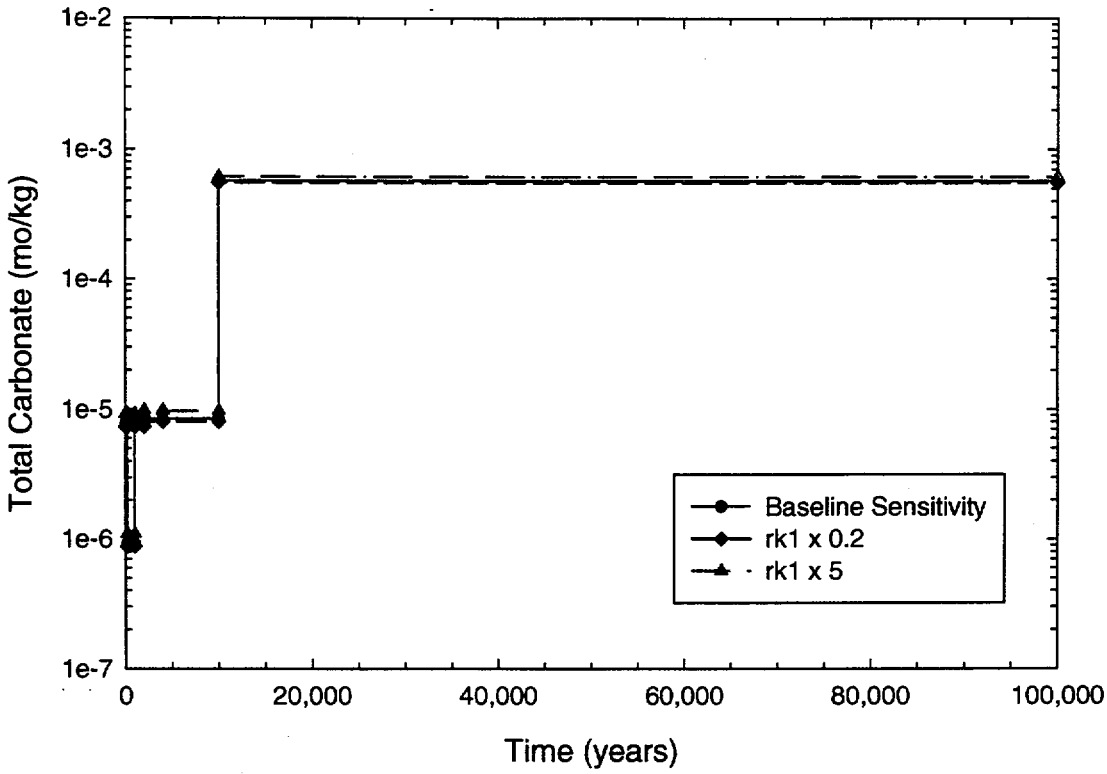

Figure 4-46. Sensitivity study showing the effect of relative reaction rates on concrete reacted fluid chemistry, total carbonate vs. time.

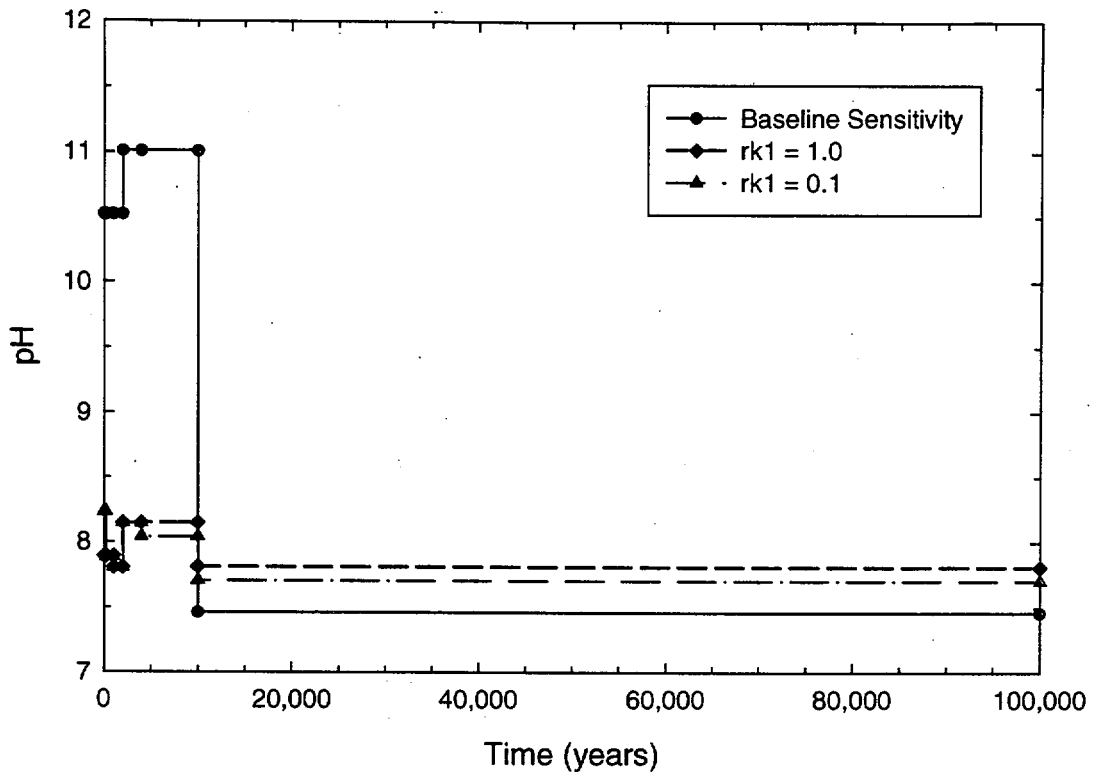

Figure 4-47. Sensitivity study showing the effect of relative reaction rates (rk1 = constant for all reactants) on concrete reacted fluid chemistry, pH vs. time.

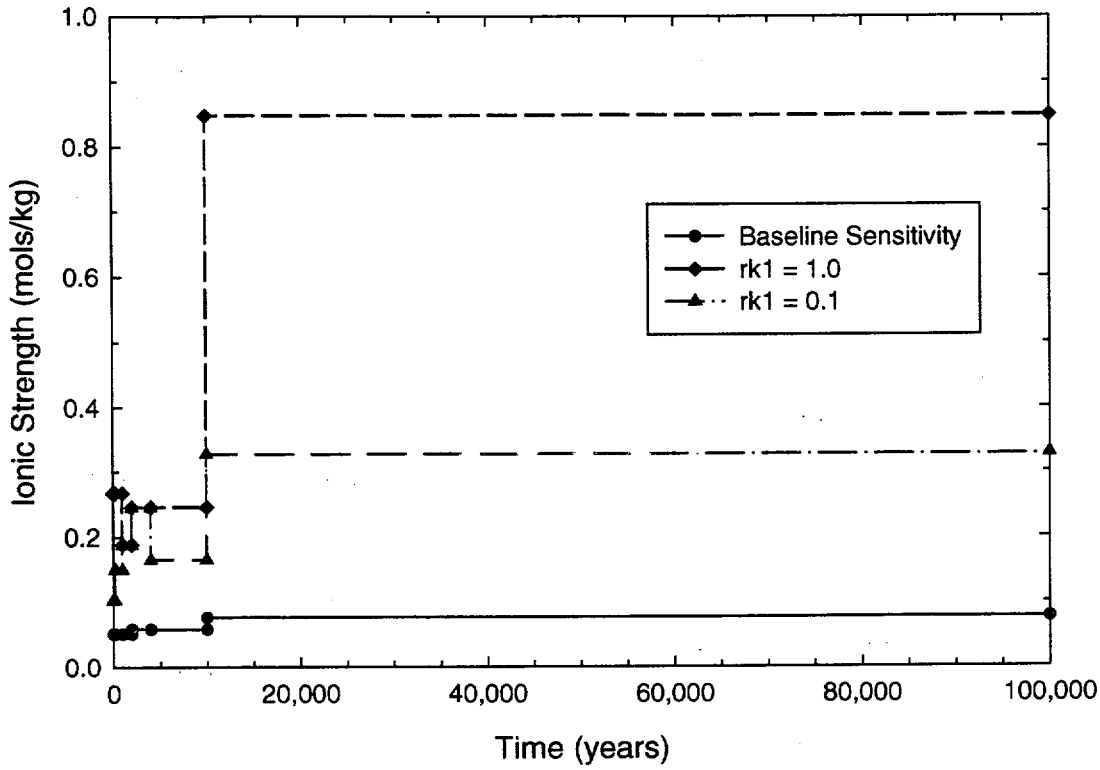

Figure 4-48. Sensitivity study showing the effect of relative reaction rates (rk1 = constant for all reactants) on concrete reacted fluid chemistry, ionic strength vs. time.

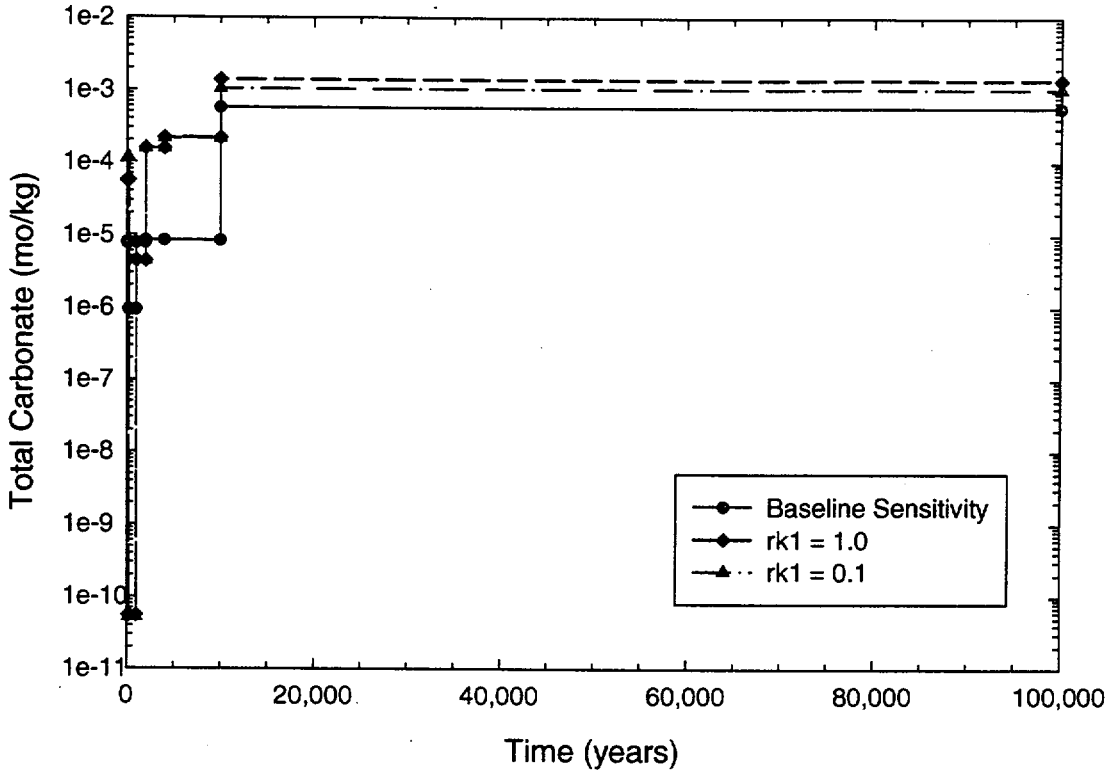

Figure 4-49. Sensitivity study showing the effect of relative reaction rates (rk1 = constant for all reactants) on concrete reacted fluid chemistry, total carbonate vs. time.

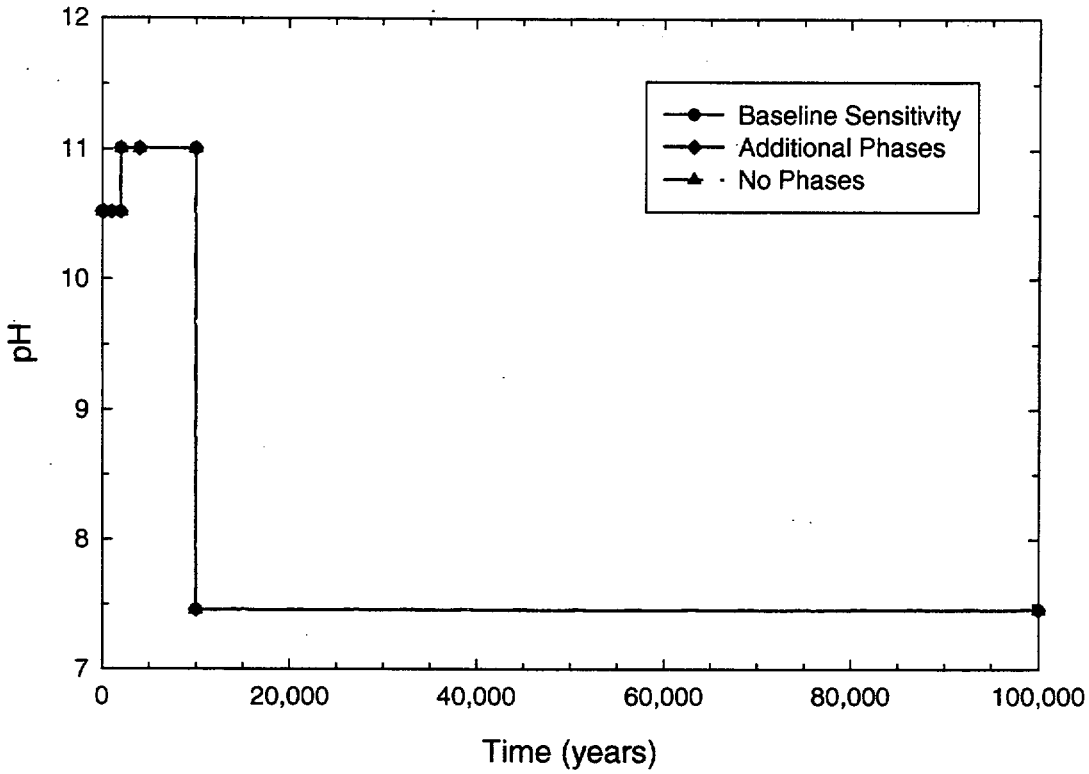

Figure 4-50. Sensitivity study showing the effect of phase suppression on the reacted fluid chemistry, pH vs. time.

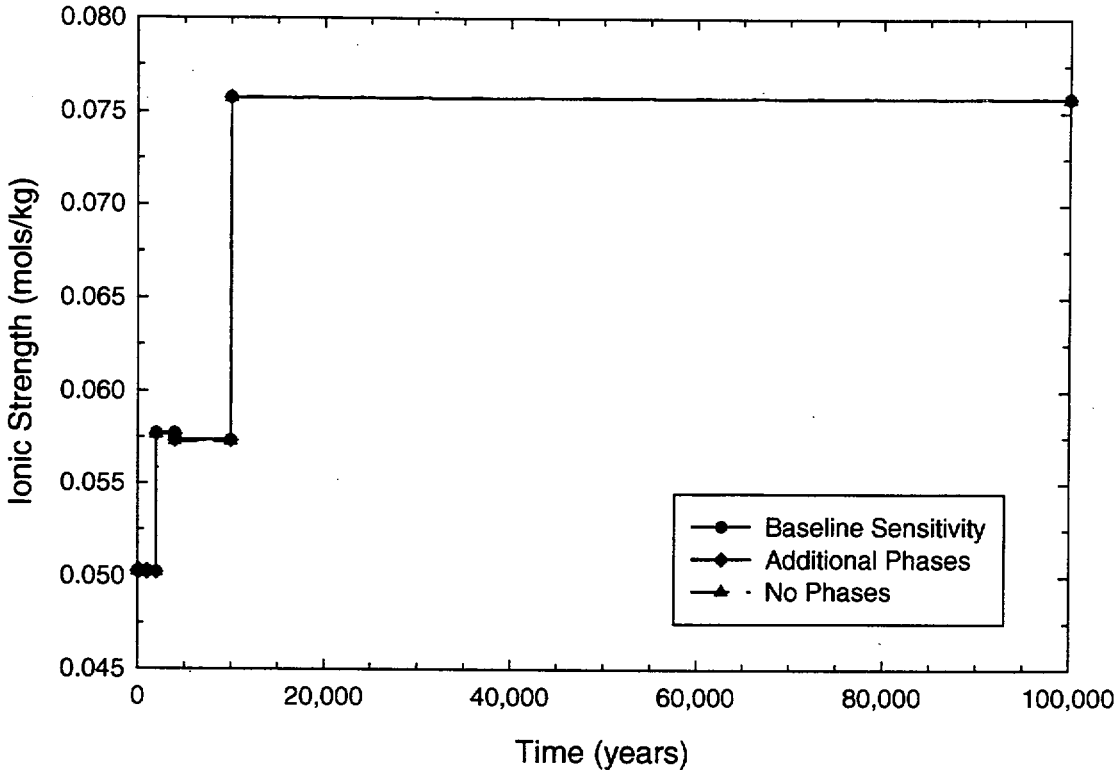

Figure 4-51. Sensitivity study showing the effect of phase suppression on the reacted fluid chemistry, ionic strength vs. time.

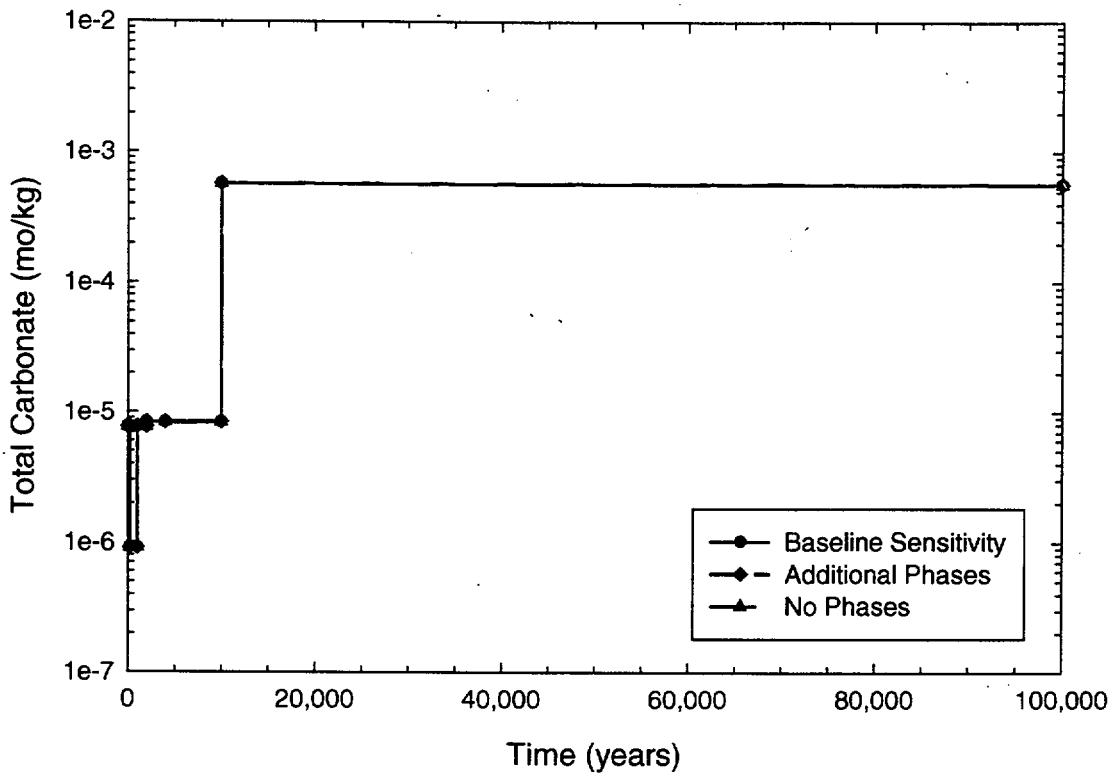

Figure 4-52. Sensitivity study showing the effect of phase suppression on the reacted fluid chemistry, total carbonate vs. time.

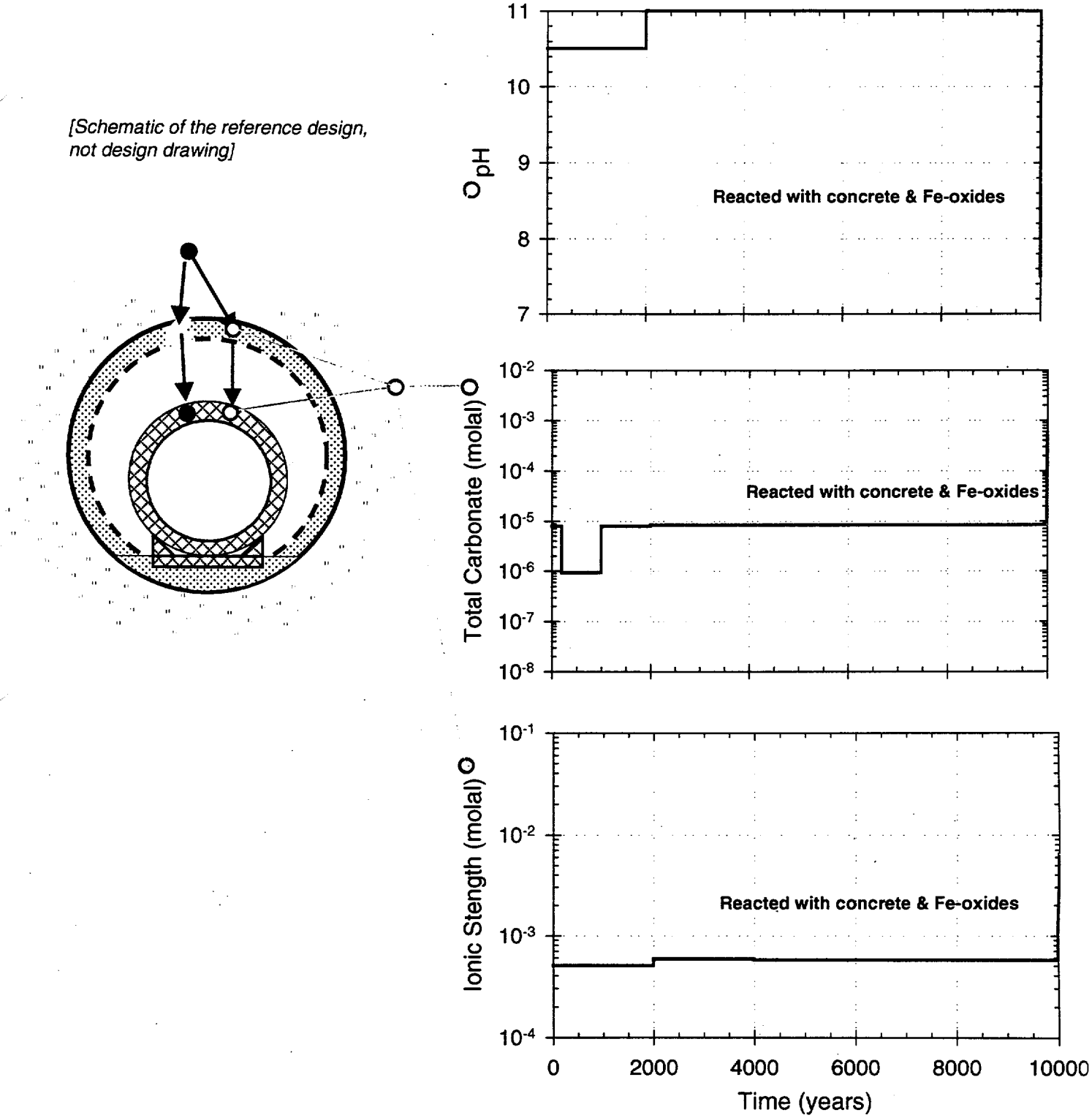

Figure 4-53. The resultant fluid compositions for incoming water to 10,000 years shown in terms of the pH, total dissolved carbonate (ΣCO_3^{2-}), and the ionic strength.

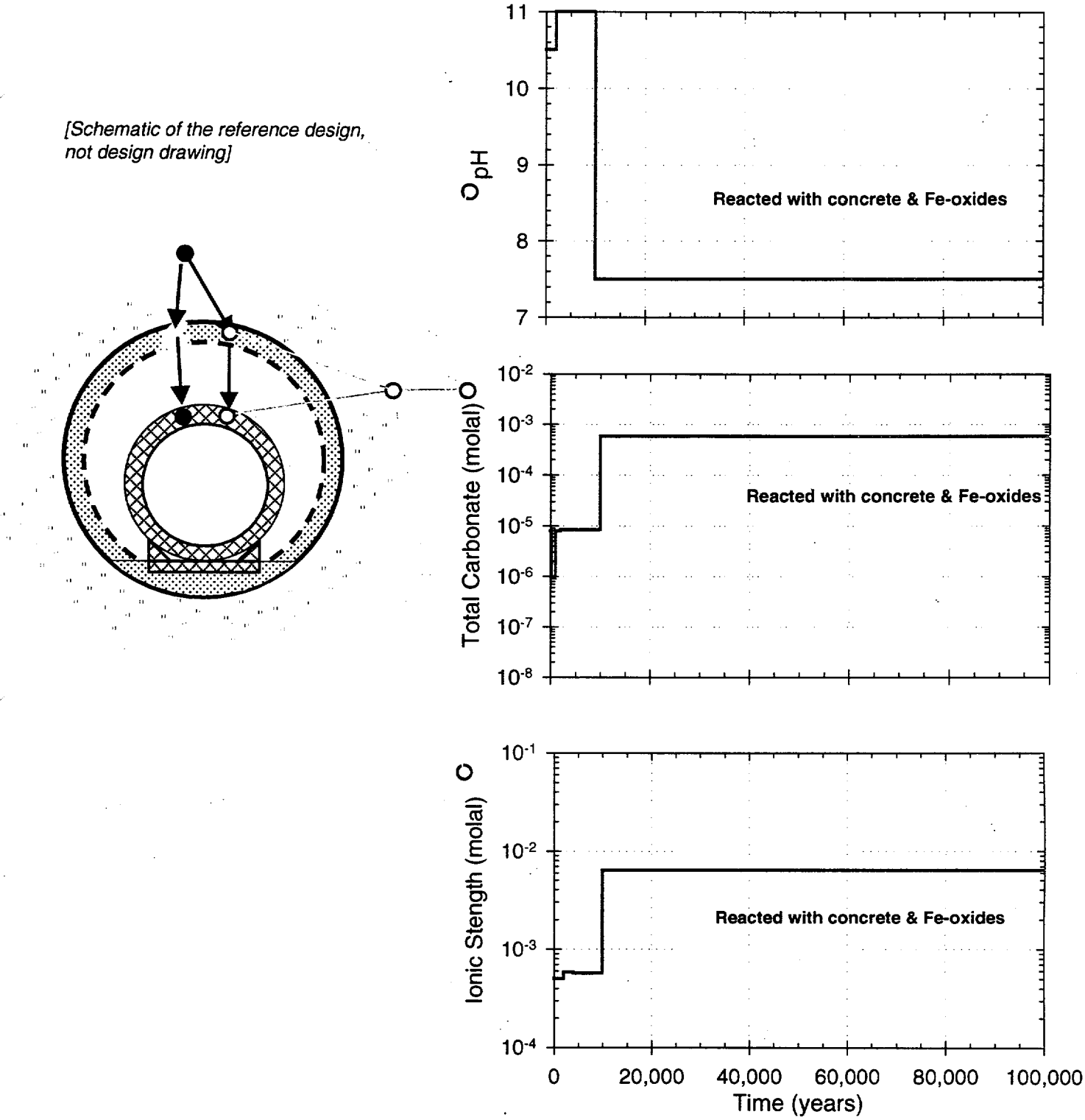

Figure 4-54. The resultant fluid compositions for incoming water to 100,000 years shown in terms of the pH, total dissolved carbonate (ΣCO_3^{2-}), and the ionic strength.

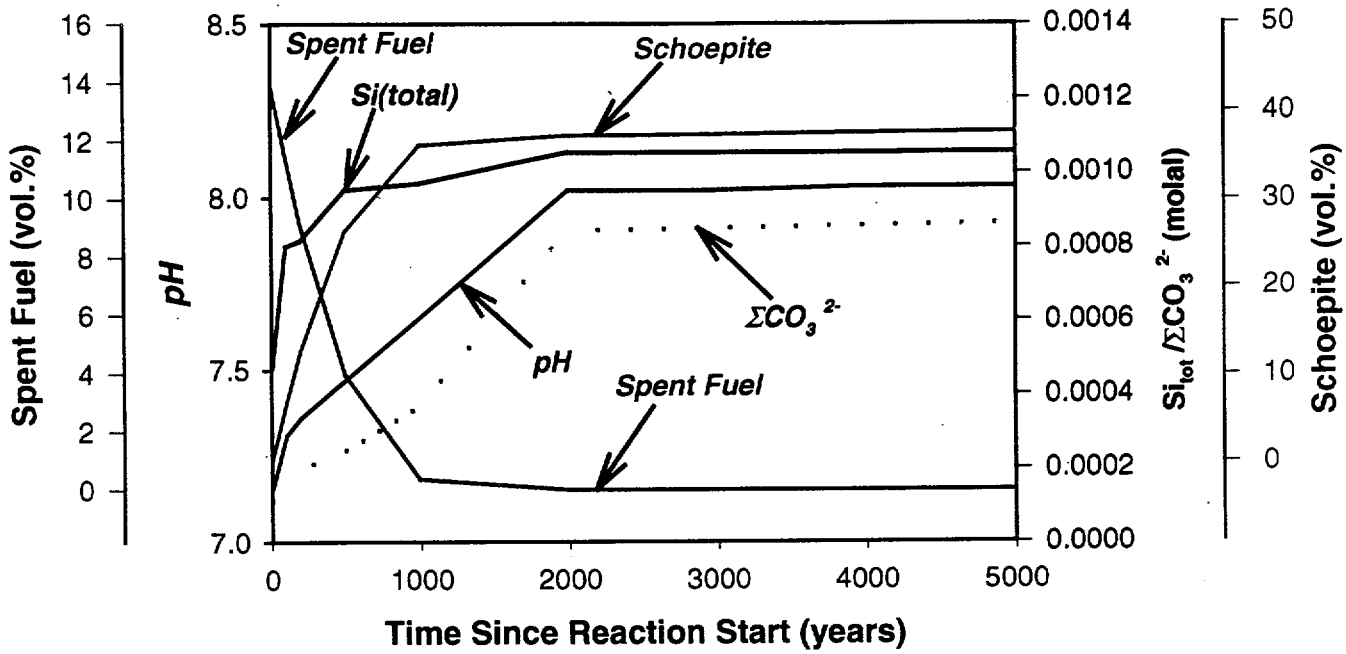

Figure 4-55. Water composition and volume fractions of major solids for Case A.

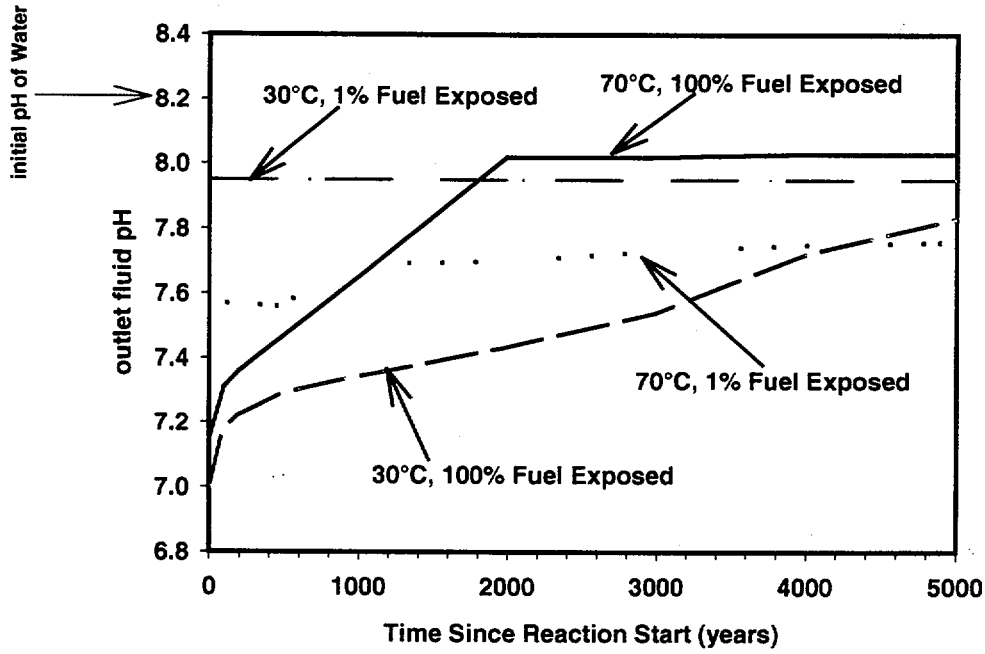

Figure 4-56. pH values of water at the bottom of CSNF waster packages.

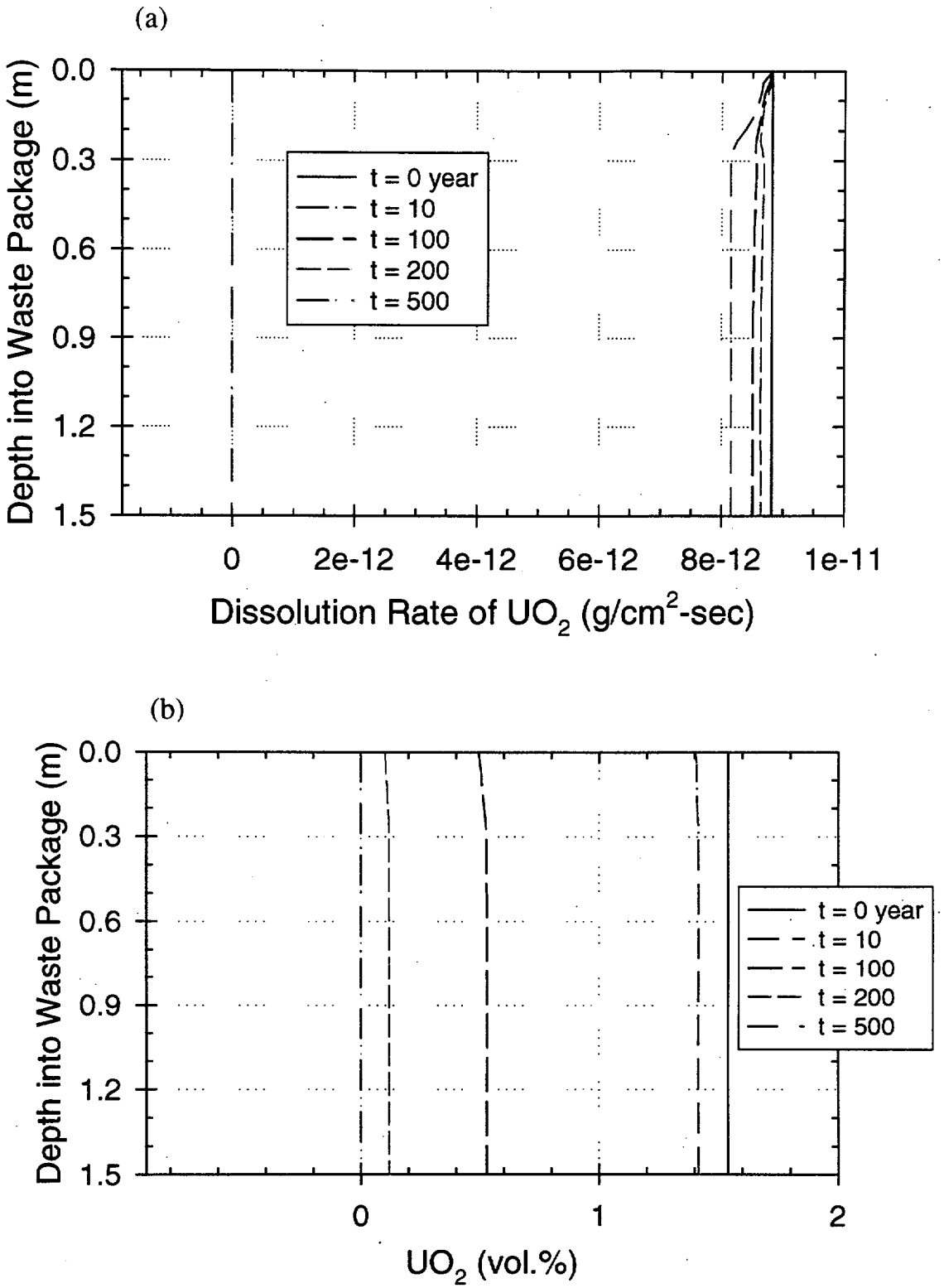

Figure 4-57. Profiles of (a) dissolution rate; and (b) volume fractions of spent fuel. The dissolution rate varies less than 15% with time and space. Available spent fuel is totally consumed after 500 years of dissolution.

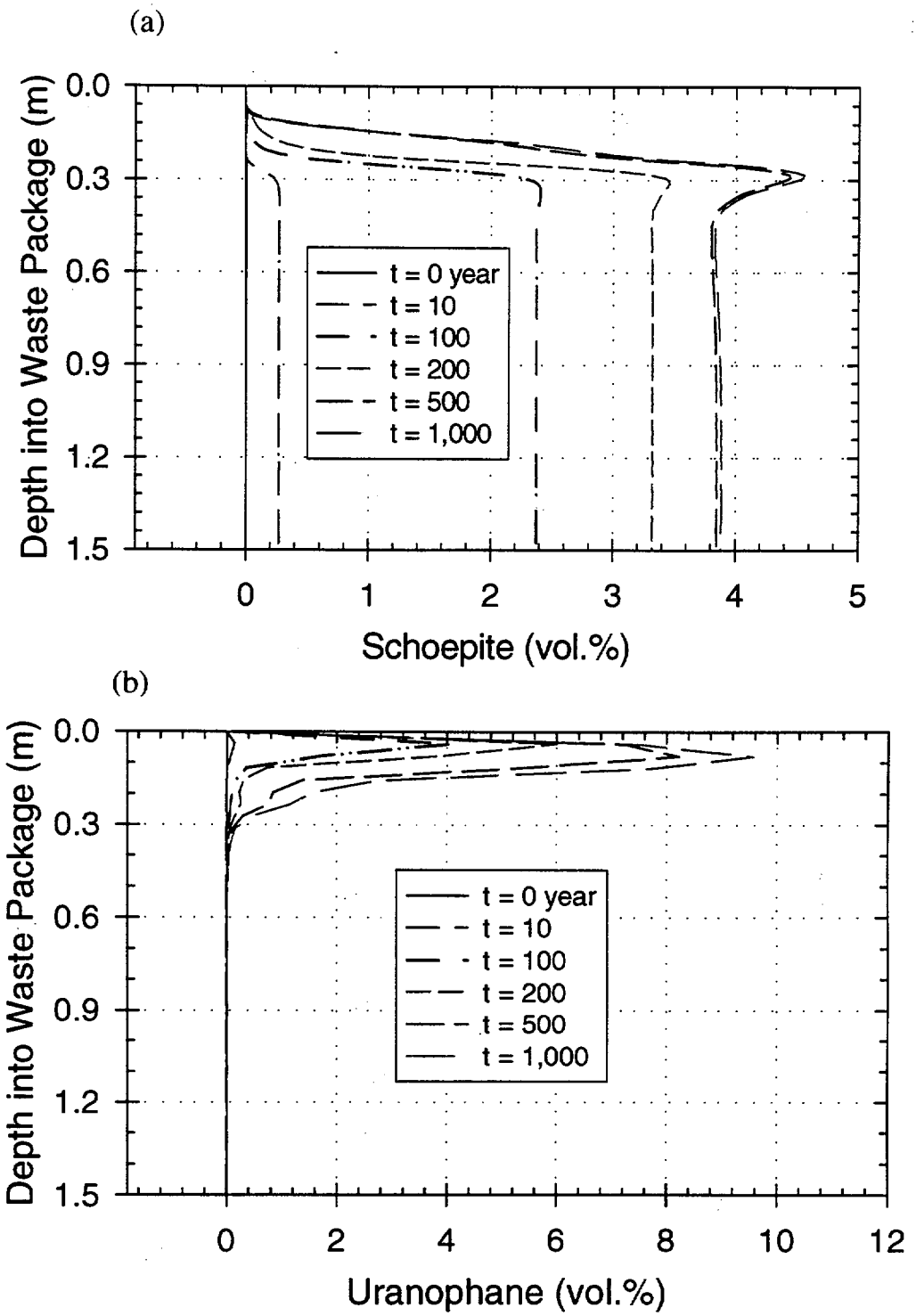

Figure 4-58. Volume profiles of secondary minerals precipitated when spent fuel dissolves. (a) schoepite, the major secondary mineral; (b) uranophane, mainly precipitates at the top of the WP.

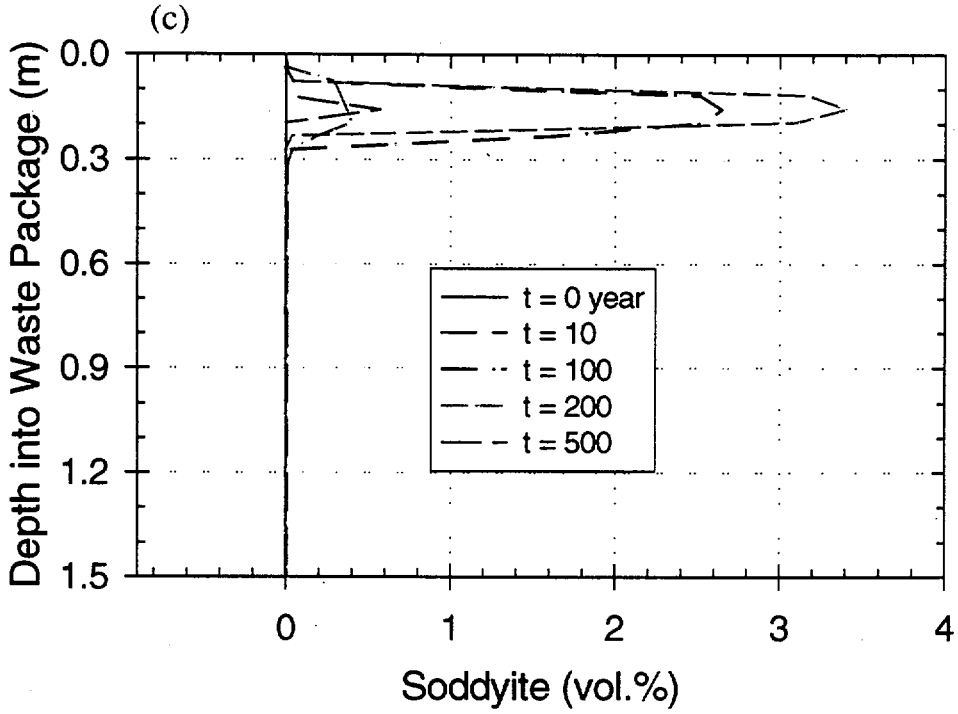

Figure 4-59. Soddyite, precipitated at the top of the WP and redissolved after spent fuel has been consumed. Closely exam the movement of precipitation fronts reveals that uranophane forms at the expense of schoepite and soddyite.

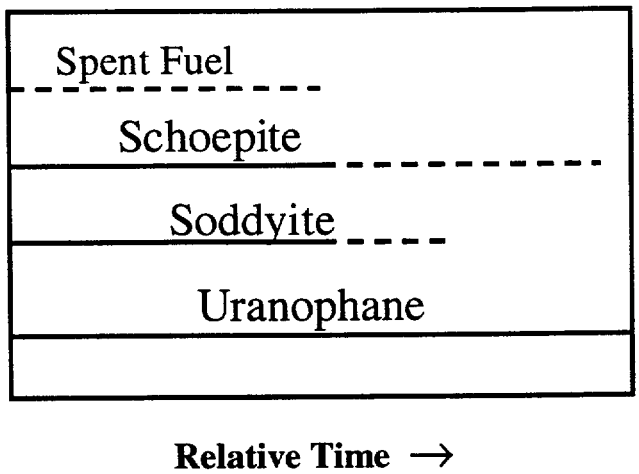

Figure 4-60. Paragenetic sequence of secondary minerals observed in the simulation results. Dashed line means meta-stable phases. Uranophane is the most stable uranyl mineral.

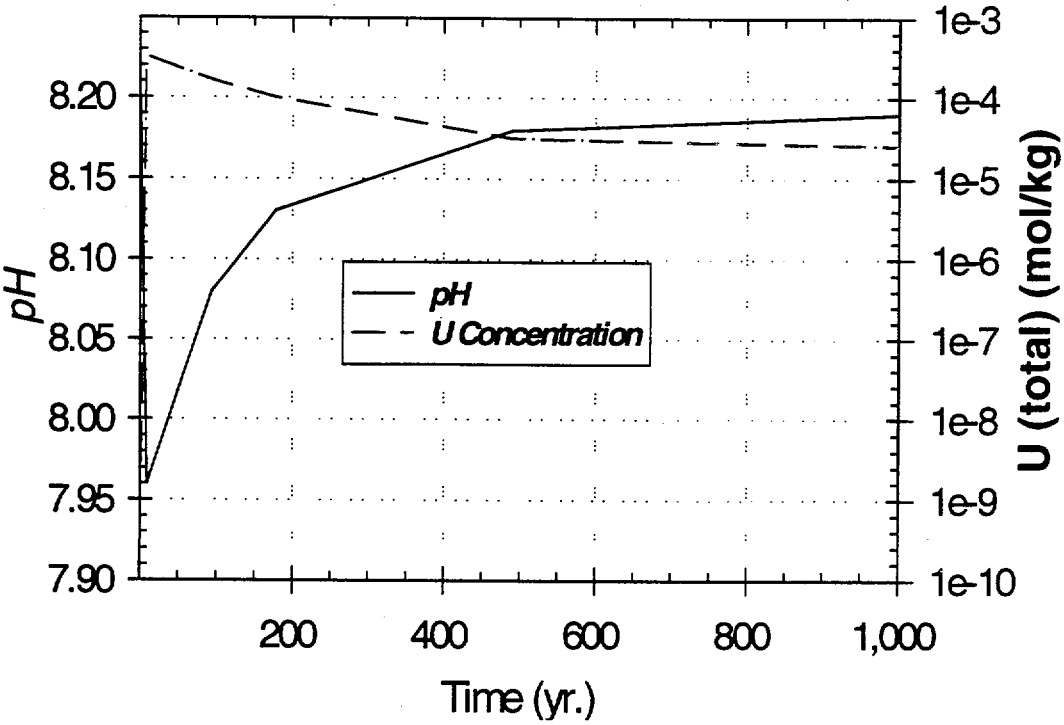

Figure 4-61. pH and U(total) concentration changes. pH drops from its original value of 8.2 to 7.95 at 10 years and then reverses to its original value. U(total) increases first and then decreases.

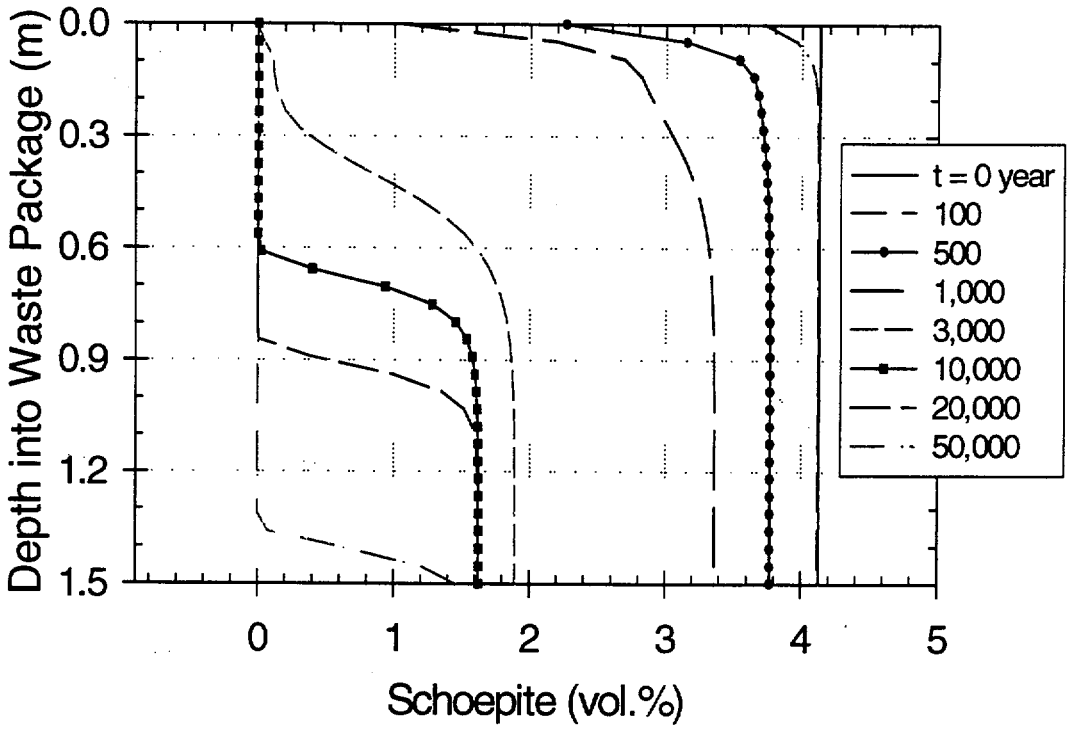

Figure 4-62. Simulated schoepite profiles for Case-1 at different time. Schoepite dissolves and disappears at 50,000 years. Before 10,000 years, the dissolution takes place across the whole WP. After, that dissolution is localized to the dissolution front, which advances with time from upstream to downstream.

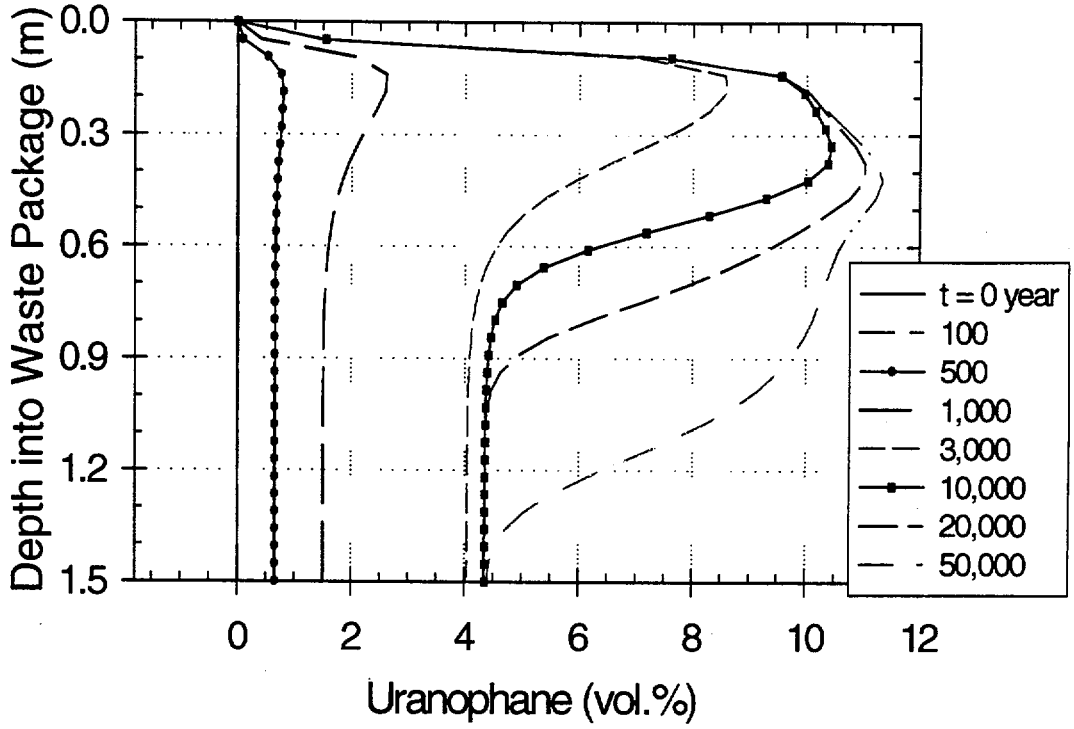

Figure 4-63. Simulated uranophane profiles for Case-1. Uranophane replaces schoepite. Before 10,000 years, it precipitates across the whole WP. After that time, the precipitation front advances from upstream to downstream.

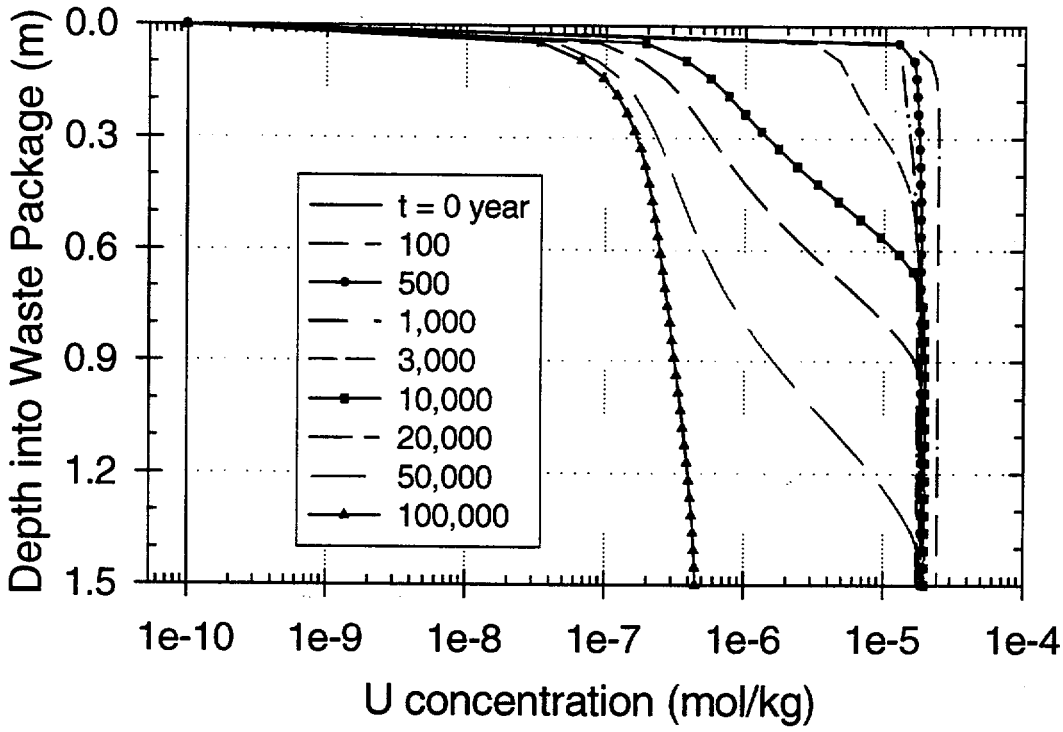

Figure 4-64. Simulated concentrations of U for Case-1. It increases with depth into WP and reaches its maximum at the bottom of WP. After 50,000 years, U concentration at the bottom decreases.

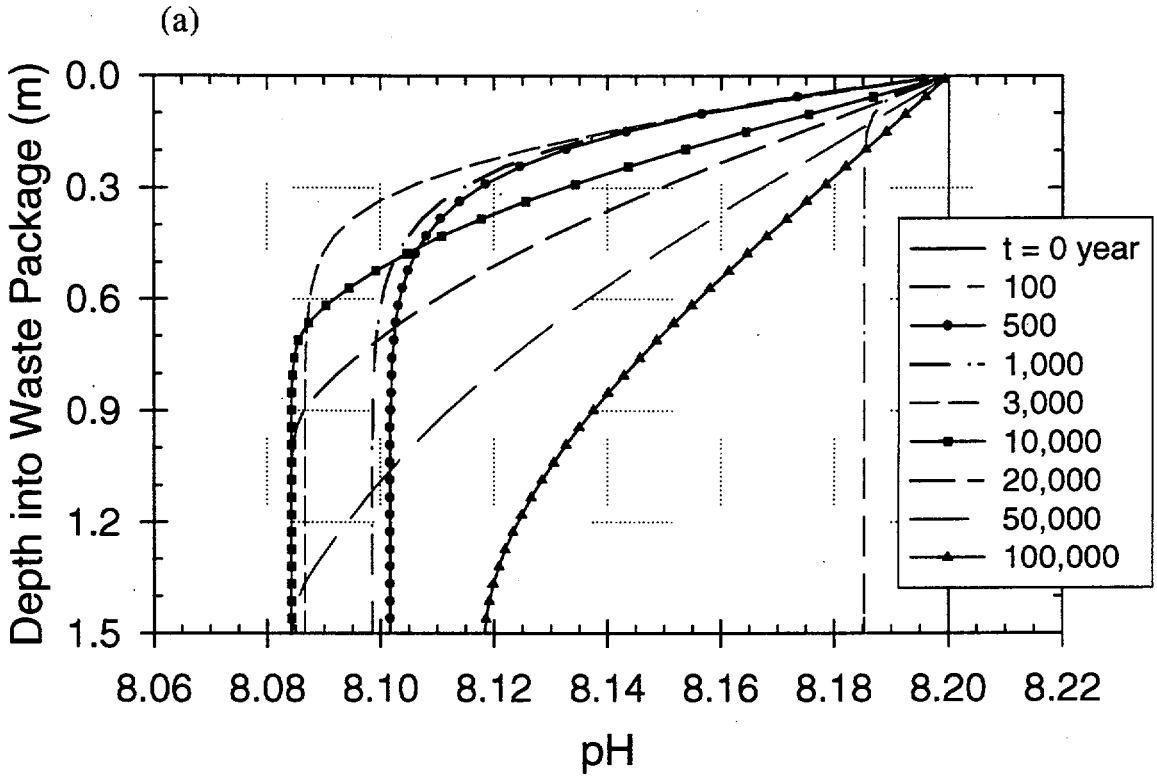

Figure 4-65. Calculated pH (a), CO_2(total). pH change is less than 0.2 unit. Changes in CO_2(total) and ionic strength are about 10%.

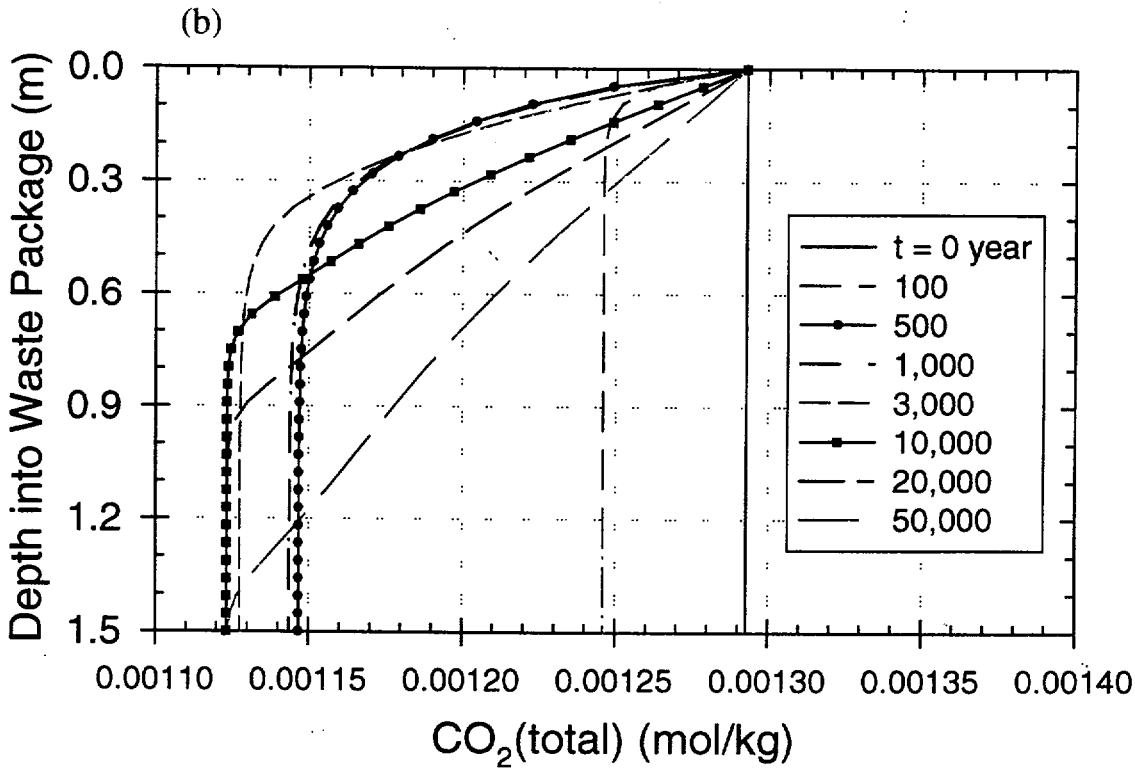

Figure 4-66. CO_2 (total) for Case-1. pH change is less than 0.2 unit. Changes in CO_2(total) and ionic strength are about 10%.

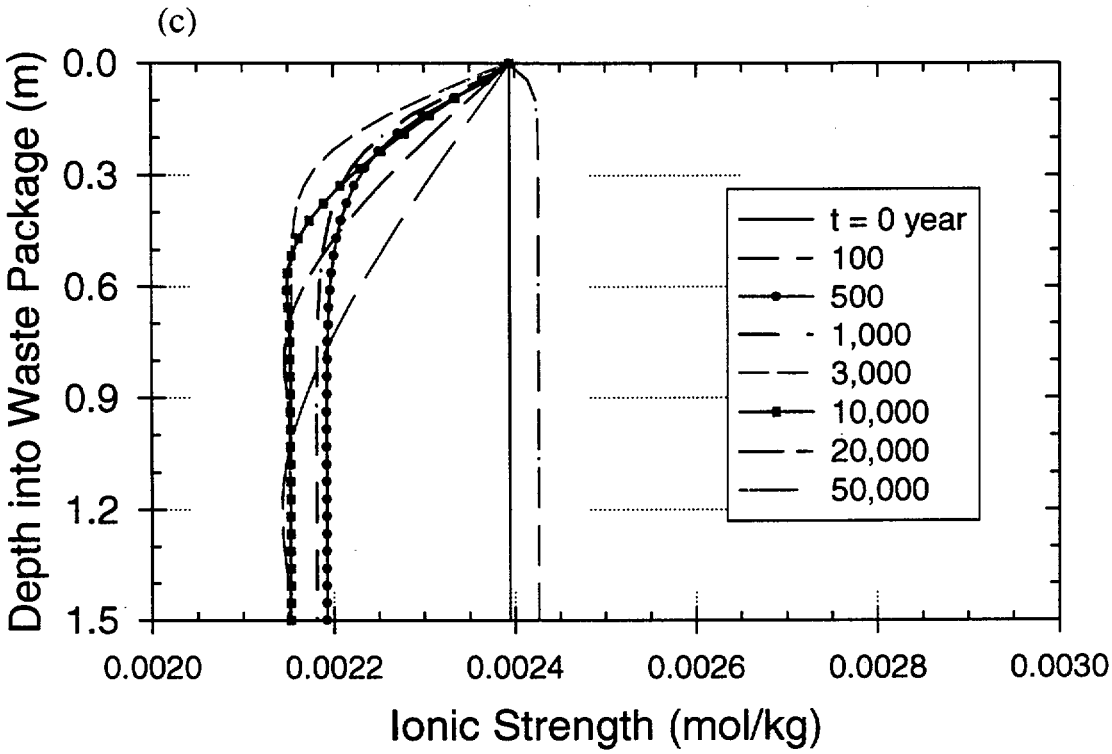

Figure 4-67. Ionic strength for Case-1. pH change is less than 0.2 unit. Changes in CO_2(total) and ionic strength are about 10%.

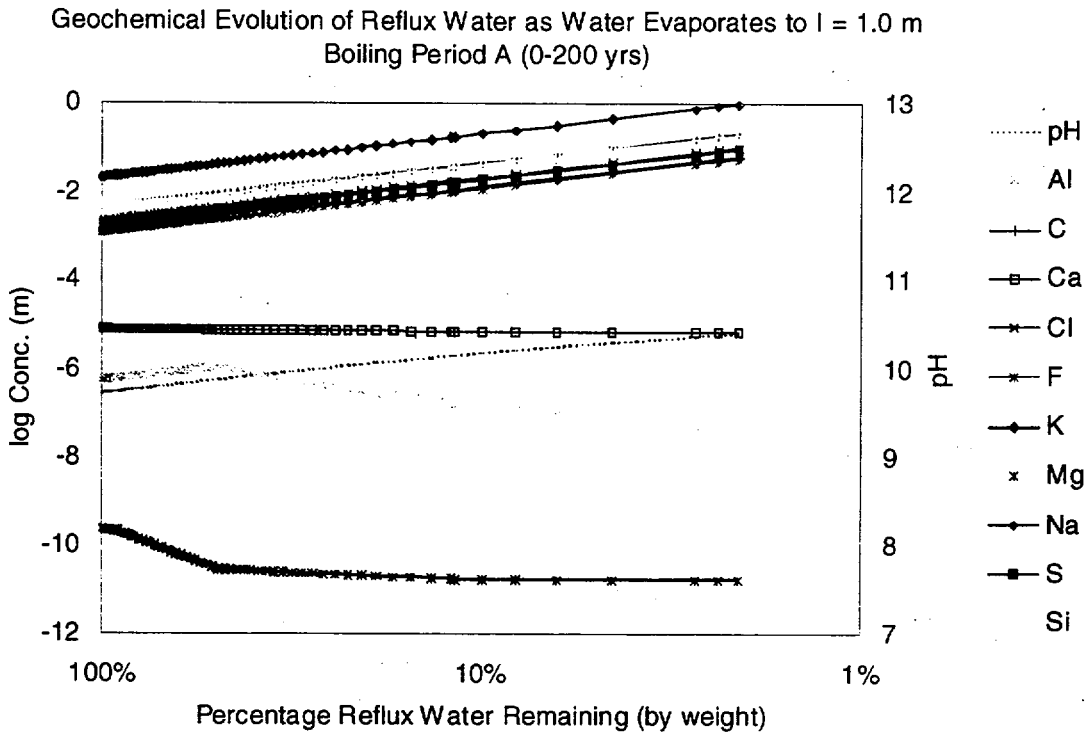

Figure 4-68. Geochemical evolution of reflux water as water evaporates to I = 1.0 m for Boiling Period A.

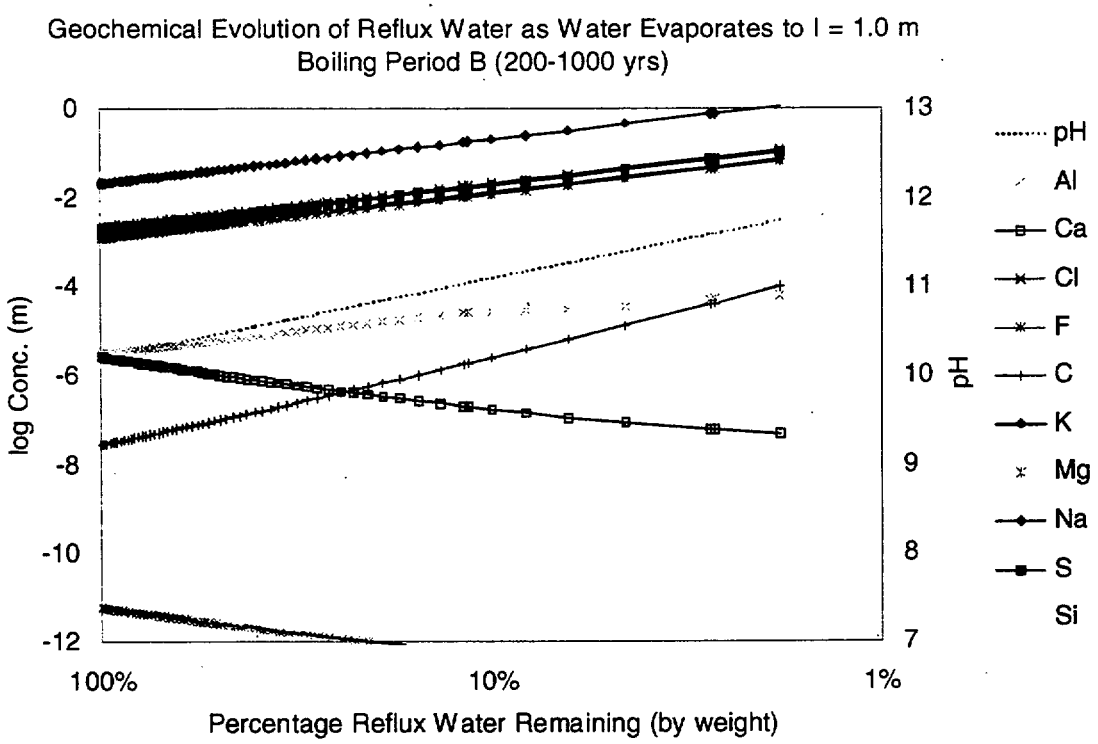

Figure 4-69. Geochemical evolution of reflux water as water evaporates to I = 1.0 m for Boiling Period B.

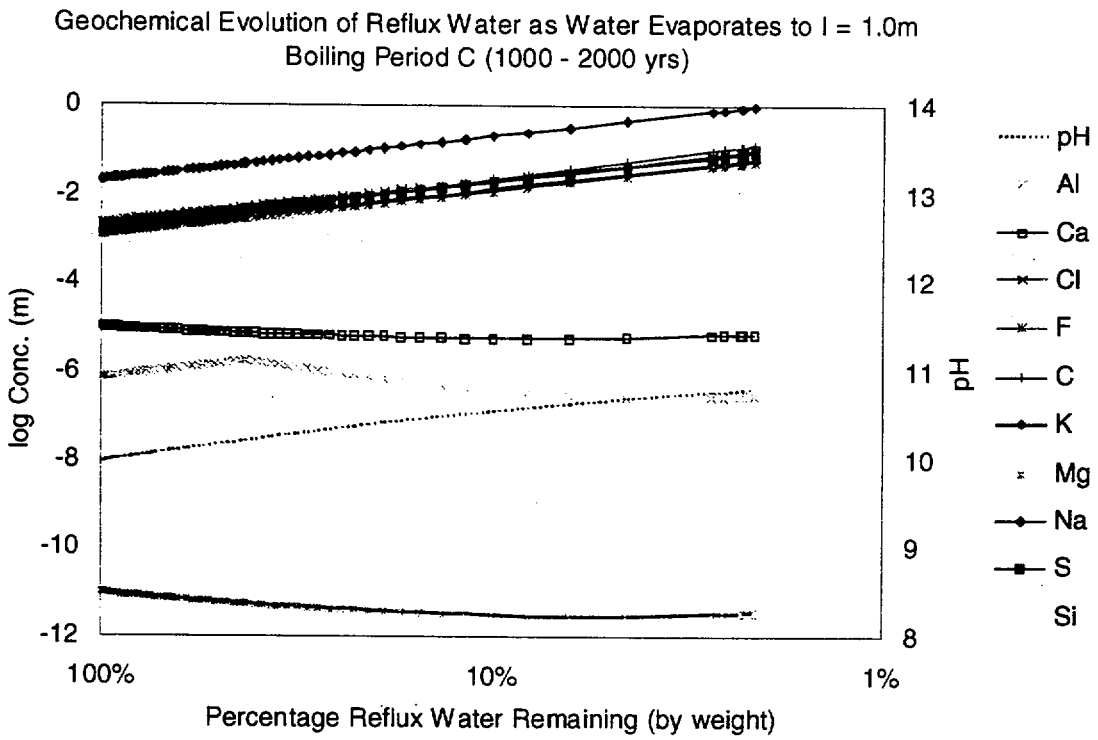

Figure 4-70. Geochemical evolution of reflux water as water evaporates to I = 1.0 m for Boiling Period C.

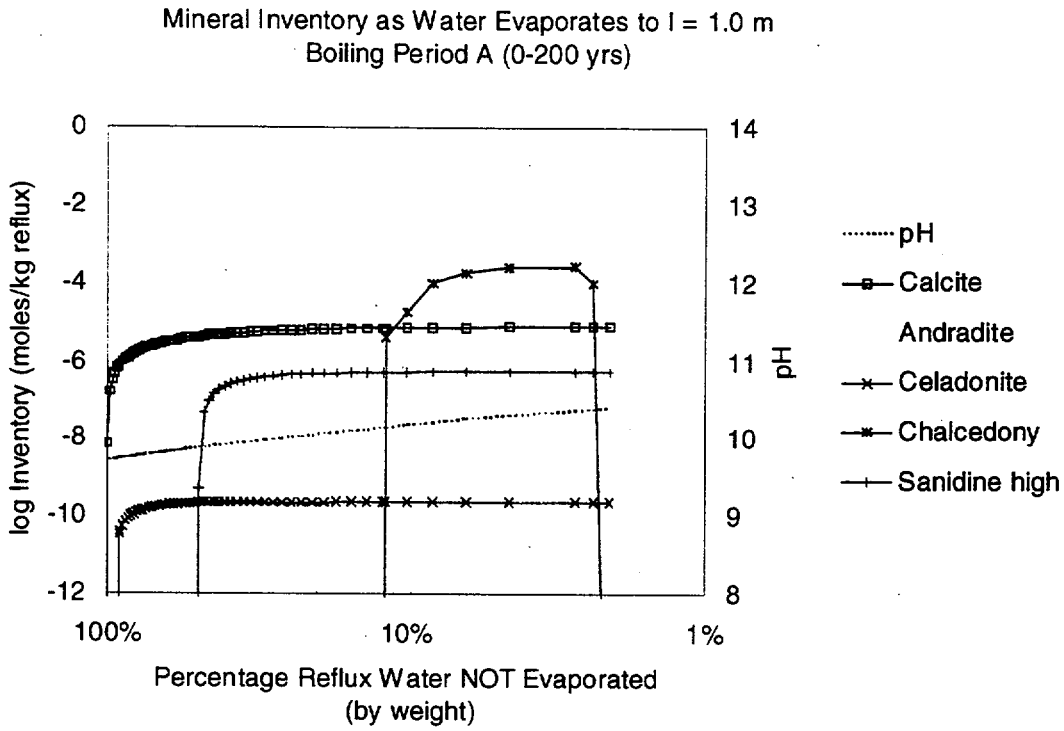

Figure 4-71. Mineral inventory as water evaporates to I = 1.0 m for Boiling Period A.

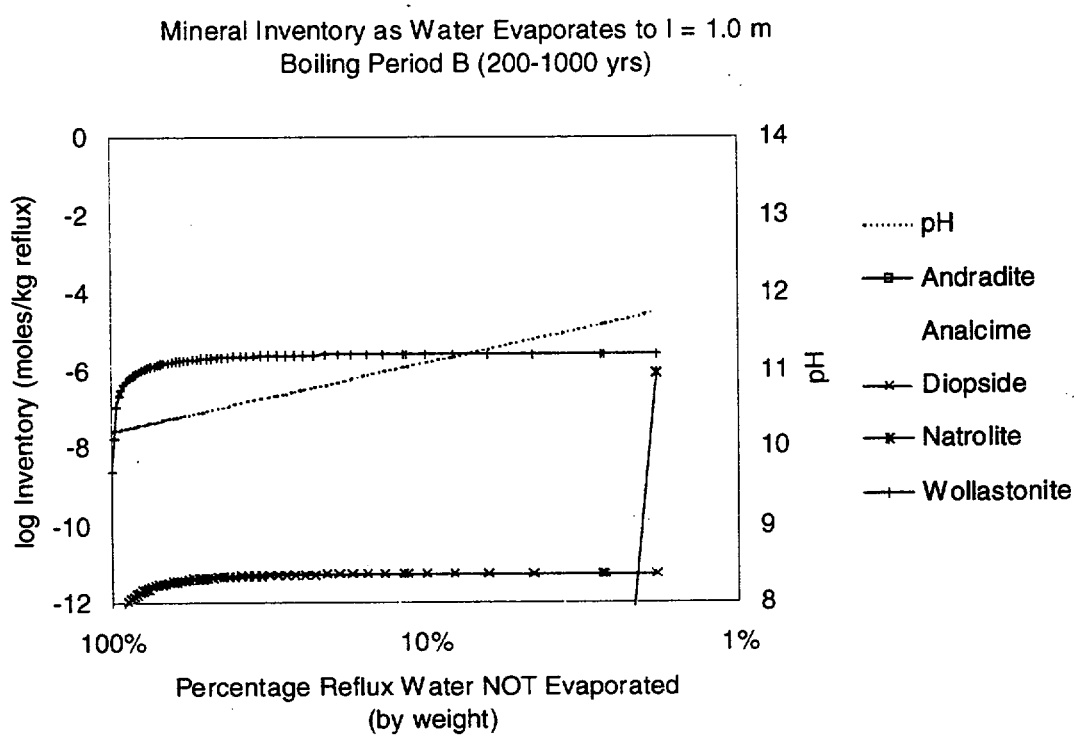

Figure 4-72. Mineral inventory as water evaporates to I = 1.0 m for Boiling Period B.

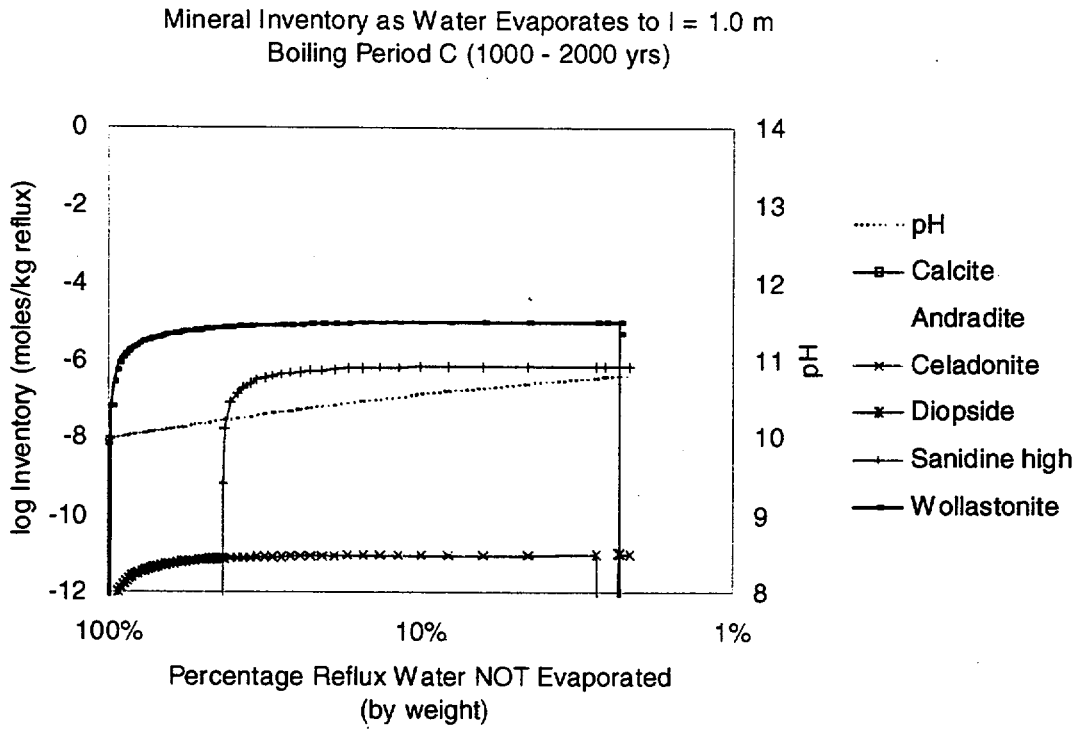

Figure 4-73. Mineral inventory as water evaporates to I = 1.0 m for Boiling Period C.

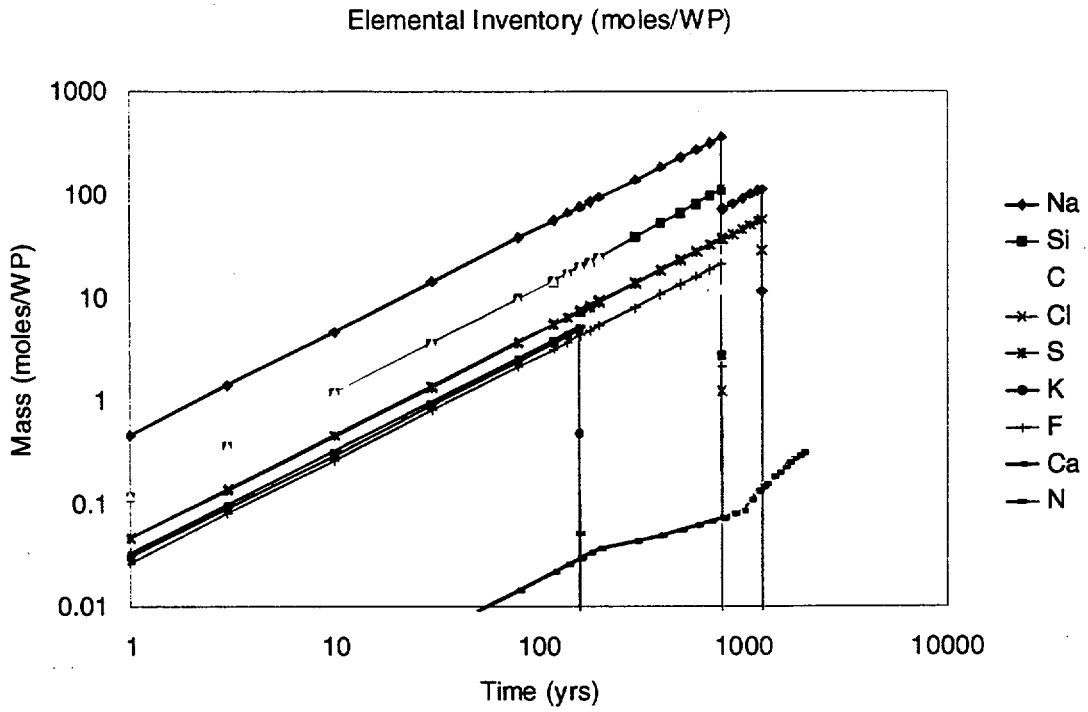

Figure 4-74. Resulting elemental inventory mass in mols per waste package for precipitates/salts model.

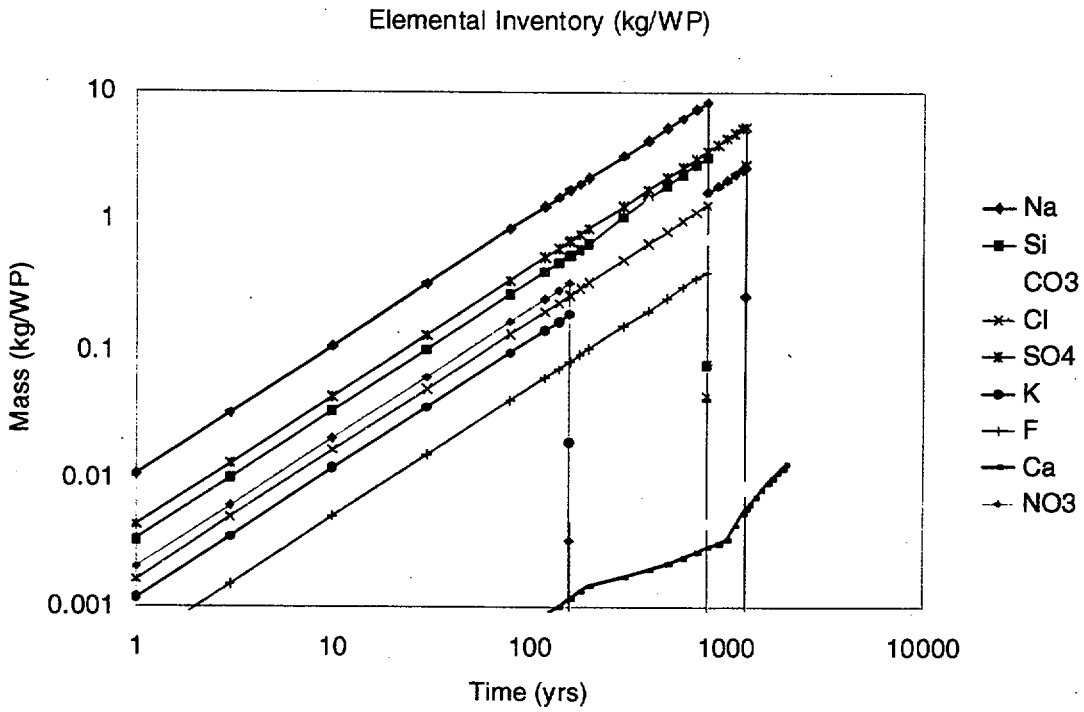

Figure 4-75. Resulting elemental inventory mass in kilograms per waste package for precipitates/salts model.

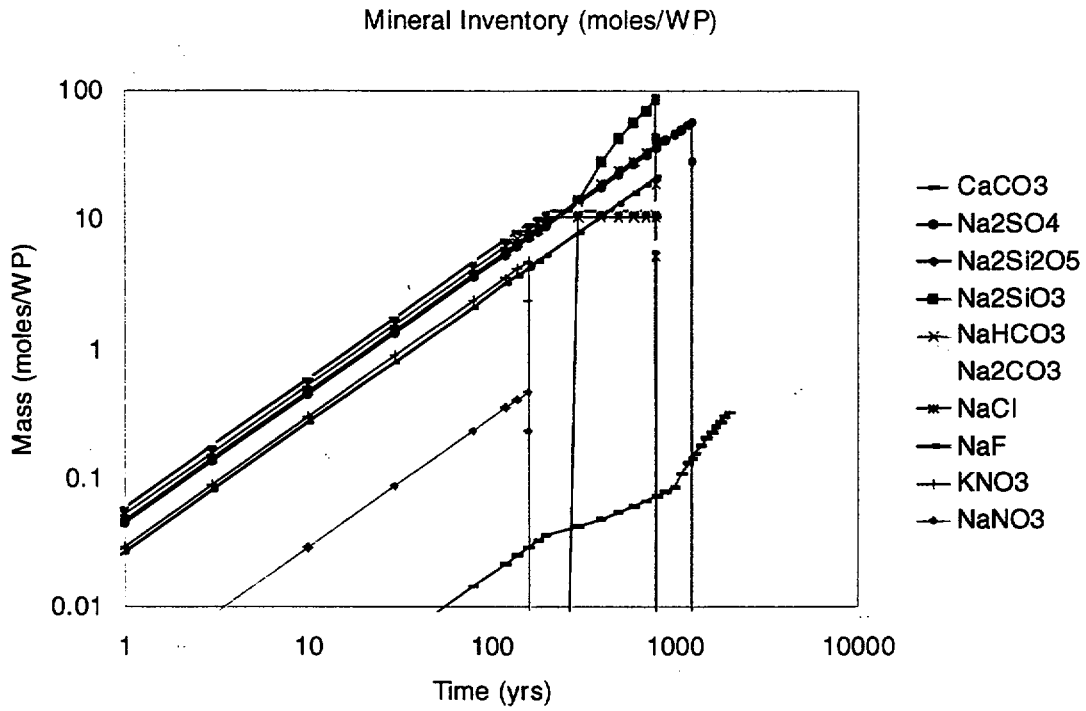

Figure 4-76. Resulting mineral inventory in mols per waste package for the precipitates/salts model.

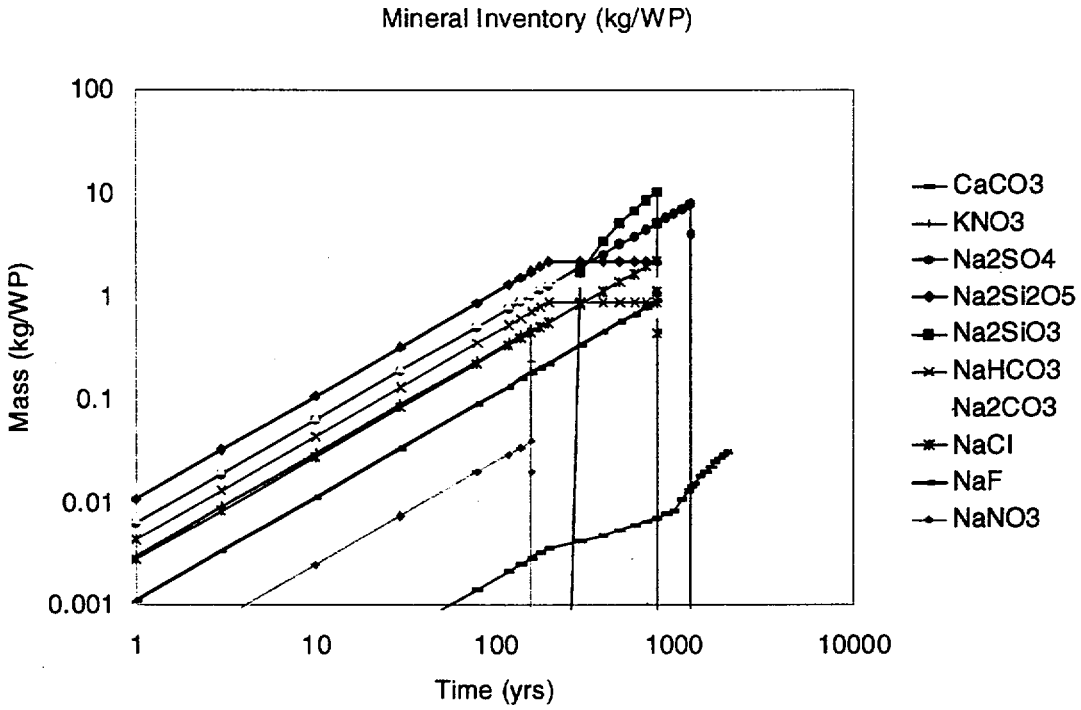

Figure 4-77. Resulting mineral inventory in kilograms per waste package for the precipitates/salts model.

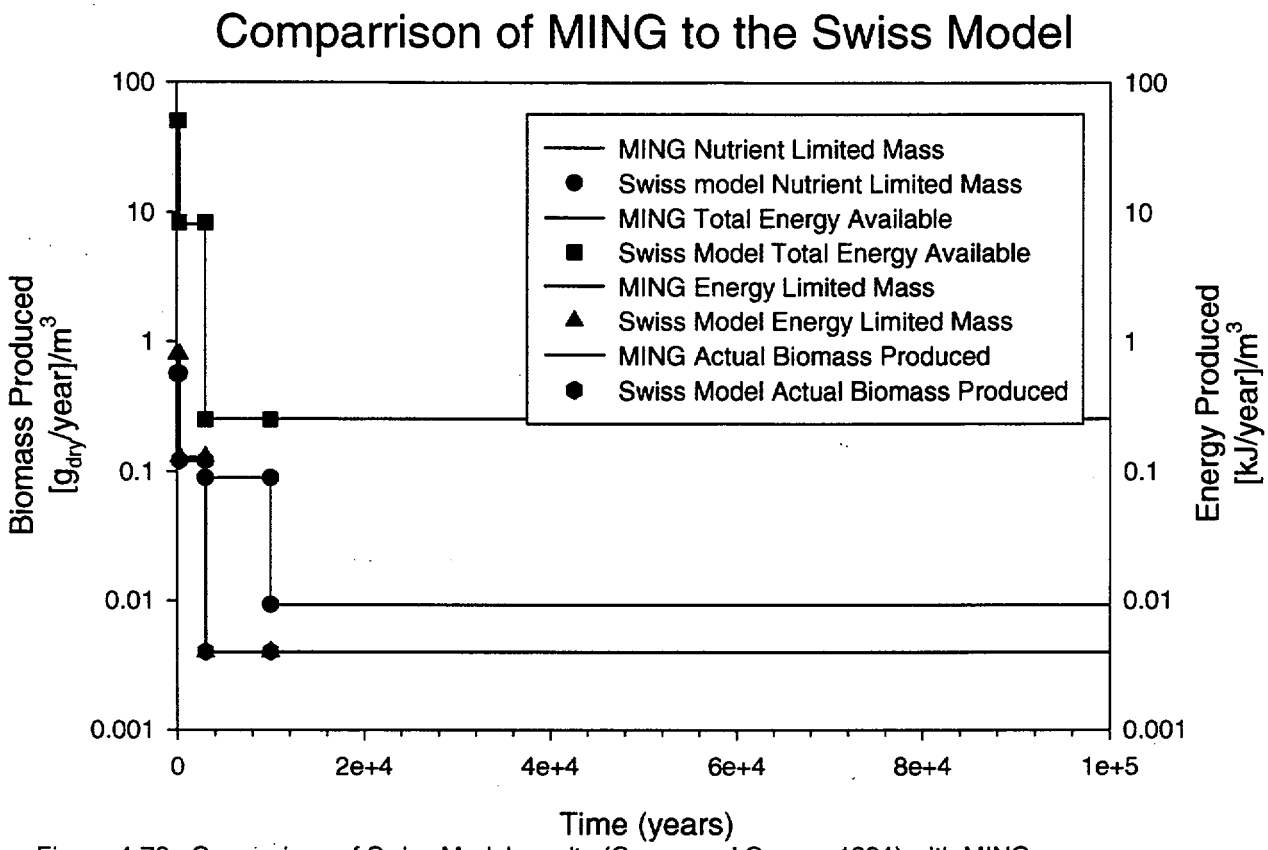

Figure 4-78. Comparison of Swiss Model results (Capon and Grogan 1991) with MING calculations of the Swiss Model.

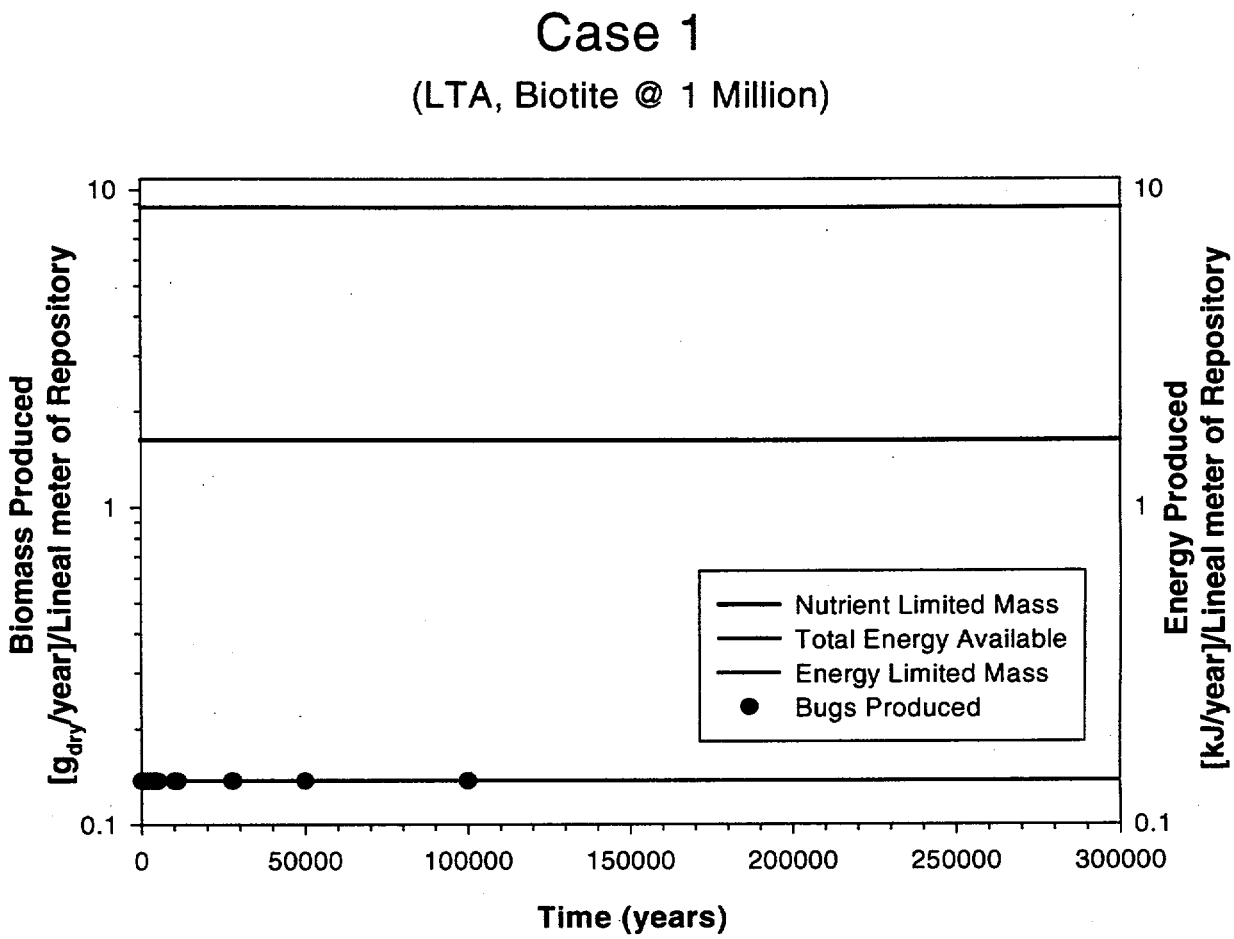

Figure 4-79. Case 1 results of the ambient system using the LTA climate with biotite degradation over 1 million years.

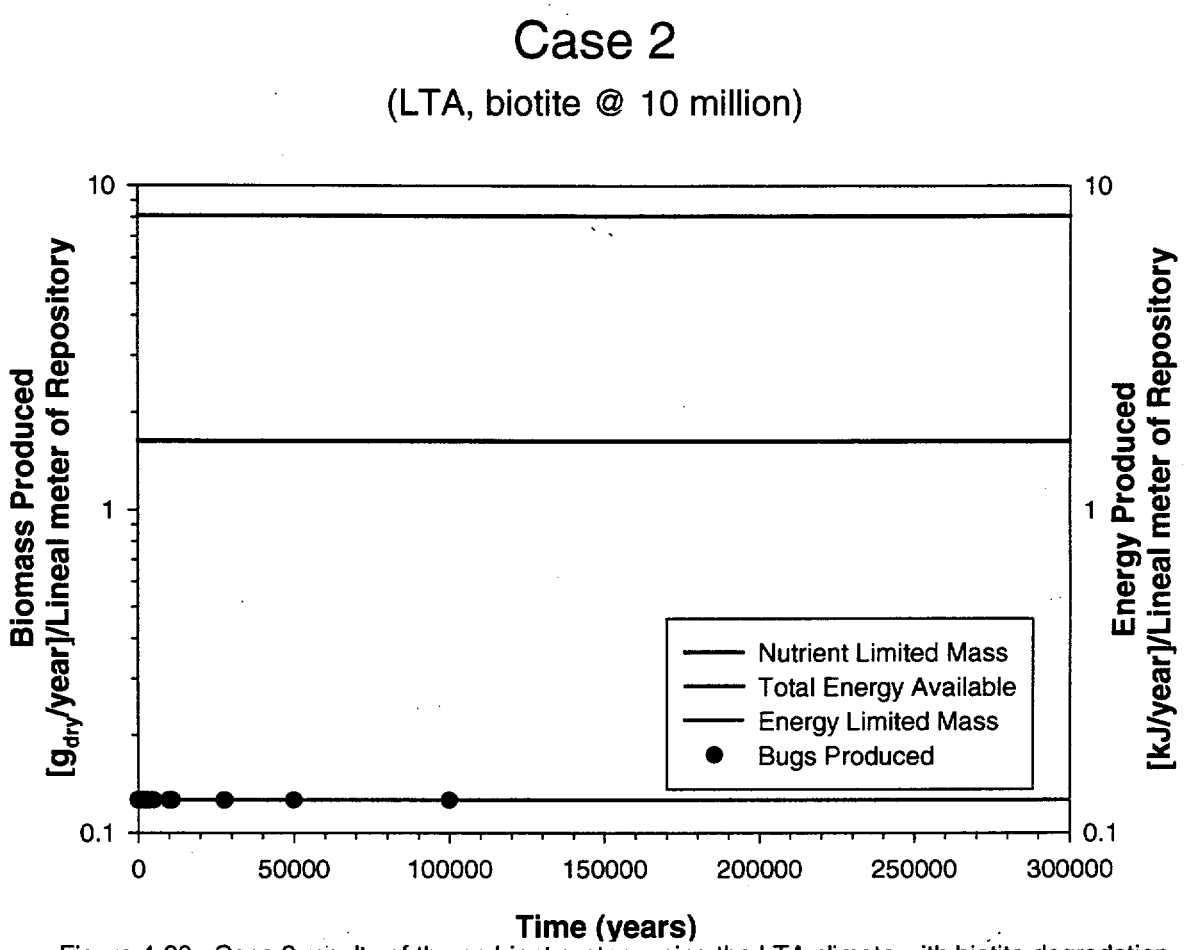

Figure 4-80. Case 2 results of the ambient system using the LTA climate with biotite degradation over 10 million years.

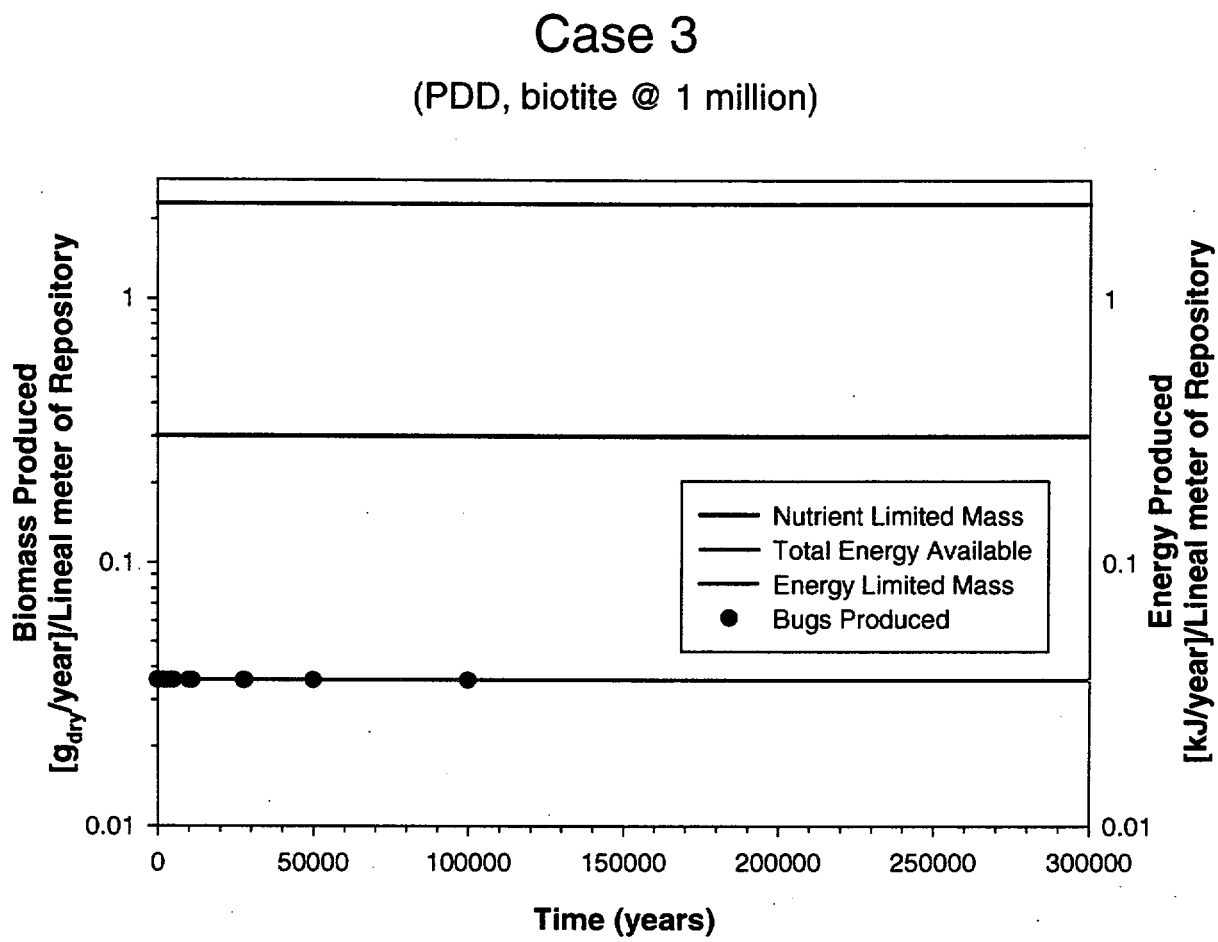

Figure 4-81. Case 3 results of the ambient system using the PDD climate with biotite degradation over 1 million years.

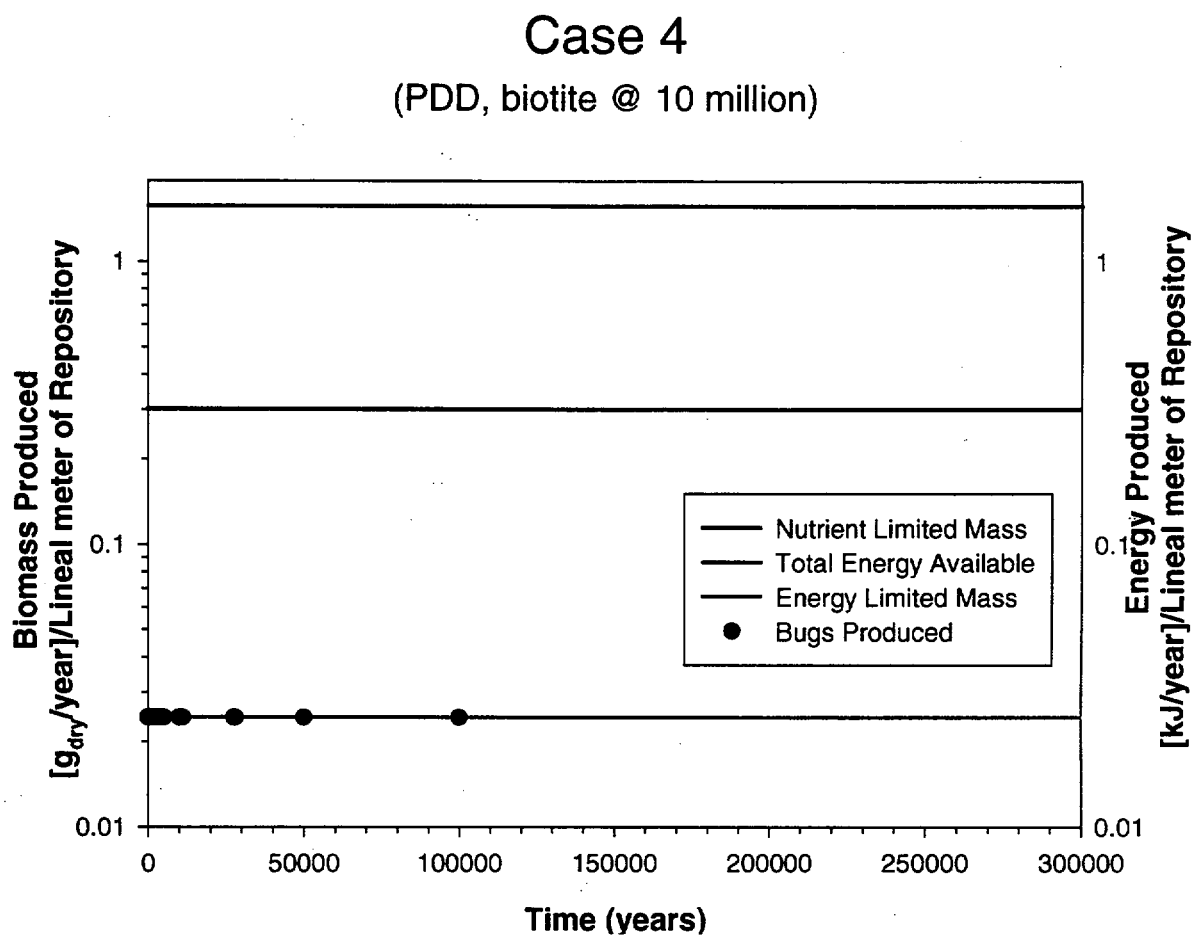

Figure 4-82. Case 4 results of the ambient system using the PDD climate with biotite degradation over 10 million years.

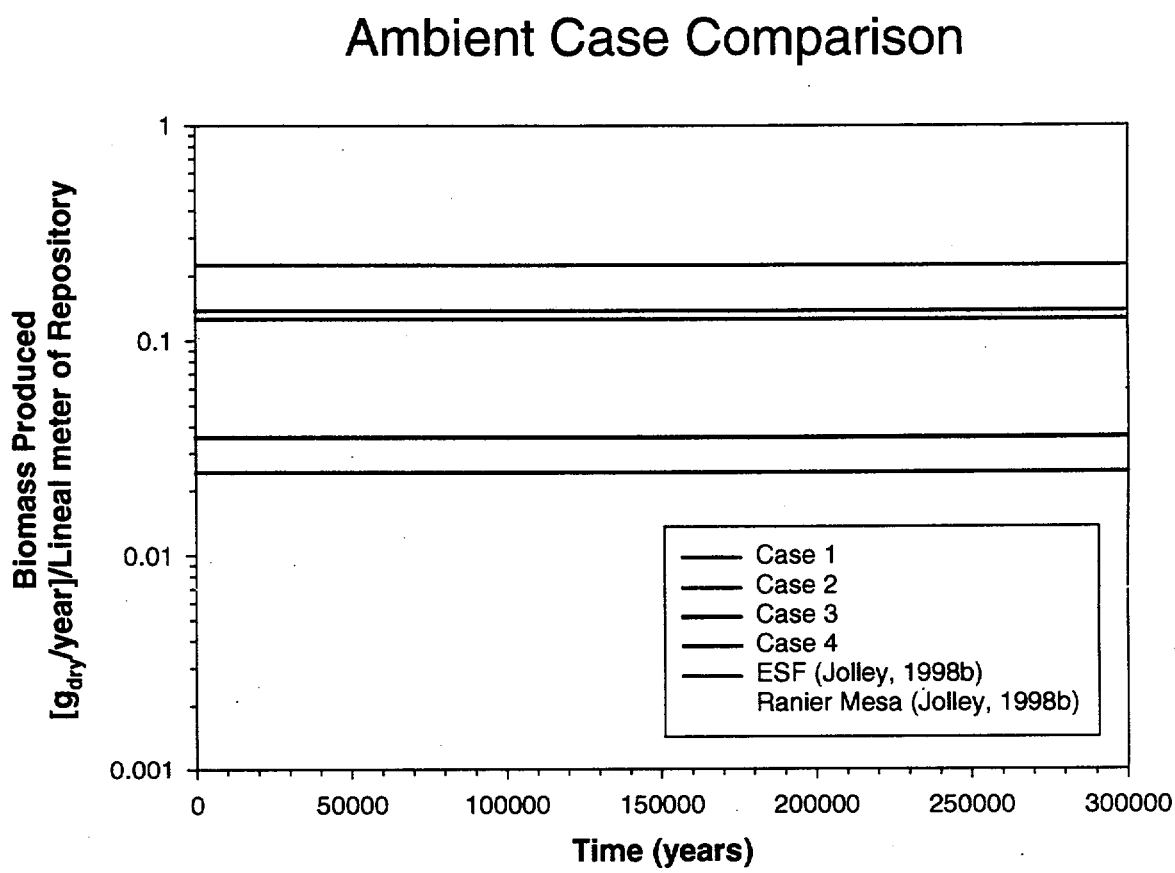

Figure 4-83. Comparison of modeled results to ambient measurements.

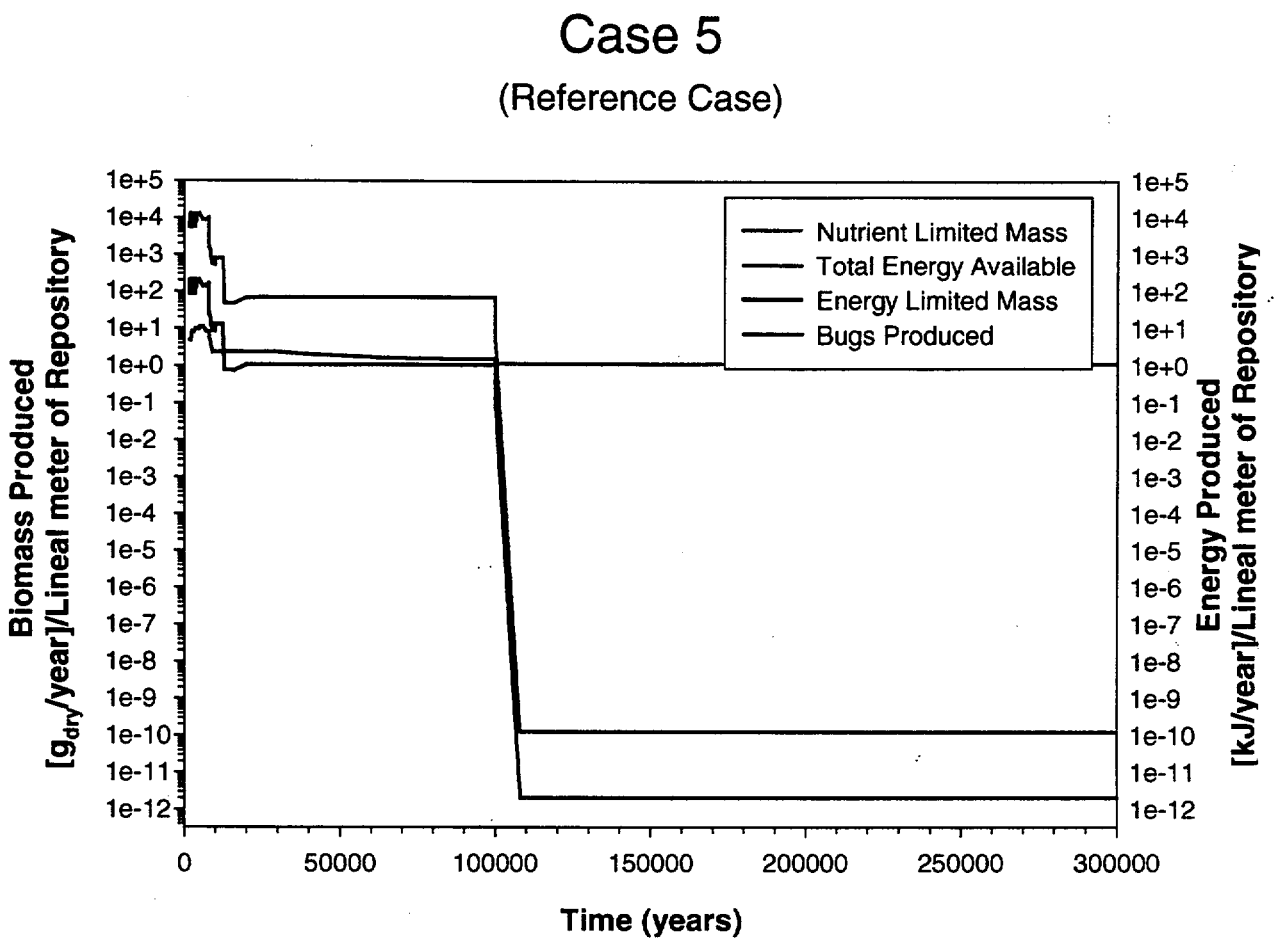

Figure 4-84. Case 5 results.

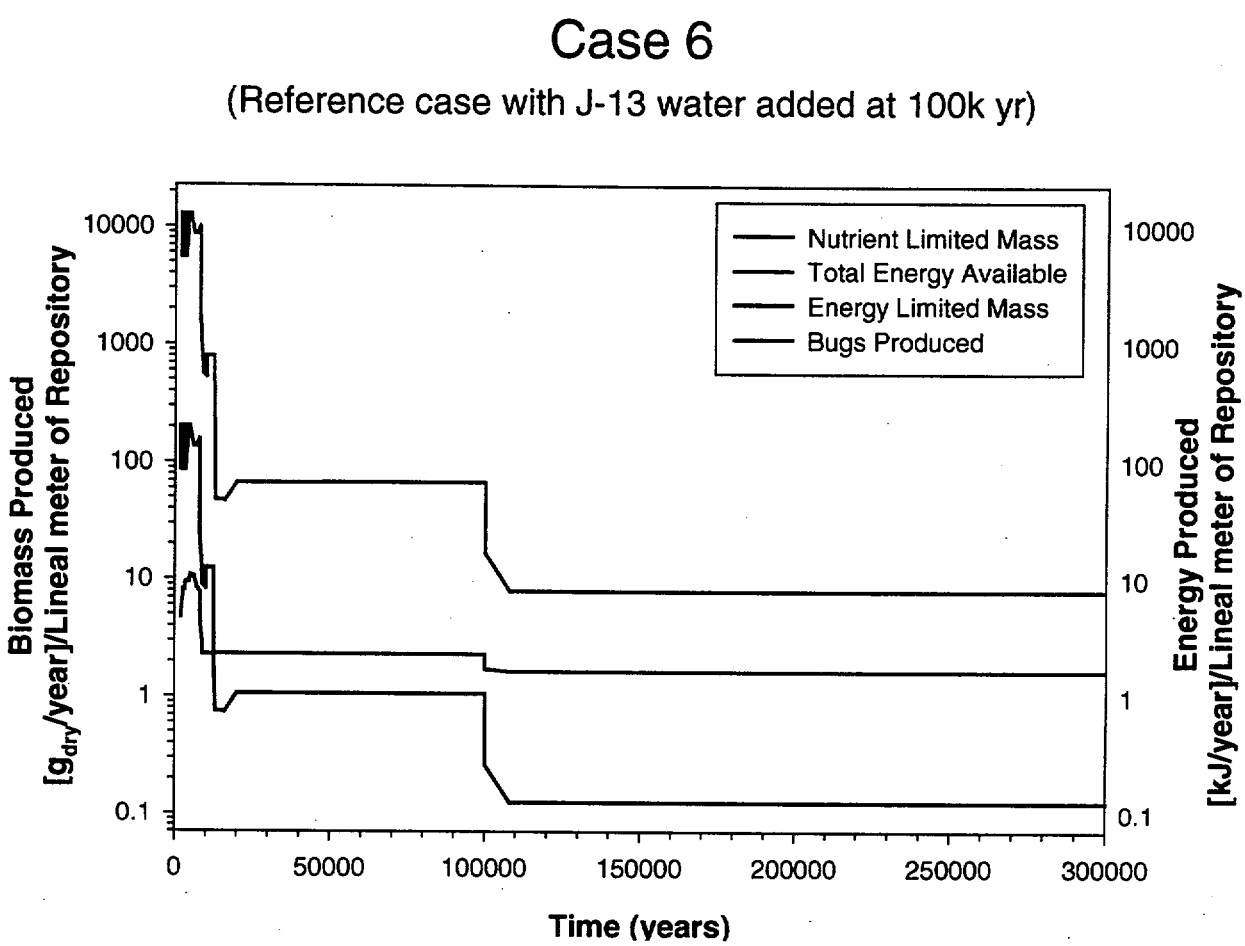

Figure 4-85. Case 6 results.

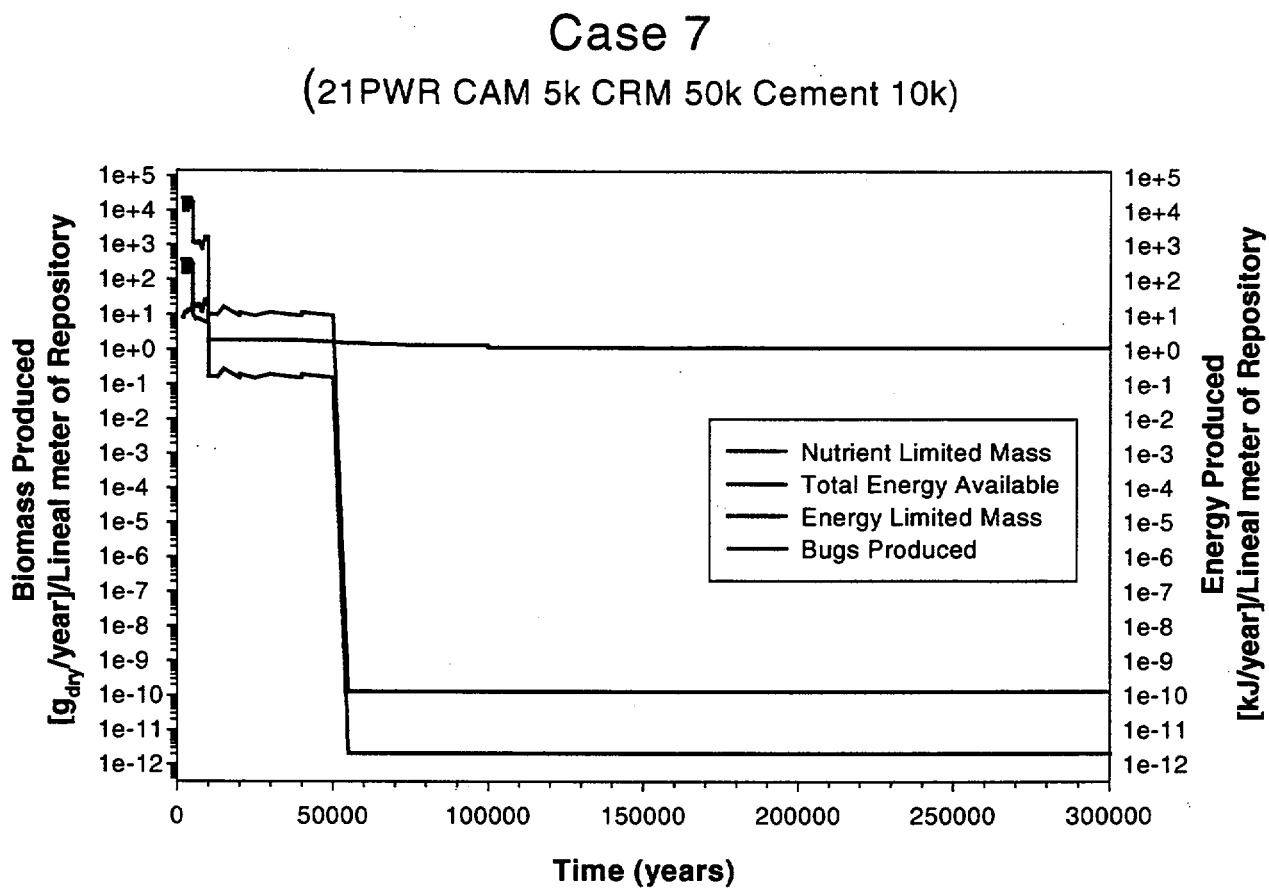

Figure 4-86. Case 7 results.

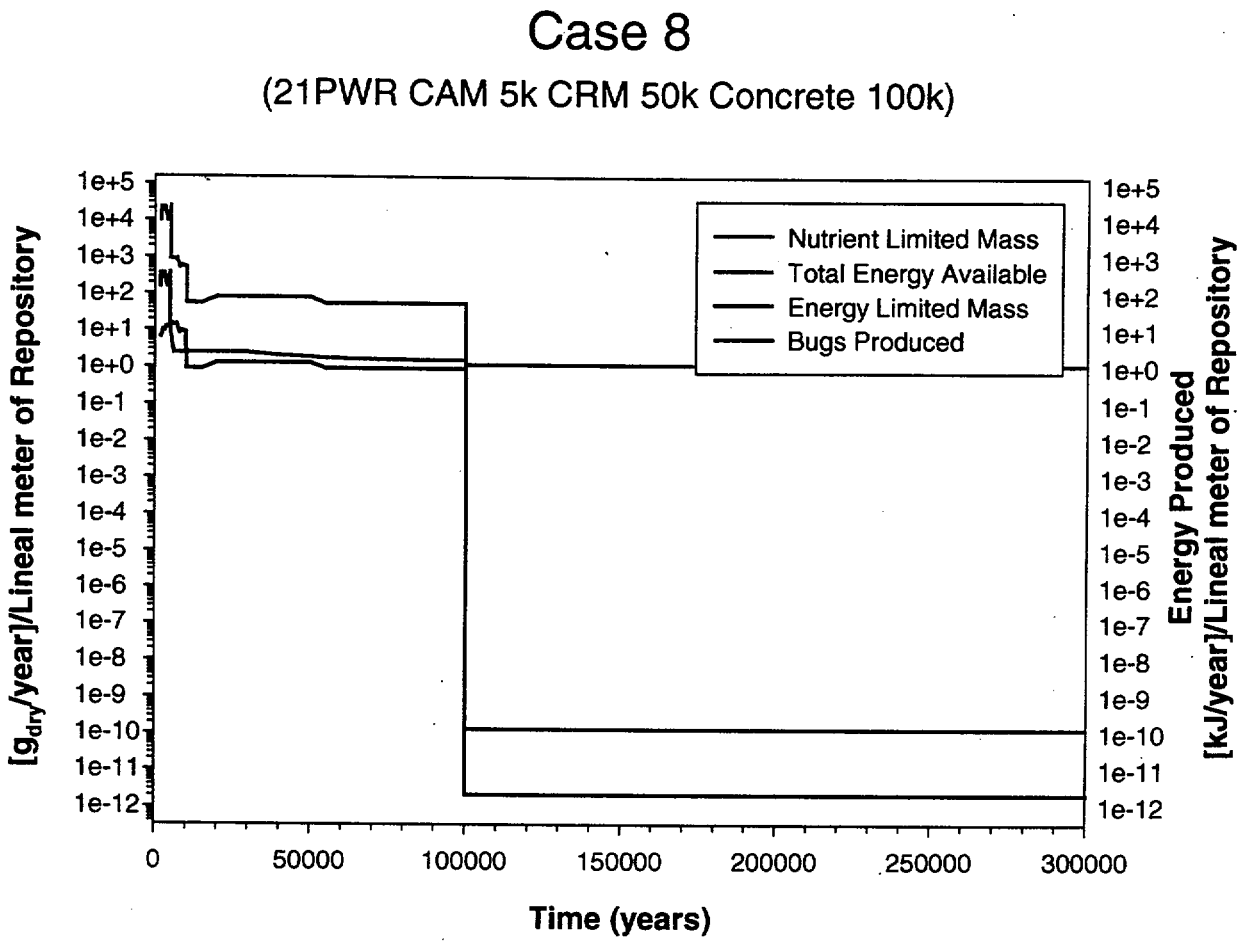

Figure 4-87. Case 8 results.

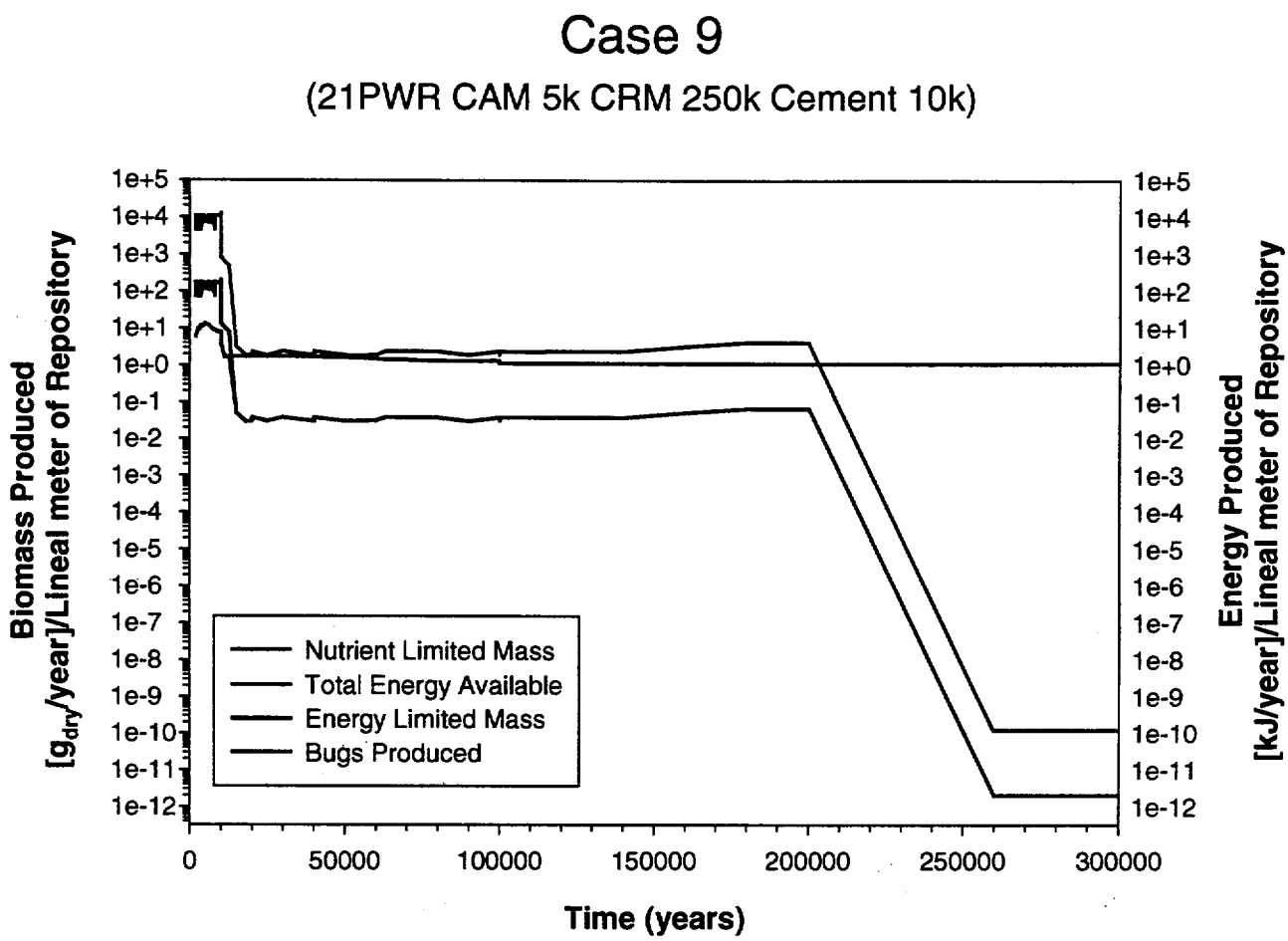

Figure 4-88. Case 9 results.

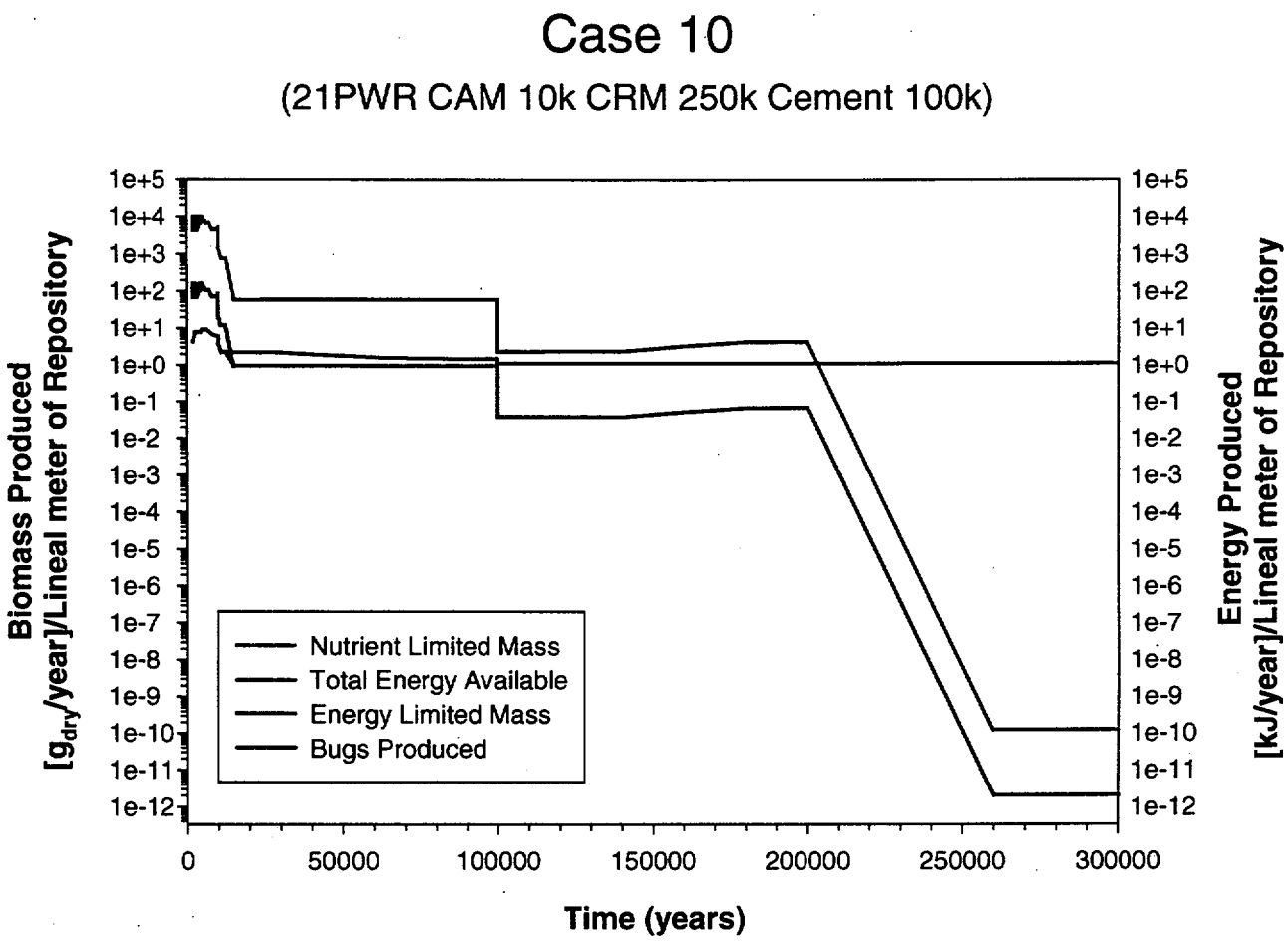

Figure 4-89. Case 10 results.

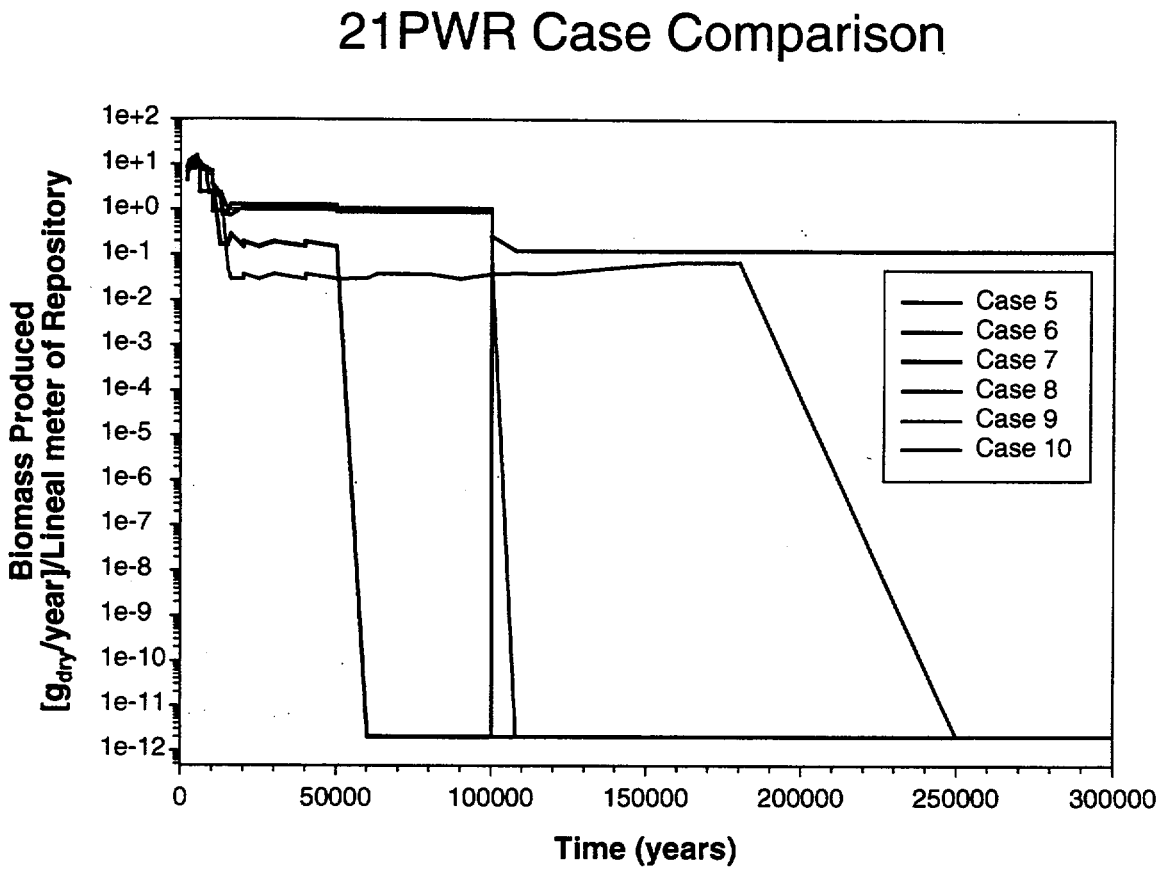

Figure 4-90. Comparison of biomass produced from Cases 5 through 10.

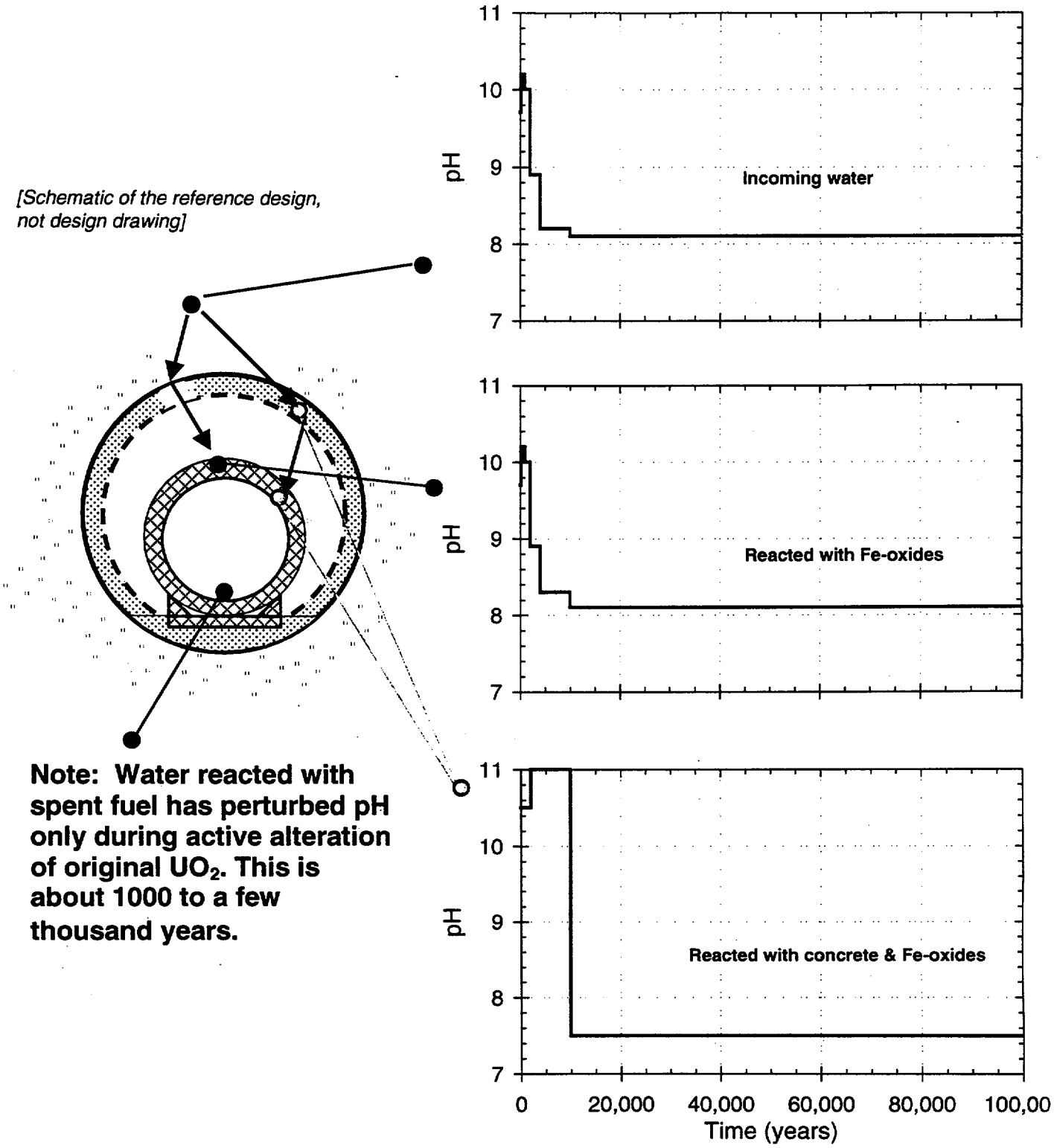

Figure 4-91. Near-field geochemical environment (NFGE) water composition summary, pH values, for the time frame from time of waste emplacement to 100,000 years later. The point along a conceptual flow pathway where the results of each plot begin to apply is indicated by reference to a schematic of a drift cross section.

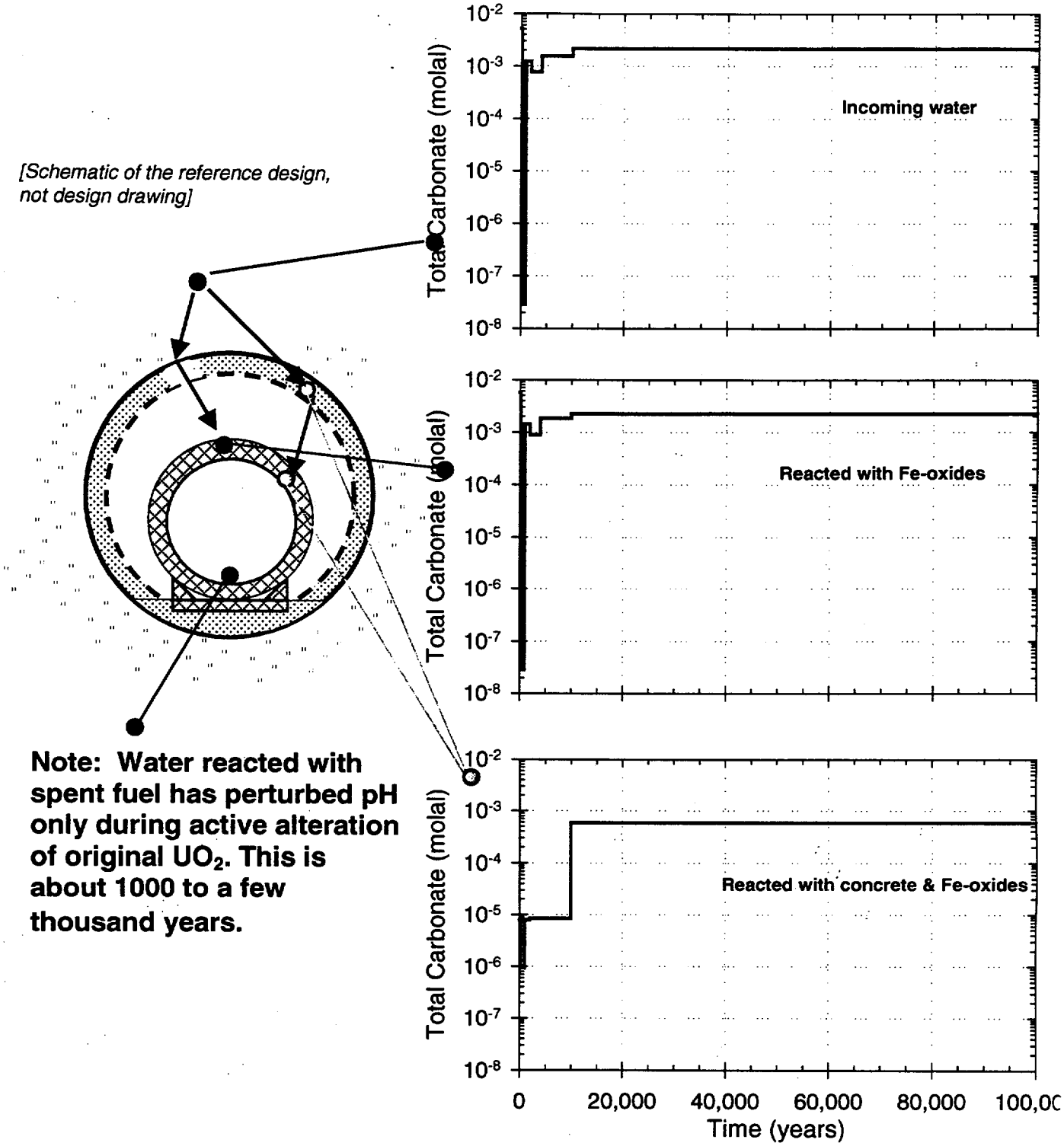

Figure 4-92. Near-field geochemical environment (NFGE) water composition summary, total carbonate values (ΣCO32-), for the time frame from time of waste emplacement to 100,000 years later. The point along a conceptual flow pathway where the results of each plot begin to apply is indicated by reference to a schematic of a drift cross section.

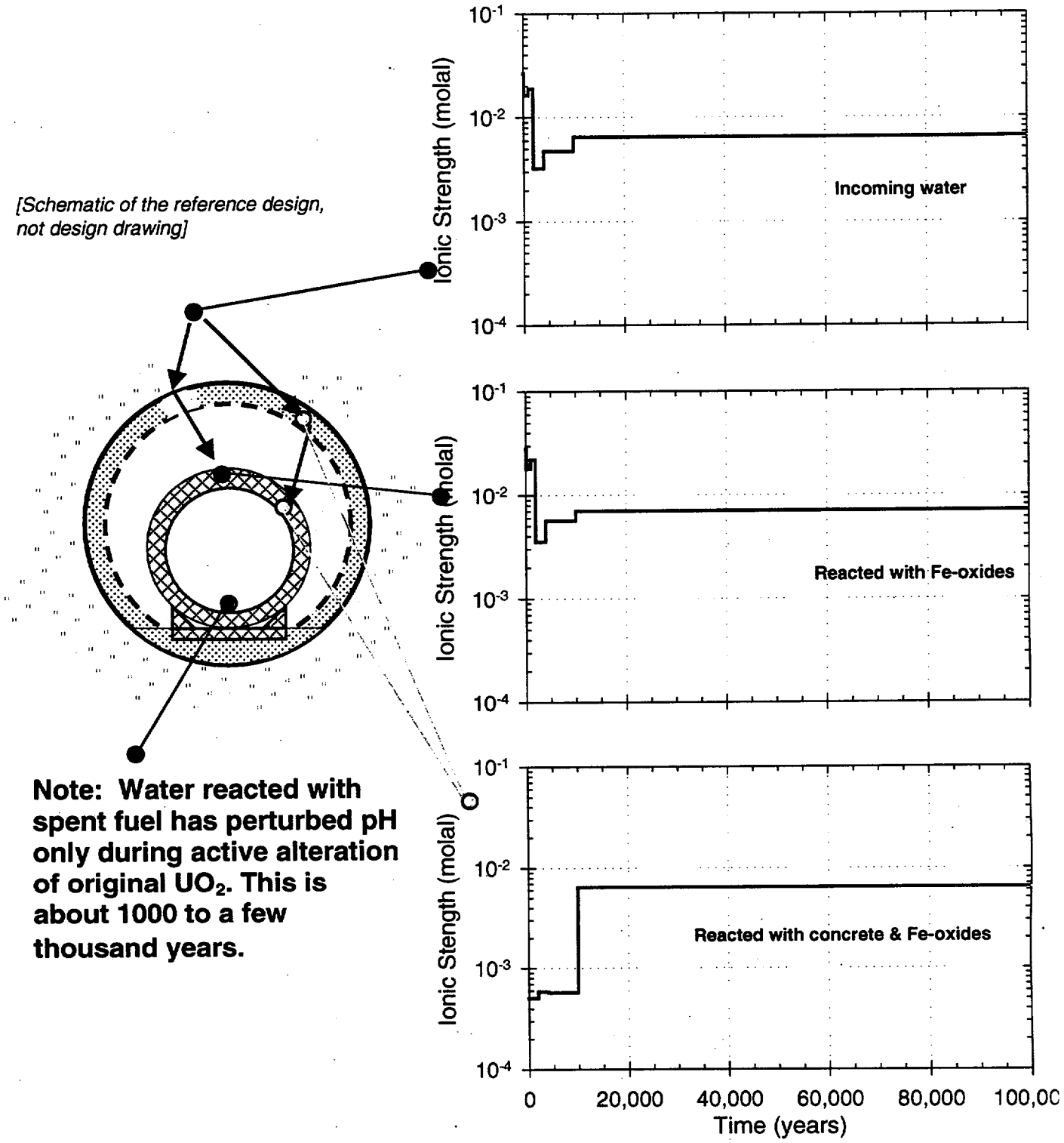

Figure 4-93. Near-field geochemical environment (NFGE) water composition summary, ionic strength values, for the time frame from time of waste emplacement to 100,000 years later. The point along a conceptual flow pathway where the results of each plot begin to apply is indicated by reference to a schematic of a drift cross section.

Chapter 4
Tables

Table 4-1. Near Field Geochemical Environment Abstraction/Testing Workshop.

NEAR FIELD GEOCHEMICAL ENVIRONMENT ABSTRACTION/TESTING WORKSHOP
March 5-7, 1997, Berkeley, CA (CRWMS M&O 1997)

Prioritization Criteria

Does the process/issue affect the

A. Dissolved radionuclide concentration?
B. Colloidal radionuclide abundances?
C. In-drift sorption capacities?
D. In-drift porosity and permeability?

Highest Priority Issues

Solid phases throughout the drift:

- Volume and flux of water in drift
- Compositions, abundances, and distribution (cement, alloys, organics, microbes, ceramics)
- Aqueous and gas reactions on materials
- Aqueous and gas reactions (corrosion) on waste package
- In-drift system open or closed

Gas phase throughout the drift:

- Gas flux
- Reactions with solids and microbes (excluding waste package)
- Reactions with waste package
- Thermal effects (water reactions)
- Temporal heterogeneity
- Climate effects

Aqueous phase throughout the drift:

- Aqueous phase reactions with major introduced materials (excluding waste package)
- Open versus closed system
- Aqueous phase reactions with waste package
- Temporal evolution of aqueous phase composition
- Perturbed water composition entering drift
- Aqueous reactions with waste form
- Thermal effects on aqueous phase compositions
- Aqueous phase reactions with evaporite minerals
- Microbial process effects on aqueous composition

Colloids throughout the drift:

- Reversibility of radionuclide sorption onto colloids
- Water-composition effects
- Waste form
- Other (introduced materials in rock)
- Temporal heterogeneity
- Microbial processes
- Temperature effects

Analysis Plans

- Incoming Gas, Water, and Colloids
- Gas composition evolution in the drift
- Water solid chemistry model
- Colloid-facilitated radionuclide transport
- Effects of microbial communities

Table 4-2. Average Compositions for Saturated Zone Water Well (J-13) and for Unsaturated Zone Water (UZ-5 and UZ-4) (nr = not reported).

Constituent	Units	J-13 AVG[a]	UE-25 UZ-5 AVG[b]	UE-25 UZ-4 AVG[c]
Ca	mg/l	12.9	45.2	99.2
Mg	mg/l	2.0	9.2	17.4
Na	mg/l	45.8	39.1	56.4
K	mg/l	5.0	8.6	14.2
SiO_2	mg/l	61.0	92.4	86.8
NO_3^-	mg/l	8.8	Nr	nr
HCO_3^-	mg/l	128.9[d]	Nr	nr
Cl	mg/l	7.1	53.2	94.0
F	mg/l	2.2	Nr	nr
SO_4^{-2}	mg/l	18.4	51.0	151.8
Li	microg/l	48.3	Nr	nr
Fe	microg/l	~30	49.1	24.3
Mn	microg/l	~45	18.5	38.6
Sr	microg/l	~50	422.6	1196.5
Al	microg/l	~30	Nr	nr
Zn	microg/l	nr	62.0	102.1
field Eh	mV	340.0	Nr	nr
field O_2	mg/l	5.6	Nr	nr
field pH	pH	7.4	7.0	7.5

a. Averages from Harrar et al. 1990, note that approximate values are estimates based on few data in Harrar et al. 1990.

b. Averages of data in Yang et al. 1998 and Yang et al. 1990.

c. Averages of data in Yang et al. 1988 and Yang 1992. d. Alkalinity as HCO_3^-.

Table 4-3. Composition of Cement Pore Fluids for a Variety of Cement Mixes, Curing Times, and Temperatures (nr = not reported).

Constituent	Units	OPC[a] 90 day	OPC+SiO_2[a] 90 day	OPC[b] 180 day	OPC+SiO_2[b] 180 day	I-09[c] 1 wk 0-20 kpsi	S-09-25[c] 6 mos	s-09-38[c] 6 mos	s-13-25[c] 6 mos	s-13-38[c] 6 mos	SPP[d] 8 mos
Ca	mg/l	110.0	120.0	nr	nr	120.0	8.0	24.0	156.0	8.0	90.0
Mg	mg/l	nr	nr	nr	nr	nr	Nr	nr	nr	nr	0.2
Na	mg/l	1470.0	1610.0	1240.0	1750.0	2510.0	2600.0	3400.0	6100.0	5106.0	1500.0
K	mg/l	7820.0	2460.0	8190.0	3430.0	12290.0	6590.0	9480.0	9360.0	7566.0	6300.0
SiO_2	mg/l	nr	nr	nr	nr	450.0	Nr	nr	nr	nr	12.9
Cl	mg/l	nr	nr	12.5	6.2	nr	17.0	38.0	780.0	1301.8	nr
F	mg/l	nr	nr	14.5	11.3	nr	Nr	nr	nr	nr	nr
$SO_4^{2!}$	mg/l	nr	nr	103.0	51.9	nr	290.0	1590.0	550.0	1440.0	nr
Fe	microg/l	nr	nr	nr	nr	nr	Nr	nr	nr	nr	500.0
Al	microg/l	2000.0	3000.0	nr	nr	17010.0	Nr	nr	nr	nr	5000.0
lab pH	pH	13.4	13.1	nr	nr	nr	13.5	13.6	nr	nr	13.4
Temperature	EC	16 to 18	16 to 18	~18	~18	nr	25.0	38.0	25.0	38.0	nr
Eh	mV	nr	nr	nr	nr	nr	Nr	nr	nr	nr	139.0

a. from Marr & Glasser (1983) where OPC means ordinary Portland cement; SiO_2 refers to Degussa silica; aging times are shown.

b. Glasser & Marr (1989) where OPC means ordinary Portland cement; SiO_2 refers to Degussa silica; aging times are shown.

c. Silsbee et al. (1986) where I-09 and S-09 designate Type I cement from Lone Star with 0.5 water /cement ratio and no added salt, S-13 designates I-09 with 0.4 wt% NaCl added, curing times and pressures (if different from atmospheric) are shown.

d. Andersson et al. (1989) where SPP refers to standard Portland cement, curing time is shown.

Table 4-4. Terms Used to Describe the O_2 Relations of Bacteria (Modified from Pederson and Karlsson (1995).

Group	O_2 Relation
Aerobes	
Obligate	O_2 is required
Facultative	O_2 is not required but growth is better with O_2
Microaerophilic	O_2 is required but at levels lower than atmospheric
Anaerobes	
Aerotolerant	O_2 is not required and growth is not better with O_2
Obligate (strict)	O_2 is harmful or lethal

Table 4-5. Bacterial Temperature Classes and Their Temperature Ranges. Data are Taken from Pederson and Karlsson (1995) and Horn and Meike (1995).

Temperature Class	Minima	Maxima	Optimum range
Psychrophiles	*	20°C	0 to 15°C
Facultative Psychrophiles	0°C	35°C	20 to 30°C
Mesophiles	15°C	45°C	20 to 45°C
Thermopiles	45°C	70°C	55 to 65°C
Hyperthermophiles	60°C	120°C	80 to 100°C

Table 4-6. pH Ranges of Differing Classes of Microbes. Data from Pederson and Karlsson (1995) and Horn and Meike (1995).

pH Class	pH Range
Acidophiles	1.0 to 5.5
Neutrophiles	5.5 to 8.5
Alkalophiles	8.5 to 11.5
Extreme Alkalophiles	>10.5

Table 4-7. Nutritional Requirements for Chemotrophic Organisms. Modified from Pederson and Karlsson (1995).

Nutritional type	Carbon sources	Electron sources (reducing power)	Examples of organisms
Chemolithotrophic autotrophy	CO_2	NH_4^+, NO_2^-, Mn^{2+}, Fe^{2+}, H_2S, S, H_2	Ammonium, nitrate, manganese, iron, sulfur, and hydrogen oxidizing bacteria, methanogenic bacteria
Chemoorganotrophic heterotrophy	Organic compound	Organic compound	Most bacteria, fungi, animals

Table 4-8. Abstractions from 2-D Thermohydrology Results.

Abstracted Period and Air Mass Fractions N233,400 Cross Section, TSPA-VA Base-Case Climate		
Infiltration = I(base-case) (I-dry + I-LTA)		
Location = Edge	***Time Frame, yrs***	***log (Air Mass Fraction)***
	0-200	-2
	200-1,000	-1
	>1,000	ambient
Location = Center	***Time Frame, yrs***	***log (Air Mass Fraction)***
	0-200	-3
	200-1,000	-7
	1,000-2,000	-2
	2,000-4,000	-1
	>4,000	ambient

Table.4-9. Calculated Water Compositions for Heated J-13-Like Water in Equilibrium with Tuff and Unsaturated-Zone Pore-Gas (see text for discussion).

J-13 Alternate Conceptual Model Resultant Fluid Compositions				
	input filename: Temperature:	**j13a31.3l 31°C**	**j13a60.3l 60°C**	**j13a90.3l 90°C**
Imposed Constraint	**Parmeter***	**Equilibrated Values (molal)***		
fO2 = 0.2 bar	redox	fO2 = 0.2 bar	fO2 = 0.2 bar	fO2 = 0.2 bar
fCO2 = 1.e-3 bar	pH	8.11	8.19	8.27
Fixed	Na+	1.99E-03	1.99E-03	1.99E-03
Fixed	K+	1.29E-04	1.29E-04	1.29E-04
Electrical balance	Ca++	3.36E-04	1.44E-04	6.76E-05
Saponite-Ca	Mg++	1.58E-05	4.97E-07	2.59E-08
Fixed	Sr++	4.56E-07	4.56E-07	4.56E-07
Fixed	Li+	6.92E-06	6.92E-06	6.92E-06
Nontronite-Ca	Fe++	2.02E-14	3.11E-15	5.93E-16
Pyrolusite (MnO2 for 90°C)	Mn++	3.99E-16	9.82E-15	4.44E-14
Montmorillonite-Ca	Al+++	5.17E-09	6.49E-08	5.62E-07
Cristobalite (alpha)	SiO2(aq)	4.58E-04	1.08E-03	2.06E-03
Fixed	B(OH)3(aq)	1.24E-05	1.24E-05	1.24E-05
Calcite	HCO3-*	1.98E-03	1.49E-03	1.07E-03
Fixed	Cl-	2.01E-04	2.01E-04	2.01E-04
Fixed	NO3-	1.42E-04	1.42E-04	1.42E-04
Fixed	SO4--	1.92E-04	1.92E-04	1.92E-04
Fixed	F-	1.15E-04	1.15E-04	1.15E-04
Fixed	HPO4-	1.25E-06	1.25E-06	1.25E-06
	Ionic Strength	6.11E-03	4.75E-03	3.76E-03
	log (I)	-2.21	-2.32	-2.43

*-Parameter represents total dissolved concentration of that constituent, unless otherwise noted. Values of pH given in pH units.

Table 4-10. Concrete Component Masses Scaled to 4.35 m^3/m of Tunnel, and Component Oxide Weight Percentages.

	Cement	Coarse Aggregate	Fine Aggregate	Water	Silica Fume	Steel Fiber	H_2O Red Admix	Superplasticizer
Mass (kg)	1713.14	4304.30	3263.39	697.13	254.43	169.46	12.43	30.51
Oxide	**wt %**	**wt %**	**wt %**	**wt %**	**wt %**	**wt %**	**wt %**	**wt %**
SiO_2	25.00	78.30	78.30	0.00	95.00	0.00	0.00	0.00
Al_2O_4	3.40	12.17	12.17	0.00	0.70	0.00	0.00	0.00
Fe_2O_3	2.80	1.00	1.00	0.00	0.30	99.80	0.00	0.00
CaO	64.40	0.47	0.47	0.00	0.30	0.00	0.00	0.00
MgO	1.90	0.12	0.12	0.00	0.20	0.00	0.00	0.00
TiO_2	0.00	0.10	0.10	0.00	0.00	0.00	0.00	0.00
Na_2O	0.00	4.08	4.08	0.00	0.30	0.00	0.00	0.00
K_2O	0.00	3.28	3.28	0.00	0.30	0.00	0.00	0.00
P_2O_5	0.00	0.02	0.02	0.00	0.00	0.04	0.00	0.00
MnO	0.00	0.05	0.05	0.00	0.00	0.08	0.00	0.00
SO_3	1.60	0.00	0.00	0.00	0.80	0.05	0.00	0.00
C	0.00	0.00	0.00	0.00	1.30	0.02	0.00	0.00
H_2O	0.00	0.00	0.00	100.00	0.00	0.00	0.00	0.00

Table 4-11. Component Elemental Masses for Concrete.

	Cement	Coarse Aggregate	Fine Aggregate	Silica Fume	Steel Fiber	Water	H_2O Red Admix	Totals
Element	Mass (kg)	Mass (kg)	Mass (kg)	Mass (kg)	Mass (kg)	Mass (kg)	Mass (kg)	Mass (kg)
Si	2.02E+02	1.58E+03	1.19E+03	1.13E+02	0.00E+00	0.00E+00	0.00E+00	3.08E+03
Al	3.11E+01	2.77E+02	2.10E+02	9.43E-01	0.00E+00	0.00E+00	0.00E+00	5.19E+02
Fe	3.39E+01	3.00E+01	2.27E+01	5.34E-01	1.69E+02	0.00E+00	0.00E+00	2.56E+02
Ca	7.96E+02	1.46E+01	1.11E+01	5.46E-01	0.00E+00	0.00E+00	0.00E+00	8.22E+02
Mg	1.98E+01	3.19E+00	2.42E+00	3.07E-01	0.00E+00	0.00E+00	0.00E+00	2.57E+01
Ti	0.00E+00	2.61E+00	1.98E+00	0.00E+00	0.00E+00	0.00E+00	0.00E+00	4.58E+00
Na	0.00E+00	1.30E+02	9.88E+01	0.00E+00	0.00E+00	0.00E+00	0.00E+00	2.29E+02
K	0.00E+00	1.17E+02	8.89E+01	0.00E+00	0.00E+00	0.00E+00	0.00E+00	2.06E+02
P	0.00E+00	3.76E-01	2.85E-01	0.00E+00	6.78E-02	0.00E+00	0.00E+00	7.28E-01
Mn	0.00E+00	1.73E+00	1.31E+00	0.00E+00	1.24E-01	0.00E+00	0.00E+00	3.17E+00
S	1.11E+01	0.00E+00	0.00E+00	8.15E-01	9.04E-02	0.00E+00	0.00E+00	1.20E+01
C	0.00E+00	0.00E+00	0.00E+00	0.00E+00	3.39E-02	0.00E+00	0.00E+00	3.39E-02
H_2O	0.00E+00	0.00E+00	0.00E+00	0.00E+00	0.00E+00	6.97E+02	1.24E+01	7.10E+02

Table 4-12. Component Elemental Moles for Concrete.

	Cement	Coarse Aggregate	Fine Aggregate	Silica Fume	Steel Fiber	Water	H_2O Red Admix	Totals
Element	Moles	Moles	Moles	Moles	Moles	Moles	Moles	Moles
Si	7.19E+03	5.61E+04	4.25E+04	4.02E+03	0.00E+00	0.00E+00	0.00E+00	1.10E+05
Al	1.15E+03	1.03E+04	7.79E+03	3.49E+01	0.00E+00	0.00E+00	0.00E+00	1.93E+04
Fe	6.06E+02	5.37E+02	4.07E+02	9.56E+00	3.03E+03	0.00E+00	0.00E+00	4.59E+03
Ca	1.99E+04	3.64E+02	2.76E+02	1.36E+01	0.00E+00	0.00E+00	0.00E+00	2.05E+04
Mg	8.15E+02	1.31E+02	9.96E+01	1.26E+01	0.00E+00	0.00E+00	0.00E+00	1.06E+03
Ti	0.00E+00	5.44E+01	4.13E+01	0.00E+00	0.00E+00	0.00E+00	0.00E+00	9.57E+01
Na	0.00E+00	5.67E+03	4.30E+03	2.46E+01	0.00E+00	0.00E+00	0.00E+00	9.99E+03
K	0.00E+00	3.00E+03	2.27E+03	1.62E+01	0.00E+00	0.00E+00	0.00E+00	5.29E+03
P	0.00E+00	1.21E+01	9.20E+00	0.00E+00	4.78E-01	0.00E+00	0.00E+00	2.18E+01
Mn	0.00E+00	3.16E+01	2.39E+01	0.00E+00	1.75E+00	0.00E+00	0.00E+00	5.72E+01
S	3.45E+02	0.00E+00	0.00E+00	2.54E+01	1.13E+00	0.00E+00	0.00E+00	3.72E+02
C	0.00E+00	0.00E+00	0.00E+00	0.00E+00	2.82E+00	0.00E+00	0.00E+00	2.82E+00
H_2O	0.00E+00	0.00E+00	0.00E+00	0.00E+00	0.00E+00	3.87E+04	3.85E+02	3.91E+04

Table 4-13. Cement Mineral Phases and Chemical Formula
(Based on Hardin et al. 1998, Section 7.1.2.1).

Phase	Chemical Formula
Ettringite	$Ca_6Al_2(SO_4)_3(OH)_{12}{:}26H_2O$
CSH17gel	$Ca_{1.7}SiO_{5.7}H_4$
Brucite	$Mg(OH)_2$
Fe-Hydrogarnet	$Ca_3Fe_2(OH)_{12}$
Al-Hydrogarnet	$Ca_3Al_2(OH)_{12}$
Portlandite	$Ca(OH)_2$

Table 4-14. Cement Phase Normalization Expressions, Total Moles, and Relative Reaction Rates.

Phase	Normalization Expression (moles phase)	Value (mols/m tunnel)	Relative Reaction Rate
Ettringite	$AFt = (S_{cem} + xS_{fume})/3$ (x = fraction of fume)	119.39	0.1
CSH17gel	$CSH = Si_{cem} + xSi_{fume}$	9204.22	1.0
Brucite	$MH = Mg_{cem} + xMg_{fume}$	821.24	0.1
Fe-Hydrogarnet	$C3FH6 = (Fe_{cem} + xFe_{fume})/2$	305.50	0.025
Al-Hydrogarnet	$C3AH6 = (Al_{cem} + xAl_{fume} - 2AFt)/2$	465.79	0.025
Portlandite	$CH = Ca_{cem} - 6AFt - (C/S)CSH - 3(C3AH6+C3FH6) + xCa_{fume}$	1182.04	5.0

Table 4-15. Aggregate Phases and Their Chemical Formula.

Aggregate Assemblage	
Phase	**Formula**
Annite	$KFe_3AlSi_3O_{10}(OH)_2$
Phlogopite	$KAlMg_3Si_3O_{10}(OH)_2$
Sanidine-high	$KAlSi_3O_8$
Albite	$NaAlSi_3O_8$
Anorthite	$CaAl_2(SiO_4)_2$
Pyrophyllite	$Al_2Si_4O_{10}(OH)_2$
SiO_2 Phase	SiO_2

Table 4-16. Coarse Aggregate Normalization Expressions.

Course Aggregate	
Phase	**Normalization Expression (moles phase)**
Annite	$Ann = Fe_{total}/3$
Phlogopite	$Phlog = Mg_{total}/3$
Sanidine-high	$San = K_{total} - Ann - Phlog$
Albite	$Alb = Na_{total}$
Anorthite	$An = Ca_{total}$
Pyrophyllite	$Py = (Al_{total} - Ann - Phlog - San - Alb - 2An)/2$
SiO_2 Phase	$Si = Si_{total} - 2An - 3(Ann + Phlog + San + Alb) - 4Py$

Table 4-17. Fine Aggregate Normalization Expressions.

Fine Aggregate	
Phase	**Normalization Expression (moles phase)**
Annite	$Ann = (Fe_{total} + (1-x)Fe_{fume})/3$
Phlogopite	$Phlog = Mg_{total} + (1-x)Mg_{fume})/3$
Sanidine-high	$San = K_{total} + (1-x)K_{fume} - Ann - Phlog$
Albite	$Alb = Na_{total} + (1-x)Na_{fume}$
Anorthite	$An = Ca_{total} + (1-x)Ca_{fume}$
Pyrophyllite	$Py = (Al_{total} + (1-x)Al_{fume} - Ann - Phlog - San - Alb - 2An)/2$
SiO_2 Phase	$Si = Si_{total} + (1-x)Si_{fume} - 2An - 3(Ann + Phlog + San + Alb) - 4Py$